Design and Development of a Novel Thermochemical Reactor Using Composite Sorbent for Solar Thermal Energy Storage

Majid Karim Nejhad

Submitted to the
Institute of Graduate Studies and Research
in partial fulfillment of the requirements for the degree of

Doctor of Philosophy
in
Mechanical Engineering

Eastern Mediterranean University
October 2019
Gazimağusa, North Cyprus

Approval of the Institute of Graduate Studies and Research

Prof. Dr. Ali Hakan Ulusoy
Acting Director

I certify that this thesis satisfies all the requirements as a thesis for the degree of Doctor of Philosophy in Mechanical Engineering.

Prof. Dr. Hasan Hacişevki
Chair, Department of Mechanical Engineering

We certify that we have read this thesis and that in our opinion it is fully adequate in scope and quality as a thesis for the degree of Doctor of Philosophy in Mechanical Engineering.

Asst. Prof. Dr. Devrim Aydın
Supervisor

Examining Committee

1. Prof. Dr. Fuat Egelioğlu
2. Prof. Dr. Arif Hepbaşlı
3. Prof. Dr. Mustafa İlkan
4. Prof. Dr. Zafer Utlu
5. Asst. Prof. Dr. Devrim Aydın

ABSTRACT

Thermochemical heat storage (THS) is being considered as a potential technology in order to enhance the utilization of renewable energy sources due to its high energy storage density and long term heat storage capacity. However, further advancement in such systems depends on the development of novel sorption materials and innovative solar-driven thermochemical processes. To this end, this work presents new sorption materials and a new solar-driven THS process suitable for building applications.

In the first part of the study, two novel composite sorbents consisting of aerated porous concrete-calcium chloride (APC-$CaCl_2$) and pumice-calcium chloride (P-$CaCl_2$), respectively, were synthesized. Other than the synthesized new composite materials, vermiculite-calcium chloride (V-$CaCl_2$) and zeolite were also selected and synthesized for a comparative performance study. A new experimental scale THS system was designed and developed for investigating the charging/discharging characteristics of all synthesized sorption materials. The experimental results show that, the values of the average energy storage density of the system operating with APC-$CaCl_2$, V-$CaCl_2$, zeolite, and P-$CaCl_2$, for five hours of discharging were 186.9 kWh/m^3, 174.2 kWh/m^3, 182.6 kWh/m^3 and 204.3 kWh/m^3, respectively. For a charging temperature of 90 ºC over three hours of charging process, the mass desorption rate of APC-$CaCl_2$ was found to be 9.84 g/min, while, it was 4.40 g/min, 13.27 g/min and 14.13 g/min for zeolite, V-$CaCl_2$ and P-$CaCl_2$, respectively. Considering their charging/discharging performances and their cyclic stability, P-$CaCl_2$ and V-$CaCl_2$ were found to be the best candidate materials for THS applications.

In the second part of the study, a solar-driven THS was designed, developed and tested under real climatic conditions of North Cyprus. V-$CaCl_2$ was selected as the working material due to its high energy density, good cyclic ability and the low cost and availability of vermiculite (host matrix) in North Cyprus. Three series of charging-discharging experiments were performed employing the newly developed solar-driven THS system. The discharging tests were performed during the night for a duration of five hours. During the discharging experiments, the temperature and relative humidity of air at the reactor inlet were in the range of 21 – 24 ºC and 80 – 90 %, respectively. Under these conditions, the average energy output over three cycles was found to be 2.1 kWh, with an average energy storage density of 156 kWh/m^3. A manufactured parabolic solar concentrator was utilized to provide the required thermal energy in the charging process. Hence, the average surface temperature of the reactor was in the range of 78 ºC to 83 ºC and the average useful energy of the charging process was 3.94 kWh. The rate of moisture desorption was 6.5 g/min while the overall efficiency was 38%.

Furthermore, an economic analysis was performed to compare the feasibility of the proposed solar-driven THS system and a typical heat-pump unit of the split air-conditioner under the climatic conditions of North Cyprus. The heating load of a house with an area of 90 m^2 was simulated in the DesignBuilder software, and from the simulation results, it was found that a solar-driven THS system with a reactor volume of 8.75 m^3 is required to meet 1366 kWh of an annual heating load of the building. The analysis showed that the net present value of THS system after ten years would be $381 with a simple payback period of 6.4 years, which illustrates the economic feasibility of the THS system.

Keywords: Thermochemical Heat Storage, Solar Energy, Thermodynamic Analysis, Porous Host Matrix, Calcium Chloride, Composite Sorbent, Experimental

ÖZ

Termokimyasal ısı depolama (TID) sistemleri, ısıl enejiyi yüksek yoğunlukta ve uzun süreli olarak depolayabilme imkanı sağladığından, yenilenebilir enerji kaynaklarından daha verimli faydalanmak için potansiyel bir teknoloji olarak görülmektedir. Ancak TID sistemlerinin gelişimi, yenilikçi ısı depolama malzemelerinin ve etkin güneş enerjili TID proseslerinin geliştirilmesine bağlıdır. Bu bağlamda sunulan çalışmada bina uygulamalarına yönelik geliştirilen yeni sorpsiyon malzemelerinin ve güneş enerjisi kaynaklı TID sisteminin performansları deneysel olarak incelenmiştir.

Çalışmanın ilk kısmında gözenekli beton-kalsiyum klorür (APC-$CaCl_2$) ve pomza-kalsiyum klorür (P-$CaCl_2$) olmak üzere iki yeni kompozit sorbent sentezlenmiştir. Bunun yanında performans karşılaştırması amacıyla Zeolit ve vermikülit-kalsiyum klorür (V-$CaCl_2$) seçilmiş ve sentezlenmiştir. Daha sonra laboratuvar ölçekli bir deneysel TID sistemi tasarlanıp üretilmiş ve hazırlanan tüm sorbentler, şarj/deşarj performans karakteristiklerinin belirlenmesi amacıyla test edilmiştir. Deneysel çalışma sonuçlarına göre, beş saat deşarj süresi için APC-$CaCl_2$, V-$CaCl_2$, Zeolit ve P-$CaCl_2$'nin enerji depolama yoğunlukları sırasıyla 186.9 kWs/m^3, 174.2 kWs/m^3, 182.6 kWs/m^3 ve 204.3 kWs/m^3 olarak hesaplanmıstır. Bunun yanında 90 ºC şarj sıcaklığı ve üç saatlik şarj süresinde, su buharı desorpsiyon hızları APC-$CaCl_2$, Zeolit, V-$CaCl_2$ ve P-$CaCl_2$ için 9.84 g/dak 4.40g/dak, 13.27g/dak ve 14.13g/dak olarak belirlenmiştir. Şarj/deşarj performansları ve çevrimsel kararlılık parametreleri göz önüne alındığında P-$CaCl_2$ ve V-$CaCl_2$ TID uygulamaları için en uygun sorbentler olarak belirlenmiştir.

Çalışmanın ikinci kısmında, güneş enerjisi kaynaklı bir TID sistemi tasarlanmış, geliştirilmiş ve Kuzey Kıbrıs iklim koşullarında test edilmiştir. Yüksek enerji depolama yoğunluğu, etkin çevrimsel kararlılığı, düşük maaliyeti ve Kuzey Kıbrıs'ta bulunabilirliği göz önüne alınarak, geliştirilen deneysel sistemde sorbent malzemesi olarak V-$CaCl_2$ kullanılmıştır. Deneysel süreçte, geliştirilen güneş enerjili TID sistem performansını ölçmek için üç tekrar eden şarj/deşarj çevrimi yapılmıştır. Deşarj testleri güneş ışınımın olmadığı akşam saatlerinde beş saatlik sürede gerçekleştirilmiştir. Deşarj testleri sırasında reaktör giriş havası sıcaklığı ve bağıl nemi sırasıyla 21 – 24 ºC ve 80% – 90% arasında ölçülmüştür. Belirtilen çalışma koşulları altında deşarj prosesi averaj ısı üretimi ve enerji depolama yoğunluğu üç tekrar eden çevrim için sırasıyla 2.1 kWs ve 156 kWs/m^3 olarak hesaplanmıştır. Sorpsiyon reaktörüne entegre edilen parabolik güneş yoğunlaştırıcısı şarj prosesinde gerekli ısıl enerjiyi üretmek için kullanılmıştır. Şarj sırasında reaktör ortalama sıcaklığı 78 ºC – 83 ºC arasında ölçülmüş, güneş ışınımından elde edilen kullanılabilir ortalama ısıl enerji değeri 3.94 kWs olarak hesaplanmıştır. Bunun yanında nem desorpsiyon hızı ve şarj verimi sırasıyla 6.5 g/dak ve %38 olarak elde edilmiştir.

Çalışmanın son bölümünde, elde edilen deneysel veriler yardımıyla güneş enerjili TID sisteminin Kuzey Kıbrıs koşullarında mahal ısıtmada kullanımının ekonomik fizibilitesi geleneksel ısı pompası sistemleri ile karşılaştırmalı olarak analiz edilmiştir. Bu amaçla, DesignBuilder programında 90 m^2 yüzey alanına sahip bir bina tasarlanarak yıllık ısı yükü hesaplanmıştır. Analiz sonuçlarına göre bina yıllık ısı yükü 1366 kWs olarak belirlenmiş, bu ısı yükünü karşılayabilmek için gerekli TID hacmi 8.75 m^3 olarak hesaplanmştır. Yapılan fizibilite analizi güneş enerjili TID sistemiyle elde edilecek 10 yıllık ekonomik kazancın bügünkü değerinin $381 ve yatırım geri

ödeme süresinin 6.4 yıl olduğunu göstermiştir. Bu bağlamda, yapılan analiz güneş enerjili TID sisteminin Kuzey Kıbrıs koşullarında uygulanmasının ekonomik olarak mümkün olduğunu göstermiştir.

Anahtar kelimeler: Termokimyasal Isı Depolama, Güneş Enerjisi, Termodinamik Analiz, Gözenekli Taşıyıcı Matris, Kalsiyum Klorür, Kompozit Sorbent, Deneysel

DEDICATION

To My Dear Mother

ACKNOWLEDGMENT

I would like to thank from the bottom of my heart to my supervisor Asst. Prof. Dr. Devrim Aydın, who has supported me through this journey with his guidance and advices. He has influenced me a lot with his passion for work. I would also like to thank the members of my dissertation committee, Prof. Dr. Fuat Egelioğlu, Prof. Dr. Arif Hepbaşlı, Prof. Dr. Mustafa İlkan and, Prof. Dr. Zafer Utlu.

I am very grateful to all of my friends who supported me in my thesis work. I am indebted to all my friends for their support and encouragement during this journey. Even if some of them were not physically here, their love and inspiration helped me during this study.

Finally, I would like to thank my family for their long-standing support and care. Above all I would like to thank my wife for her love and constant support. My heartfelt thanks to my late mother for her eternal love and to my father for his love and dedications. Also, I am very grateful to all of my brothers. Their love and understanding made it possible for me to complete this journey.

TABLE OF CONTENTS

LIST OF TABLES

LIST OF FIGURES

LIST OF SYMBOLS

C_p	specific heat at constant pressure, J/(kg K)
E_{cum}	cumulative thermal energy, Wh, kWh
E_d	energy density, kJ/kg, kWh/m^3
f	mass uptake ratio, g_{wv} /g_{abs}
H	enthalpy, kJ/s
$\dot{m}_a$	mass flow rate of air, kg/s
m	mass, g, kg
P	density, kg/m^3
$\dot{Q}$	thermal power rate, W, kW
RH	relative humidity, %
S	entropy, kJ/kg
T	temperature, ºC, K
T	time, s, h
T_{reg}	regeneration temperature, ºC, K
V	volume, m^3
W	absolute humidity, g/kg
X_{cum}	cumulative thermal exergy, Wh, kWh
$\dot{X}$	exergy rate, W, kW
y	sorption/desorption rate, g/min
Δ	difference
η_I	first law efficiency
η_{II}	second law efficiency

LIST OF ABBREVIATIONS

a	air
ads	adsorbent
APC	Aerated Porous Concrete
aq	aqueous solution
avg	average
COP	Coefficient Of Performance
cr	charging
cum	cumulative
dcr	discharging
des	desorption
I	Irradiance
in	inlet
IRR	Internal Rate of Return
LHS	Latent Heat Storage
mat	material
NPV	Net Present Value
out	outlet
P	Pumice
r	regeneration
SEM	Scanning Electron Microscope
SHS	Sensible Heat Storage
SIM	Salt In Matrix
SIR	Saving to Investment Ratio

SPP	Simple Payback Period
sur	surroundings
TES	Thermal Energy Storage
THS	Thermochemical Heat Storage
v	volumetric
wv	water vapor

Chapter 1

INTRODUCTION

1.1 Background and Problem Description

Energy demand is increasing continuously as the population grows and prosperity rises around the world. In 2017, fossil fuels (oil, coal, natural gas) were still the main sources of energy in the world with a share of 81 % in the total energy production, whereas, biofuels/waste, renewables, and nuclear power contributed 10 %, 4 %, and 5 %, respectively to the global energy production. Energy consumption has increased by 2.25 times from 1971 to 2017. The share of residential energy demand was 22 % of the total while, industry and transport had a share of 37 % and 29 %, respectively. The heat was the largest energy end-use. Heating accounted for around half of the total energy consumption. Of the produced heat, 46 % was used in the residential sector for space and water heating and cooking [1]. In 2017, the share of renewables in heat production accounted for 10 % and based on its percentage growth of 20 %, it is expected to reach a share of 12.4 % in 2023 [2]. Currently, renewable energy is produced mainly from bioenergy, although the use of solar thermal, renewable electricity and geothermal energy has significantly increased in recent years (see Figure 1). Solar thermal systems have seen a rapid growth recently. These systems are mostly small-sized systems used for domestic hot water production and in some cases for space heating.

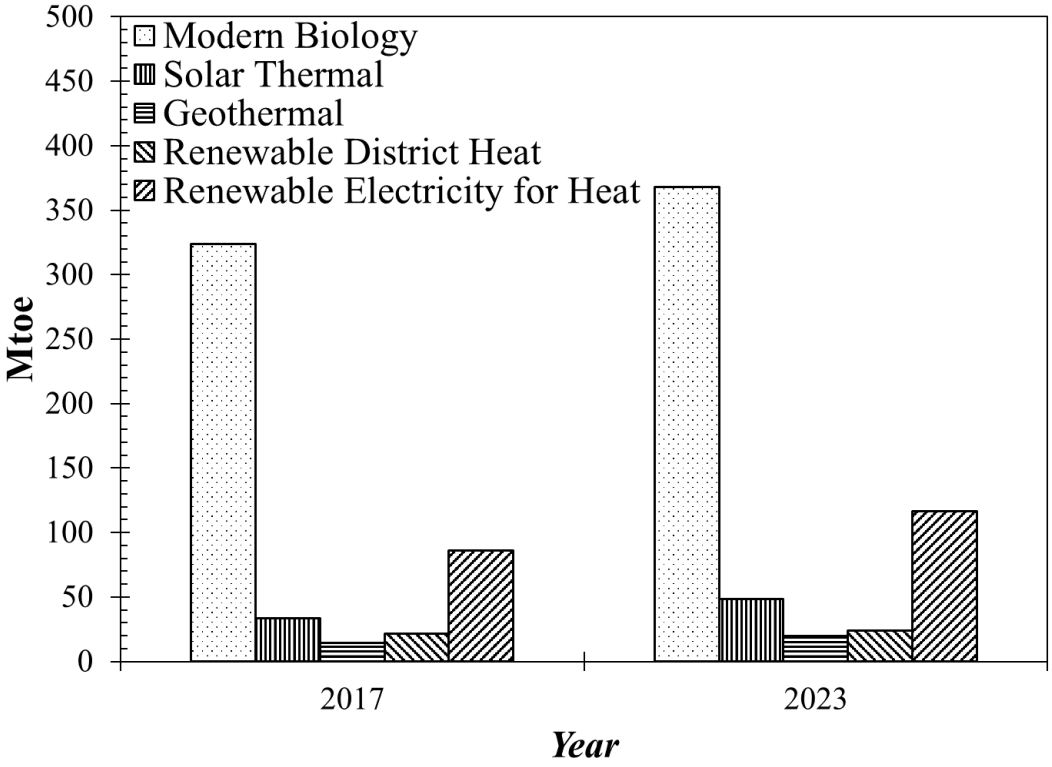

Figure 1: Renewable heat consumption corresponding to different sources, for the years 2017 and 2023(estimated) (adapted from [3])

1.2 Energy Storage Systems

Energy storage (ES) is a vital technique used for storing energy from any intermittent energy sources to meet a wide range of energy demands. Energy storage systems are classified into five categories, namely, thermal, chemical, mechanical, magnetic and biological.

1.2.1 Thermal Energy Storage Systems

Recently, due to pollution, expense and depletion of fossil fuel sourced energy, thermal energy storage (TES) systems and technologies are expected to play a vital role in the supply of clean, inexpensive and sustainable thermal energy [4, 5]. There are three main types of thermal energy storage: sensible heat storage, latent heat storage and thermochemical heat storage.

Thermochemical Heat Storage

Thermochemical heat storage (THS) systems offer higher thermal storage density as compared to conventional sensible heat storage (SHS) systems and latent heat storage (LHS) systems [6, 7]. Unlike the other TES technologies, THS systems are not widely available in markets and are still at the research and development stage. The materials used in THS systems can take the required charging energy from any renewable or non-renewable source and discharge the required thermal energy during the peak times of electricity consumption or at the times needed by the consumer to heat their living space [8]. In the case of solar-assisted THS systems, in summer, due to the availability of solar energy for a longer duration, THS materials can be charged and stored and can be used during periods of scarce availability of solar energy in winter [9]. In addition, THS systems could be utilized for storing of electricity during off-peak times and the electricity generated by photovoltaic panels in the form of thermal energy. This could allow achieving energy supply-demand balance and help in reducing fossil fuel usage in building space heating applications. On the other hand, THS systems provide an opportunity for medium temperature waste heat recovery in industrial applications. Many industrial processes are energy-intensive, once used, much of the heat from these processes, at relatively low but potentially useful temperatures, is exhausted into the atmosphere thus making the processes obviously inefficient and economically wasteful [10]. It is estimated that 48 TWh of heat is being wasted by the UK industry per year [11], while, energy-intensive industries (e.g., the cement industry) account for nearly 50 % of energy consumption in China [12]. Nearly 30 % of large steel furnaces and the majority of the cement manufacturers in China do not capture and reuse waste heat and therefore, the savings potential in this sector is substantial. On the other hand, according to the report of the United States Department of Energy (DOE), selected 25

energy-intensive industries in the US, together produce 439 TWh waste heat per year [13]. In this context, a THS could be designed as a portable device/thermal battery that could enable loss-free storage and transportation of waste heat from industrial plants in a mobilized form. This approach could allow the economic utilization of "waste" heat from larger industrial plants, typically located away from cities and large towns.

In order to successfully utilize THS systems in the above-mentioned solar thermal, photovoltaic and waste heat recovery applications (see: Figure 2), development of composite sorbents with improved properties and an optimized process/reactor design are crucial. Therefore, further advancements are required in these fields.

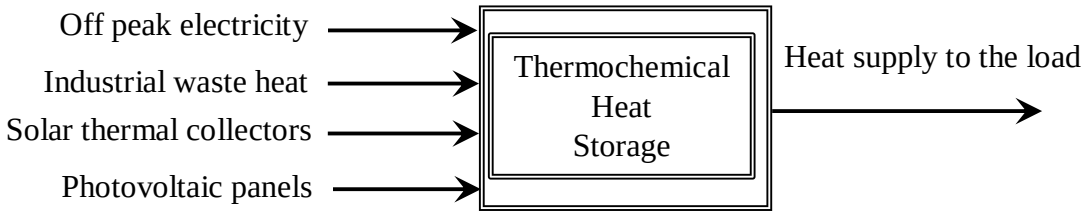

Figure 2: Potential application areas of thermochemical heat storage systems

1.3 Aim of the Thesis

Recently, some attempts have been made to design and develop solar-driven thermochemical heat storage systems. However, considerable improvements are still required, particular, in material development and in the process and reactor design, for improving this technology. The main aim of this research work was to develop a novel thermochemical heat storage system, to be used for solar thermal energy storage. In order to achieve this goal, studies on the development and testing of a solar-driven THS unit have been carried out. Furthermore, novel composite sorbents, namely, vermiculite-$CaCl_2$, aerated porous concrete-$CaCl_2$ and pumice-$CaCl_2$, having

improved structural properties and high surface area, in order to enhance heat and mass transfer between air and salt, have been developed. Zeolite 13X has also been used in the study as reference material for a comparative performance study due to its widely known properties. A laboratory-scale open THS system has been designed and manufactured for carrying out an experimental testing of the sorption materials. Based on the results obtained from the investigation of the charging/discharging cycles, sorption/desorption kinetics, the thermal and cyclic performances of the materials have been comparatively investigated. From these investigations, $CaCl_2$ was selected as the sorption salt due to its low cost, low regeneration temperature, high sorption heat, and high sorption capacity.

The main objectives of this experimental research are listed below:

1. To synthesize novel composite sorbents, namely, pumice-$CaCl_2$, aerated porous concrete-CaCl2, vermiculite-$CaCl_2$.
2. To design and manufacture a lab-scale open THS system.
3. To carry out an experimental investigation on the composite sorbents in the developed THS system.
4. To analyze and compare the performance of the THS system for composite sorbent candidates.
5. To design and fabricate a novel solar-assisted THS reactor consisting of a sorption pipe unit and a compound parabolic concentrator (CPC) unit.
6. To investigate the performance of the novel THS reactor under the climatic conditions of North Cyprus.

1.4 Organization of the Thesis

The aim and motivation of the present study are introduced in Chapter 1. Chapter 2 contains a literature review of the previous studies related to THS materials and reactors. In Chapter 3, synthesizing, testing and performance analysis of the composite materials for THS applications have been described. An experimental investigation of the sorption pipe unit integrated with a CPC unit has been presented in Chapter 4. Furthermore, based on the results obtained, the energetic and economic feasibility analysis, for applying the THS system to a domestic building, has been investigated via simulations by using the DesignBuilder software package. Conclusions from the present work, discussions, and recommendations for future work have been presented in Chapter 5.

Chapter 2

LITERATURE REVIEW

2.1 Overview

The performance of a THS system mainly depends on the working materials and reactor design. This chapter provides a literature review on the types of materials and reactors that have been used in previous studies.

2.1.1 THS Sorption Materials

The working principle of a THS system is based on reversible chemical reactions and the sorption process between two separate substances (sorbent and sorbate), in which a high amount of thermal energy is produced. The THS method has two phases:

1. Desorption (charging) process, which separates the sorbate from the sorbent when the latter is heated.
2. Sorption (discharging) process, which starts when the sorbate comes in contact with the sorbent.

Thus, without a time constraint, the binding energy can be stored as long as the two reactive materials (sorbent and sorbate) are separated. Unlike the sensible heat storage (SHS) and latent heat storage (LHS) methods, heat is not stored in a storage container in THS systems and this advantage enables them to be considered as a promising candidate for long term energy storage applications [14]. Moreover, the storage density of THS materials is nearly 8-10 times higher than SHS materials and almost 2 times more than LHS materials. Figure 3 illustrates the storage density of some THS materials, such as silica gel, zeolite, SHS materials like rock and concrete and the LHS

material such as paraffin wax. However, in the THS method, an efficient reaction between the sorbent and the sorbate is highly dependent on the storage volume, which is not the case in LHS and SHS methods.

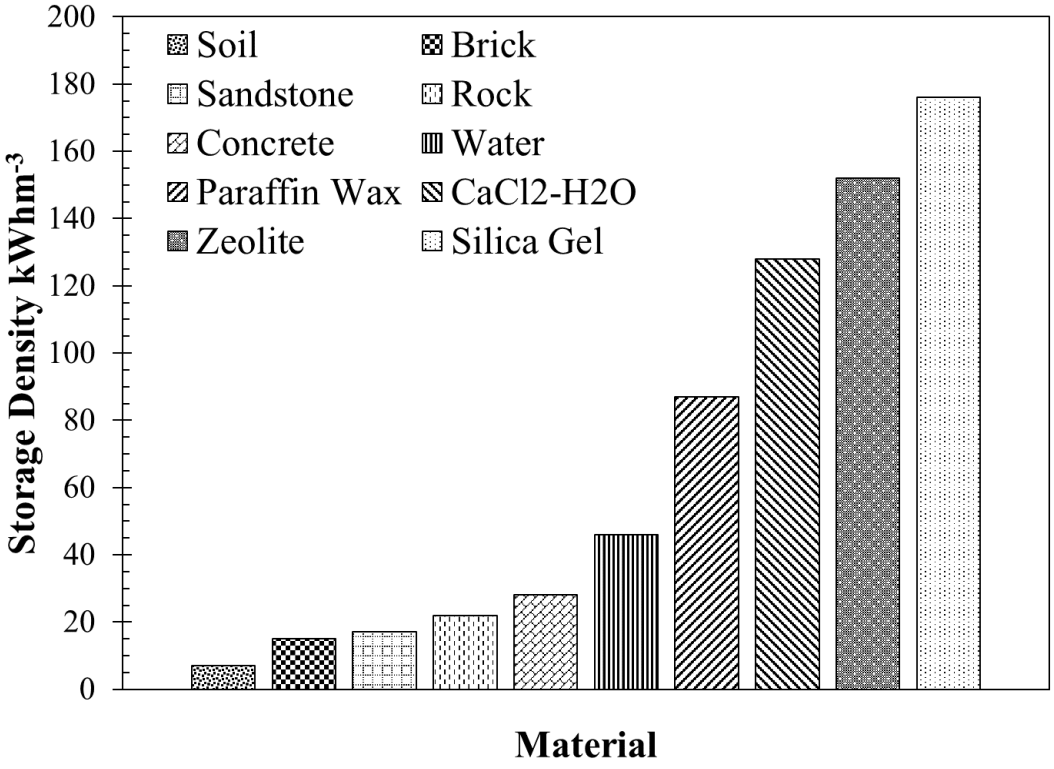

Figure 3: Storage density of some THS, LHS and SHS materials (adapted from [15])

The term adsorption refers to the enrichment of one or more components in an interfacial layer. The material that is adsorbed onto the surface of material(s) is called the adsorbate and the material that adsorbs other materials on its surface is called adsorbent. The process of penetration of adsorbate molecules into the absorbent structure is called absorption. Sorption thermal storage methods are classified into four categories (see Figure 4) [16]:

1. Solid adsorption,
2. Liquid absorption,

3. Chemical reaction,
4. Composite materials

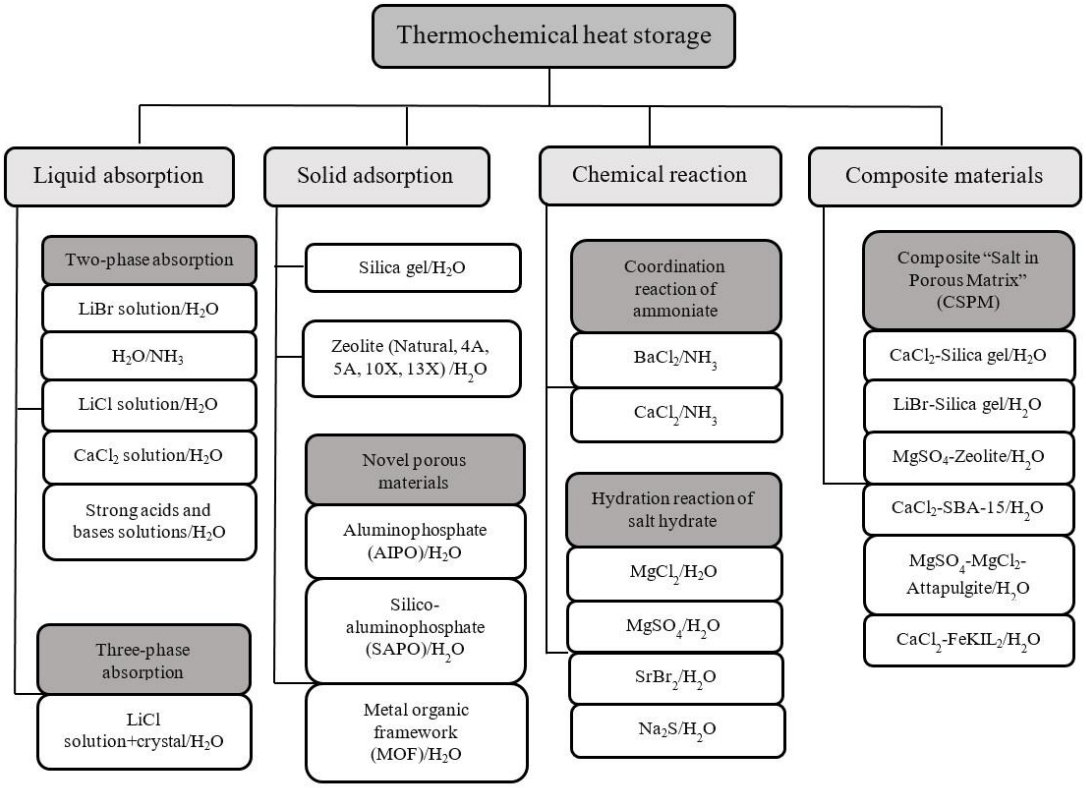

Figure 4: Classification of the different sorption thermal storage methods (adapted from [16])

The sorption process can be named based on the state of the sorbent and sorbate. For example, if the sorbent is a solid and the sorbate is a gas, the process can be called solid-gas adsorption or solid adsorption. A chemical reaction is classified into two groups: hydration reaction of salt hydrate and coordination reaction of ammonia. In both, the reaction involves the attraction of molecules of ammonia and water by metal ions.

Recently, in order to improve the sorption properties of THS materials, a new composite called composite salt in porous matrix (CSPM) has been added to the

sorption thermal storage family. The sorbent of CSPM is composed of two components: a porous host material (vermiculite, pumice, silica gel, zeolite, aerogel, etc.) and an inorganic salt ($CaCl_2$, $MgCl_2$, $MgSO_4$, $LiNO_3$, LiCl, etc.) [17-20] embedded into the host material. For the cases in which water acts as the sorbate material, these composites are called selective water sorbents (SWS). In fact, the sorption process in SWS has two steps: liquid absorption and chemical reaction between inorganic salt and water, and due to this reason the sorption process in SWSs is regarded as a combination process [21-26]. The porous host matrix serves two main functions in the sorption process of CSPMs: it holds the adsorbent and avoids its dispersion. Moreover, some of the host matrices provide an enhanced contact surface area and, consequently, increase the rate of heat and mass transfer and performance of the reaction (see Figure 5).

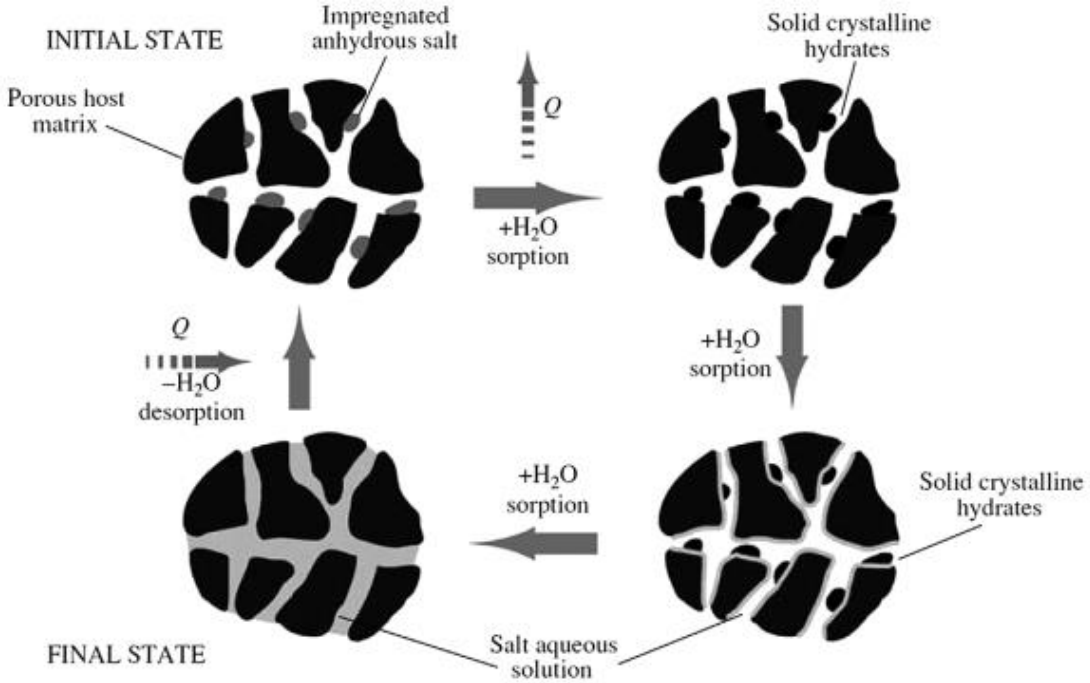

Figure 5: Sorption process in SWS composites [27].

Recently, several studies have been performed on the development and characterization of sorption materials. A typical sorption material for THS systems exhibits the following characteristics [14, 15, 28]: i) higher energy storage density (kWh/m^3 or Wh/kg), ii) higher mass ratio of sorbate uptake to the sorbent (g of sorbate/ g of sorbent), iii) high heat and mass transfer rates, iv) being non-toxic and low cost per unit of energy production, v) low charging temperature and vi) structural stability.

Various parameters such as the material type, airflow rate, size and features of the reactor, etc., affect the performance of the THS system. Selecting appropriate material has a crucial influence on the performance of the whole THS system. Zeolite/H_2O and silica gel/H_2O are well-known examples of solid adsorption materials, that have been widely investigated previously. Despite silica gel/H_2O and zeolite/H_2O having good adsorption characteristics, they suffer from high regeneration temperature, which is an obstacle for their usage in solar driven THS systems. Furthermore, hygroscopic inorganic salts such as $MgSO_4$, $MgCl_2$, LiNO3 and $SrBr_2$ have also been investigated as potential liquid absorption materials. Although these salts provide high energy density, their major drawback is the saturation of the liquid salt at certain relative humidity (RH) level (deliquescence). The composite absorbents are mainly synthesized from hydrated salt(s) and a porous host material (host matrix). Using the host matrix eliminates the problem of deliquescence of salt in the discharging phase, however, their structural instability and deformation and also salt leakage are major concerns of these composite materials [7].

In recent years, various sorption materials have been tested and examined for THS applications. Liu et al. [29] designed an open THS system and impregnated $CaCl_2$ as the sorbent to their novel mesoporous ceramic honeycomb filter used as the host

matrix. The result achieved by the authors showed that the composite sorbent has a high volumetric heat storage density of 616 MJm^{-3} for (Wakkanai siliceous shale) (WSS) + 13.0 wt% $CaCl_2$ and 1181 MJm^{-3} for WSS + 22.4 wt% $CaCl_2$. The researchers suggested that the developed material could be regenerated at low temperatures (around 90ºC).

In another study, Gaeini et al. [30] used different characterization methods to stabilize various salt hydrate samples using $CaCl_2$ as the salt impregnated into graphite/vermiculite and ethyl cellulose as host matrix. The effect of the different stabilization methods on the performance of the materials, such as, kinetics and energy density were investigated. The volumetric energy density of the twice-impregnated vermiculite was found to be the highest (about 1.2 GJ/m^3) among the three composite materials. Composite sorbent of vermiculite and $CaCl_2$ was employed by Aydin et al. [31] in their open-sorption pipe reactor. Their proposed system offered a volumetric energy density of 290 $kWhm^{-3}$ for four-cycle testing of the system. The energetic and exergetic efficiency of their system was in the range of 0.64 – 0.69 and 0.14 – 0.21, respectively.

Michel et al. [32] used $SrBr_2$/ H_2O as the reactive pair in an open type reactor and observed that the variation of mass transfer within the reactive porous bed depended on the reactive bed density and the duration of the reaction. Zhang et al. [33] performed an experimental investigation on a 1 kWh open type THS system. Activated alumina/LiCl was used as the composite sorbent. The authors stated that the energy storage density and output power were directly proportional to the variation of the relative humidity, but inversely proportional to the variation of the airflow rate. For a

discharging period of 7.1 h, the total energy storage of the system was found to be 191 $kWhm^{-3}$.

In an experimental study, D'Ans et al. [34] analysed the effect of sorbate (water) concentration on heat and mass transfer effectiveness of the sorbent material of $CaCl_2$ 40 – 43 wt% encapsulated in silica. The variation of thermal conductivity was between 0.129 and 0.155 W/(m.K) and the water mass diffusivity coefficient changed from 3×10^{-10} to 2×10^{-8} m^2/ s. In another research work, Tatsidjodoung et al. [35] used zeolite 13X and water in an open type THS system. For 40 kg of zeolite, an average outlet temperature of 38 ºC was recorded for eight working hours. The absolute humidity and airflow rate were respectively 10g/kg of dry air and 180 m^3/h. In an experimental study, Janchen et al. [36] used Linde-type 4A-zeolite beads and honeycomb structures in an open-sorption system. Their results showed that the binderless honeycomb zeolite offered higher adsorption kinetics performance among the other candidates. In a recent study, Shere et al. [37] characterized zeolite 13X impregnated with $MgSO_4$ and $MgCl_2$. According to their experimental results, 400 kJ/kg energy density for a temperature range of 30 – 150 ºC and 35% rise in thermal conductivity was achieved by 1% addition of multiwall carbon nanotubes to the composite.

In another study, Alebeek et al. [38] investigated the experimental performance of an open type THS system based on zeolite 13X and water. For an airflow rate of 50 g/s, their developed system with four working segments, offered a maximum power of 4.4 kW, which was 30% percent less than the theoretically expected power (1.55 kW per each segment). The average energy storage density of each segment was 13 kWh, which was slightly higher compared to the theoretical value of 12.5 kWh per segment. In a comparative research work, Xu et al. [39] the studied hydration behaviour of

different zeolite–$MgSO_4$ composites. From which a saturation time of hydration was found to be the same (14 h) for all composite types as well as zeolite 13X, however the amount of water adsorbed by the $MgSO_4$-zeolite composite to reach the saturation state was approximately 40 % higher than pure zeolite 13X. The hydration ability of composites increased significantly at higher relative humidity and air temperature (just below 50ºC). Mehrabadi and Farid [40] investigated the energy density and charging performance of five different salts; $Al_2(SO_4)_3.18H_2O$, $MgSO_4.7H_2O$, $CaCl_2.6H2O$, $MgCl_2.6H_2O$, and $SrCl_2.6H_2O$. The energy storage performance of two host porous matrices, pumice and expanded clay, was tested by using the most suitable salt, $SrCl_2.6H_2O$, reported in their investigation. They found that, expanded clay-$SrCl_2.6H_2O$ and pumice-$SrCl_2.6H_2O$ could store up to 29 kWh/m^3 and 7.3 kWh/m^3 energy, respectively. On the other hand, pumice-$SrCl_2.6H_2O$ showed almost constant thermal cycling performance over repetitive cycles. In another study, Kuznik et al. [41] numerically analysed the characteristics of an open THS system using zeolite 13X as the adsorbent and water as adsorbate. The acquired results suggested that 50% of the total input heat was lost during the charging phase and 30% of stored energy was transferred to the fluid during the discharging phase. From their investigation, overall efficiency of the system was estimated to be 36%.

2.1.2 THS Reactors

Besides the material based studies on THS systems, several studies have been done on the development of THS reactors and designing THS processes. Based on the type of reactor, THS systems can be divided into open and closed types [42, 43]. An open type THS system operates under ambient environmental conditions and the air is mostly used as the process fluid and thus, only water can be used as the sorbate material. In the charging phase, a stream of hot and dry air goes into the reactor, absorbs water

from the sorbent material and exits the reactor bed. Solar energy or off-peak electricity can be used for the production of hot air in the charging phase. During the discharging phase, cool and humid air passes through the reactor bed and some of the water vapor in the air is absorbed by the dry sorbent material. Due to the heat produced by the sorption process, the air exiting from the outlet of the reactor becomes hot and dry. The working principle of an open THS system is shown in Figure 6.

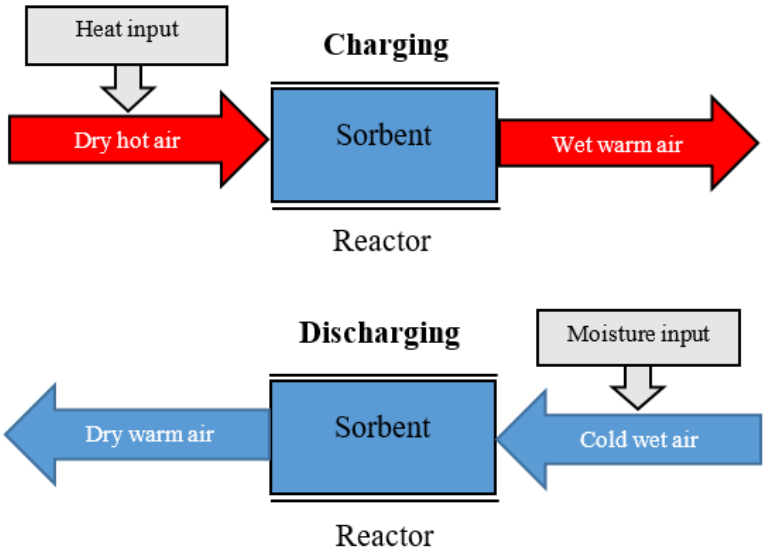

Figure 6: Working principle of an open THS system (adapted from [16])

On the other hand, a closed THS system operates at pressures below the atmospheric pressure and water is used as the process fluid. The working principle of a closed sorption system is presented Figure 7. A Closed sorption system contains two main components: a reactor and a condenser/evaporator. During the charging process, high-temperature heat is transferred from a solar collector into the reactor and separates the sorbate from the sorbent. By passing through the condenser, the vapor changes into its liquid state and the heat of condensation is released into a heat sink. The discharging can be done in the reverse direction.

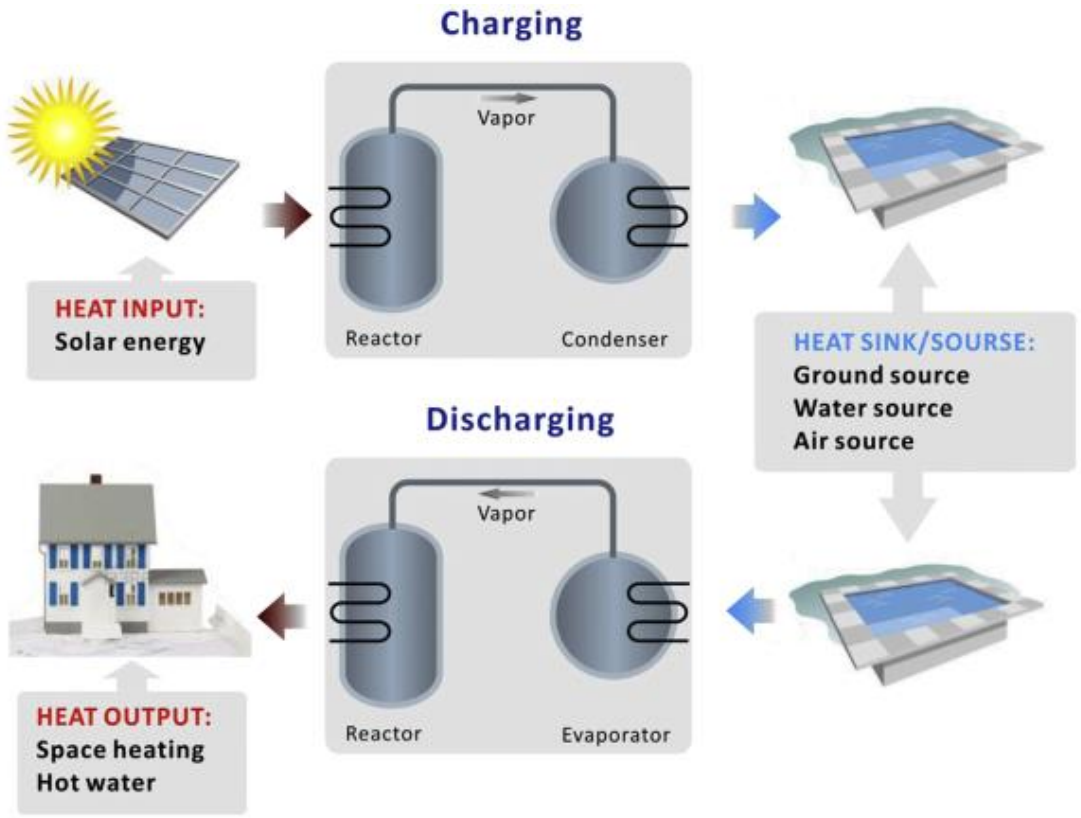

Figure 7: Working principle of a closed THS system [16]

An open THS releases heat directly to the space to be heated and due to its simple design and operational practicality, it is considered as a promising method for thermal energy storage [44]. Mette et al. [45] developed a solar-assisted open THS system within the chemical heat storage project and investigated the characterizations of the system for different reactors and various types of materials. Among the tested materials, a composite of salt impregnated zeolite showed a higher energy storage density and better mechanical stability. In another experimental study, Aydin et al. [46] developed a solar assisted hybrid thermal system consisting of a heat pump and a modular sorption reactor. Four salt-based composites and zeolite 13X were tested in the reactor from which a maximum energy storage capacity of 6 kWh was achieved. In addition, the sorbent SIM-3cl provided the highest energy storage densities of 0.84 kW/g and 1.98 kW/g for high and low humidity levels respectively. A closed THS

system consisting of a valve-less adsorber and a separate reservoir has been developed by Xu et al., [47]. A composite of zeolite 13X/ $MgSO_4$/ ENG-TSA (expanded natural graphite treated with sulphuric acid) was used in this experimental measurement. The energy density of the system was calculated to be 120.3 kWm^{-3} at a charging temperature of 250 ºC. Al-Zareer et al., [48] proposed a thermal energy system consisting of a solid-gas charging reactor, a solid-gas discharging reactor, condenser and evaporator with $SrCl_2$-$8NH_3$ as the reactive pair. The maximum energy and exergy efficiencies obtained in heating applications using their system were 65.4% and 50.8 % at T = 87 ºC. For cooling applications at T = 0 ºC and T = -35 ºC, energy and exergy efficiencies were found to be 29.3% and 22.9% respectively.

The reactive pair of $MgCl_2$/water was used in a laboratory scale closed THS system developed by Zondag et al. [49]. The developed system provided an energy density of 0.5 GJ/m^{-3} over 40 h of operation. Another open THS system developed by Zettl et al. [50] which consisted of a rotating drum as the reactor and zeolite 4A/water and zeolite MSX/water as working pairs. For 10.5 h of testing, the thermal energy produced with zeolite 4A and zeolite MSX were 10.5 kWh and 11.9 kWh respectively. Accordingly, the energy storage densities of the system were determined to be 148 $kWhm^{-3}$ for zeolite-4A, and 154 $kWhm^{-3}$ for MSX composite. Johannes et al. [51] designed a modular open THS system made up of two reactors and using zeolite/water as the reactive pair. The thermal power generation rate of 2250 W for 6 h of discharging operation was achieved using their system. Kronauer et al. [52] investigated the characteristics of an open type, mobile THS system based on zeolite/water. The project was developed by ZAE Bayern for industrial waste heat utilization and tested for more than one year. The pilot plant consisted of two storage tanks. The charging heat was

provided from the extraction steam of a turbine belonging to a waste incineration plant. During the discharging process, the produced heat was utilized as a fuel saver of the gas burner.

The thermal energy storage capacity of the system was measured to be 2.3 MWh. Wyttenbach et al. [53] designed and manufactured a THS reactor with a circular shape and a vibrating bed. The continuous movement of the solid hydrate enhanced the rate of heat and mass transfer inside the reactor. A composite of $CaCl_2$-silica gel was used in the performance testing of the novel reactor and the test results revealed an average heating power of 356 W with an average temperature rise of +6 K, while a cooling power of 278 W with an average temperature decrease of 4.5 K was recorded in the desorption phase. The energy density of the system for a reactor volume of 0.163 m^3 was 200.4 Wh/kg of 9% $CaCl_2$-silica gel composite. Michel et al. [32] designed and manufactured an experimental bench to analyse the mass transfer and sorption/ desorption kinetics of an open THS system. The reactor consisted of two perforated plates in which a hydrated salt bed was bounded between them. The storage density of the system was found to be in the range of 300 – 600 kWh/m^3. Even though a large variety of hygroscopic salts (i.e., LiCl, $LiNO_3$, $MgCl_2$, $CaCl_2$ etc.) and natural sorbents (i.e., zeolite, silica gel) have been widely investigated for their use in THS systems, only a limited number of porous host matrices (activated alumina, Wakkanai siliceous shale, vermiculite, pumice and activated carbon) have been investigated previously for salt impregnation. Therefore, it can be evidenced by the literature that there is a gap in this area, and new porous materials suitable for salt impregnation need to be sought. Vermiculite-$CaCl_2$ composite has been previously investigated by Aydin et al. and Casey et al. [9, 31, 46] and the ‘salt-in-matrix’ concept has been observed to show a

good potential to be used in open THS systems. The main problem found with the use of vermiculite as the host matrix was its physical degradation due to moisture absorption in repeating cycles. Porous matrices that are physically more stable, easy to manufacture, have low cost, and offer a high surface area to mass ratio need to be sought for achieving THS systems with steady performance in a long term operation. Accordingly, in this research, a new composite consisting of $CaCl_2$ as the sorbent and aerated porous concrete as the host matrix has been developed and experimentally investigated. The developed composite is novel and there are no previous studies that have investigated its performance in the THS systems. In addition, this research provides a comparative study between the performance of zeolite, vermiculite-$CaCl_2$, pumice-$CaCl_2$ and APC-$CaCl_2$ under similar operating conditions. In previous studies, the charging/discharging behaviours of different sorbents have been mainly investigated on a small scale by using characterization techniques. However, no study has been found in the literature that, provides a comparative investigation of the sorption/desorption characteristics of different sorbents at the experimental prototype scale by considering both mass (water vapour), energy and exergy exchanges in repeating cycles. Consequently, the performance parameters (mass adsorption / desorption capacities, charging/discharging temperature, heat storage density and energy/exergy efficiency) of the investigated materials obtained in this work are promising compared to those described in the literature and could considerably contribute to a further development of the THS systems.

Furthermore, a simple configuration and practical operational aspects of the laboratory scale reactor prototype, developed in this work, could be of interest to researchers working in the field of design and development of THS systems. Such THS units could

be integrated with photovoltaic panels or solar air heaters for the regeneration of the sorbent with sustainable energy sources. This could lead to a substantial reduction in fossil fuel consumption in building heating applications. In addition, THS units could also be used for industrial heat recovery applications for enhancing energy efficiency in industrial plants. The developed and tested new innovative sorption materials could be a step forward for such applications, due to their high energy storage density and reasonable (80 – 90 ºC) regeneration temperature, and for their integration with solar systems or industrial waste heat sources. Table 1 represents the summary of related studies in the literature.

Table 1: Summary of the related studies

Author	Year	Working material	THS type	Working condition	Energy storage density
Liu et al.[29]	2013	Wakkanai Siliceous Shale + 13.0 wt% $CaCl_2$ Wakkanai Siliceous Shale + 22.4wt% $CaCl_2$	open	$T_{cr\text{-}in}$=80–100 ºC	616MJm^{-3} 1181MJm^{-3}
Zondag et al.[49]	2013	$MgCl_2 + H_2O$	closed	$T_{cr\text{-}in}$=130 ºC	0.5 GJ/m^{-3}
Zettl et al.[50]	2014	Zeolite MSX + H_2O Zeolite 4A + H_2O	open	$T_{dcr\text{-}in}$ = 20 ºC	154 kWhm^{-3} 148 kWhm^{-3}
Johannes [51] et al.	2015	Zeolite Na-X+ H_2O	open	$T_{cr\text{-}in}$=120&100 ºC $T_{dcr\text{-}in}$ = 20 ºC	27.5 Wkg^{-1}
Tatsidjodoung et al. [35]	2015	Zeolite 13X + H_2O	open	$\dot{m}_{a\text{-}in}$=180m^3/h $T_{dcr\text{-}in}$ = 20 ºC w_{in}=10g/kg	–
Kronauer et al. [52]	2015	Zeolite 13X + H_2O	open	$T_{cr\text{-}in}$=130 ºC	0.164 MWh/tone
Michel et al. [32]	2016	$SrBr_2 + H_2O$	open	$T_{cr\text{-}in}$ ~ 80 ºC $T_{dcr\text{-}in}$ ~ 25 ºC	300-600 kWhm^{-3}
Aydin et al. [31]	2016	Vermiculite-$CaCl_2$ + H_2O	open	Δw <81(g/kg) 8<Δw <12 12<Δw	290kWhm^{-3}
Zhang et al. [33]	2017	Activated alumina/ LiCl + H_2O	open	$RH_{dcr\text{-}in}$=80% $T_{dcr\text{-}in}$ = 20 ºC	191kWhm^{-3}
Shere et al [37].	2018	$MgSO_4$+7H_2O+Zeolite 13X $MgCl_2$+6H_2O+Zeolite 13X	–	$RH_{dcr\text{-}in}$=95%	400 kJ/kg
Alebeek et al [38].	2018	Zeolite 13X + H_2O	open	$T_{cr\text{-}in}$ = 180 ºC $RH_{dcr\text{-}in}$=85% $\dot{m}_{a\text{-}in\text{-}dcr}$=35g/s $\dot{m}_{a\text{-}in\text{-}cr}$=50g/s	208kWhm^{-3}
Xu et al. [39]	2018	Zeolite 13X+$MgSO_4$+H_2O	open	$RH_{dcr\text{-}in}$ =85%, 75%, 65%, 55%	–

		Zeolite 4A+$MgSO_4$+H_2O Zeolite 3A+$MgSO_4$+H_2O Pure Zeolite		T_{dcr-in} = 25, 35,45,55 ºC	
Mehrabadi and Farid [40]	2018	$Al_2(SO_4)_3$+18H_2O $MgSO_4$+7H_2O $CaCl_2$+6H2O $MgCl_2$+6H2O $SrCl_2$+6H_2O Pumice - expanded clay	open	T_{cr-in}= 90-130ºC	29 kWh/m^3 for expanded clay-$SrCl_2$+6H_2O 7.3 kWh/m^3 for Pumice-$SrCl_2$+6H_2O
Aydin et al. [7]	2018	Zeolite 13X Vermiculite+43 wt% $CaCl_2$ (SIM-3a) Vermiculite+35 wt% $MgCl_2$ (SIM-3m) Vermiculite+22 wt% $CaCl_2$+17% wt LiCl (SIM-3cl) Vermiculite+18 wt% $MgCl_2$+17% wt LiCl (SIM-3ml)	closed	RH_{dcr-in} =60% & T_{dcr-in} =17 ºC (Low humidity condition) RH_{dcr-in} =80% & T_{dcr-in} =17 °C (high humidity condition)	**low humidity (**Wh/g) Zeolite 13X→1.1 SIM-3a→1.2 SIM-3m→1.3 SIM-3cl→1.98 SIM-3ml→1.47 **high humidity** (Wh/g) Zeolite 13X→0.6 SIM-3a→0.7 SIM-3m→0.7 SIM-3cl→0.84 SIM-3ml→0.73
Xu et al [47]	2018	Zeolite 13X/ $MgSO_4$/ ENG-TSA	closed	T_{cr-in} =250 ºC	120.3 $kWhm^{-3}$
Al-Zareer et al. [48]	2018	$SrCl_2$ - 8NH_3	–	$T_{heating}$= 85 ºC $T_{cooling}$= 0 ºC	2010 kJ/kg (heating) 902 kJ/kg (cooling)
Wyttenbach et al. [53]	2018	$CaCl_2$-Silica gel + H_2O	open	T_{cr-in} = 90 ºC	200.4Wh/ kg

Chapter 3

SYNTHESIS AND EXPERIMENTAL INVESTIGATION OF NOVEL COMPOSITE SORBENTS FOR THERMOCHEMICAL HEAT STORAGE

3.1 Design and Thermal Analysis of the THS System

Careful designing of a THS system is crucial for obtaining high heat storage efficiency. Otherwise, insufficient heat-mass transfer and non-uniform air flow could result in a drastic drop in the system's performance. Thus, efficient designing of the system becomes an extremely vital requirement for the working conditions of a reactor. An optimal THS design should provide a steady discharge temperature output, uniform moisture sorption rate, an efficient heat transfer and minimal heat losses.

3.1.1 Experimental Prototype

A schematic of the designed THS system and a photograph of the actual setup are shown in Figure 8 (a) and 8 (b), respectively. The prototype of the THS system consists of two main components, an air conditioning unit and a THS reactor. The air conditioning unit comprises a fan, electric heaters (only used during charging) and an ultrasonic humidifier (only used during discharging). The reactor is a rectangular shaped box (52 cm × 40 cm × 60 cm) with a trapezoidal outlet. It is insulated with 40 mm thick glass wool and an internally placed tray (45 cm × 45 cm × 7 cm) is used for holding the composite material perpendicular to the air-flow. The air flow rate of the prototype can be adjusted with accuracy of ±1 % m^3/s using a radial fan. An air

conditioner is used for controlling the temperature of the experimental space. The charging temperature is supplied using four electrical heaters (two 0.5 kW and two 1 kW) and is adjusted by a temperature control unit. A household humidifier has been used to increase the relative humidity of the supplied air. The system components and the sensor locations for measuring ambient, inlet and outlet temperature and humidity in the charging/discharging cycles are indicated in Figure 8. The sensors that have been used to record the inlet, outlet, and ambient temperature and humidity are Sensirion SHTC3 type with a typical accuracy of ±2 % RH and ±0.2 ºC.

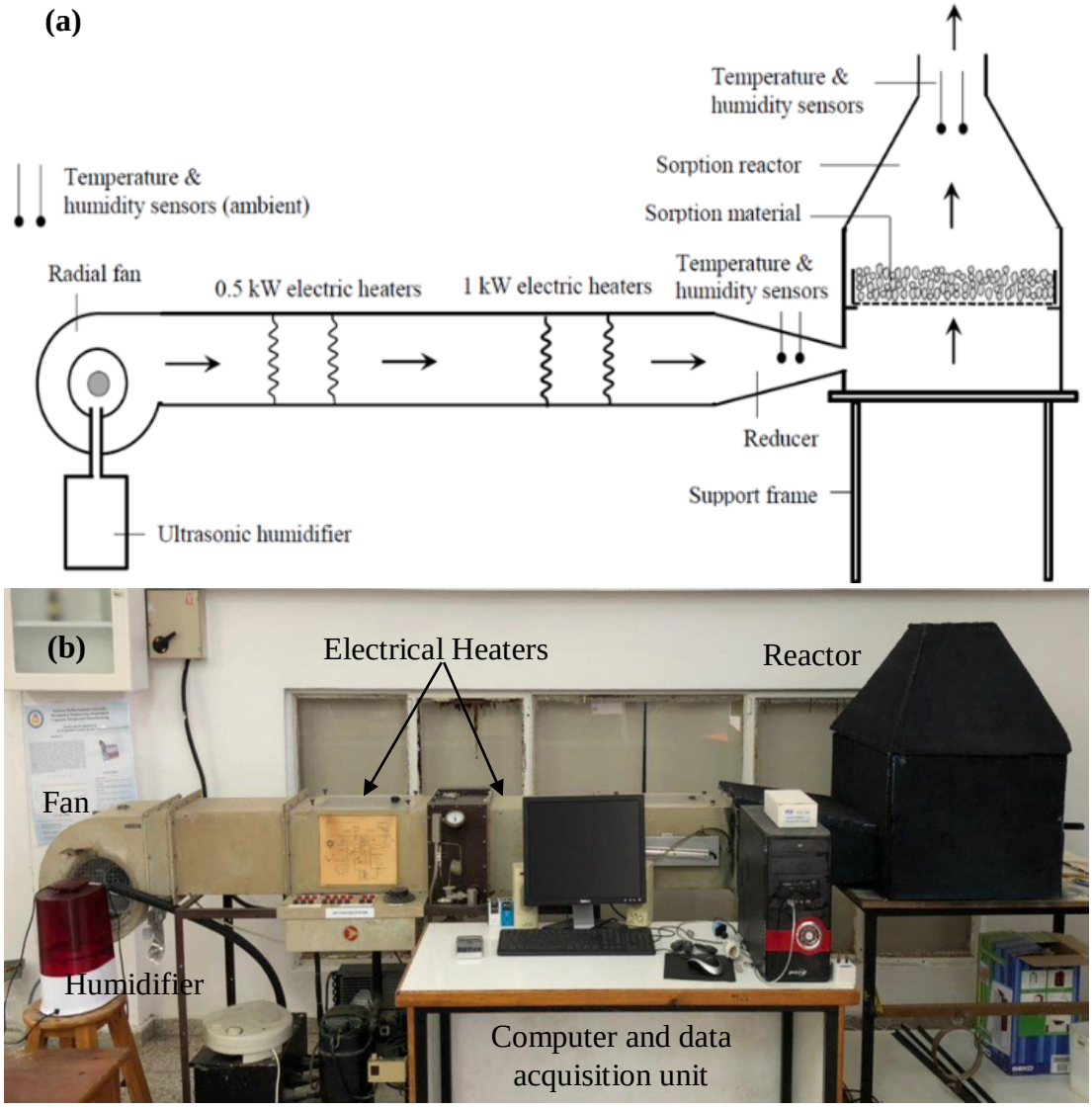

Figure 8: (a) Schematic of the designed open sorption thermal storage prototype. (b) Photograph of the developed experimental unit

3.1.2 Experimental Study and Thermodynamic Analysis

The THS system operation can be explained in a cyclic order. In the system developed in the present work, during the discharging process, the ambient air is moisturized up to an RH of about 85 – 90% and blown through the channel to the sorption reactor. The air temperature at the reactor inlet is 20 – 21ºC. The humid air then passes across the sorption bed, where moisture is absorbed and heat is generated. Finally, hot air with low moisture content leaves the system. In the charging mode, air is heated up to 85 – 95 ºC and hot dry air passes across the sorption bed. As a result, the moisture inside the sorbent is removed and wet moist air is exhausted.

The performance of the developed THS system for three different sorbent materials has been examined according with the first law and second law of thermodynamics. The parameters measured by the fitted sensors can be used for calculating several thermodynamic factors such as energy output (E), exergy (X), first law efficiency (η_I), second law efficiency (η_{II}), sorption and desorption rate (y) and, uptake ratio and mass loss ratio (f).

Instantaneous heat output ($\dot{Q}_{out}$) during the sorption phase is calculated based on the enthalpy changes as given in Equation (1a) and (1b) below [54]:

$$\dot{Q}_{out} = \dot{H}_{out} - \dot{H}_{in} \quad (1a)$$

$$\dot{Q}_{out} = \dot{m}_{dcr} C_p (T_{out} - T_{in}) \quad (1b)$$

where, $\dot{H}_{in}$ and $\dot{H}_{out}$ are the rate of change of enthalpies at the reactor inlet and outlet, $\dot{m}_{dcr}$ is the mass flow rate during the discharging stage, C_p is the specific heat and T_{in} and T_{out} are the temperatures at the inlet and outlet of the reactor, respectively.

Both the charging ($\dot{E}_{out,cum}$) and discharging cumulative energy ($\dot{E}_{in,cum}$) output rates, as indicated by Equations (2) and (3), are calculated by taking a time integral of Equation (1b);

$$\dot{E}_{out,cum} = \dot{m}_{dcr} C_p \int_0^{t_{dcr}} (T_{out} - T_{in}) dt \quad (2)$$

$$\dot{E}_{in,cum} = \dot{m}_{cr} C_p \int_0^{t_{cr}} (T_{in} - T_{out}) dt \quad (3)$$

Where, $\dot{m}_{cr}$ is the mass flow rate during the charging stage and t_{cr} and t_{dcr} are the charging and discharging durations, respectively.

The instantaneous exergy output rate for the discharging phase ($\dot{X}_{out,dcr}$) is determined on the basis of exergetic variation of air at the outlet and inlet of the reactor [54]:

$$\dot{X}_{out,dcr} = (\dot{X}_{out} - \dot{X}_{in}) \quad (4a)$$

The exergy output rate can also be expressed in terms of the air enthalpy (*h*) and the entropy (*s*) differences across the reactor as,

$$\dot{X}_{out,dcr} = \dot{m}_{dcr} [(h_{out} - h_{in}) - T_a (s_{out} - s_{in})] \quad (4b)$$

Where, T_a is the air temperature, h_{in}, h_{out} are the enthalpy of air while s_{in}, s_{out} are the entropy values at the inlet and outlet of the reactor, respectively.

Using Equation (1b) in Equation (4b) and from the definition of the change in entropy of a system at constant pressure, the exergy output rate can also be further written as:

$$\dot{X}_{out,dcr} = \dot{m}_{dcr} C_p \left[(T_{out} - T_{in}) - T_a ln(\frac{T_{out}}{T_{in}}) \right] \quad (4c)$$

In the same manner, the instantaneous input exergy rate is calculated using,

$$\dot{X}_{in,cr} = \dot{m}_{cr} C_p \left[(T_{in} - T_{out}) - T_a ln(\frac{T_{in}}{T_{out}}) \right] \quad (5)$$

The cumulative exergy output ($\dot{X}_{out,dcr,cum}$) and cumulative exergy input ($\dot{X}_{in,cr,cum}$) rates, are determined by taking a time integral of $\dot{X}_{out,dcr}$ (Equation (4c)) and $\dot{X}_{in,cr}$ (Equation (5)):

$$\dot{X}_{out,dcr,cum} = \dot{m}_{dcr} C_p \int_o^{t_{dcr}} \left[(T_{out} - T_{in}) - T_a ln(\frac{T_{out}}{T_{in}}) \right] dt \quad (6)$$

$$\dot{X}_{in,cr,cum} = \dot{m}_{cr} C_p \int_o^{t_{cr}} \left[(T_{in} - T_{out}) - T_a ln(\frac{T_{in}}{T_{out}}) \right] dt \quad (7)$$

The first law efficiency (energetic efficiency) and the second law efficiency (exergetic efficiency) of the THS are defined as,

$$\eta_I = \frac{\dot{E}_{out,cum}}{\dot{E}_{in,cum}} \quad (8)$$

$$\eta_{II} = \frac{\dot{X}_{out,cum}}{\dot{X}_{in,cum}} \quad (9)$$

The absolute humidity of air (w) is calculated using [55],

$$w = 216.7 \left[\frac{\frac{\phi}{100\%} 6.112 \exp(\frac{17.62T}{243.12+T})}{273.15+T} \right] \quad (10)$$

The water vapour pressure (P_w) is calculated based on the relative humidity of air (ϕ) and the water vapour saturation pressure ($P_{w,\,sat}$).

$$P_w = \frac{\phi P_{w,sat}}{100\%} \quad (11)$$

The rate of moisture adsorption in the discharging phase (y_{ads}) and the rate of moisture desorption in the charging phase (y_{des}) at any instant of the process is calculated as follows [31]:

$$y_{ads} = \int_{t_{x,dcr}}^{t_{x+1,dcr}} [60 \dot{m}_{dcr} (w_{in} - w_{out}) dt] \quad (12)$$

$$y_{des} = \int_{t_{x,cr}}^{t_{x+1,cr}} [60 \dot{m}_{cr} (w_{out} - w_{in}) dt] \quad (13)$$

where w_{in} is the amount of moisture adsorbed by the sorbent and w_{out} is the amount of moisture desorbed from the sorbent surface.

The mass of the sorbate adsorbed in the discharging phase(Δm) is calculated using the mass change of the sorbent (see Equation (14)). A similar logic is applicable for calculating the weight of the sorbate desorbed during charging phase;

$$\Delta m = m_w = m_{ads,wet} - m_{ads,dry} \tag{14}$$

Referring to Equations (12) and (13), the mass uptake (Δm_{dcr}) and mass loss (Δm_{cr}) of the sorbent are calculated [31],

$$\Delta m_{dcr} = \int_0^{t_{dcr}} \dot{m}_{dcr}\,(w_{in} - w_{out})dt \tag{15}$$

$$\Delta m_{cr} = \int_0^{t_{cr}} \dot{m}_{cr}\,(w_{out} - w_{in})dt \tag{16}$$

The ratio of the total adsorbed sorbate to the weight of the dry adsorbent defines the total mass uptake ratio (f_{dcr}) (Equation (17)) in the discharging phase. Similarly, the ratio of the total desorbed sorbate to the weight of the wet adsorbent determines the total mass loss ratio (f_{cr}) (Equation (18)) [31]:

$$f_{dcr} = \frac{\left[\int_0^{t_{dcr}} \dot{m}_{dcr}(w_{in} - w_{out})dt\right]}{m_{ads,dry}} \tag{17}$$

$$f_{cr} = \frac{\left[\int_0^{t_{cr}} \dot{m}_{cr}(w_{out} - w_{in})dt\right]}{m_{des,wet}} \tag{18}$$

Energy density (E_d) is a factor used to measure the storage performance of the selected sorption material. It could be defined in two different ways: i) ratio of the cumulative output energy of sorbent to the absorbed mass of sorbate (Equation (19)) and ii) ratio of the cumulative energy produced per volume of sorbent material used (Equation (20)) [31];

$$E_d = \frac{E_{out,cum}}{\Delta m_{dcr}} \tag{19}$$

$$E_d = \frac{E_{out,cum}}{\mathrm{V}_{ads}} \tag{20}$$

3.1.3 Uncertainty Analysis

The accuracy of the experimental results of this work has been determined using the uncertainty analysis, in which, the experimental uncertainties were determined based on the error propagation formula. The resulting w_R is obtained as a function of several independent variables. In the analysis, w_1, w_2, w_3, …, w_n represent the uncertainties in the different independent variables.

In the developed experimental rig, three sensor locations were used in order to determine the temperature and relative humidity of air at the inlet and outlet of the reactor as well as that of the ambient air. Air mass flow rate (m_a) was also measured and recorded during the charging and discharging cycles. Thus, the uncertainty, w_R, is defined as [56, 57]:

$$w_R = \left[\left(\frac{\partial R}{\partial x_1} w_1\right)^2 + \left(\frac{\partial R}{\partial x_2} w_2\right)^2 + \left(\frac{\partial R}{\partial x_3} w_3\right)^2 + \cdots + \left(\frac{\partial R}{\partial x_4} w_4\right)^2\right]^{1/2} \quad (21)$$

From Equations (1) to (3) it can be seen that the heat storage efficiency (η_I) is a function of T and m_a obtained in charging-discharging cycles, each subject to uncertainty:

$$\eta_I = f\left(T_{in,cr}, T_{out,cr}, T_{in,dcr}, T_{out,dcr}, m_{cr}, m_{dcr}\right) \quad (22)$$

Thus, the total uncertainty in the overall system efficiency can be expressed as;

$$w_R = \left[\left(\frac{\partial \eta_I}{\partial T_{in,cr}} w_{T_{in,cr}}\right)^2 + \left(\frac{\partial \eta_I}{\partial T_{out,cr}} w_{T_{out,cr}}\right)^2 + \left(\frac{\partial \eta_I}{\partial T_{in,dcr}} w_{T_{in,dcr}}\right)^2 + \right.$$

$$\left.\left(\frac{\partial \eta_I}{\partial T_{out,dcr}} w_{T_{out,dcr}}\right)^2 + \left(\frac{\partial \eta_I}{\partial m_{cr}} w_{m_{cr}}\right)^2 + \left(\frac{\partial \eta_I}{\partial m_{dcr}} w_{m_{dcr}}\right)^2\right]^{1/2} \quad (23)$$

The overall uncertainty affecting the efficiency of the developed heat storage system was determined by using Equations (21) to (23). The estimation shows that the total uncertainty in the analysis of η_I is found to be 3.38 %. The uncertainties in the other calculated parameters are obtained in a similar way and their values are given in Tables 5 – 7.

3.2 Material Synthesis and Experimental Methodology

The Incipient Wetness Technique (IWT) has been used for synthesizing the composite sorbents. This impregnation method uses the natural wetting or liquid absorption capacity of the host matrix materials to fill the pore structure with the applied salt solution. More details on this method can be found in an earlier report [58]. For preparing vermiculite-$CaCl_2$, pumice-$CaCl_2$ and APC-$CaCl_2$ composites, 43wt% $CaCl_2$ salt solution was prepared. The synthesis procedure applied for preparing the composite sorbents is presented in Figure 9. Basic properties of the sorption materials used in this study are briefly described below. Some important key parameters of the materials are presented in Table 2.

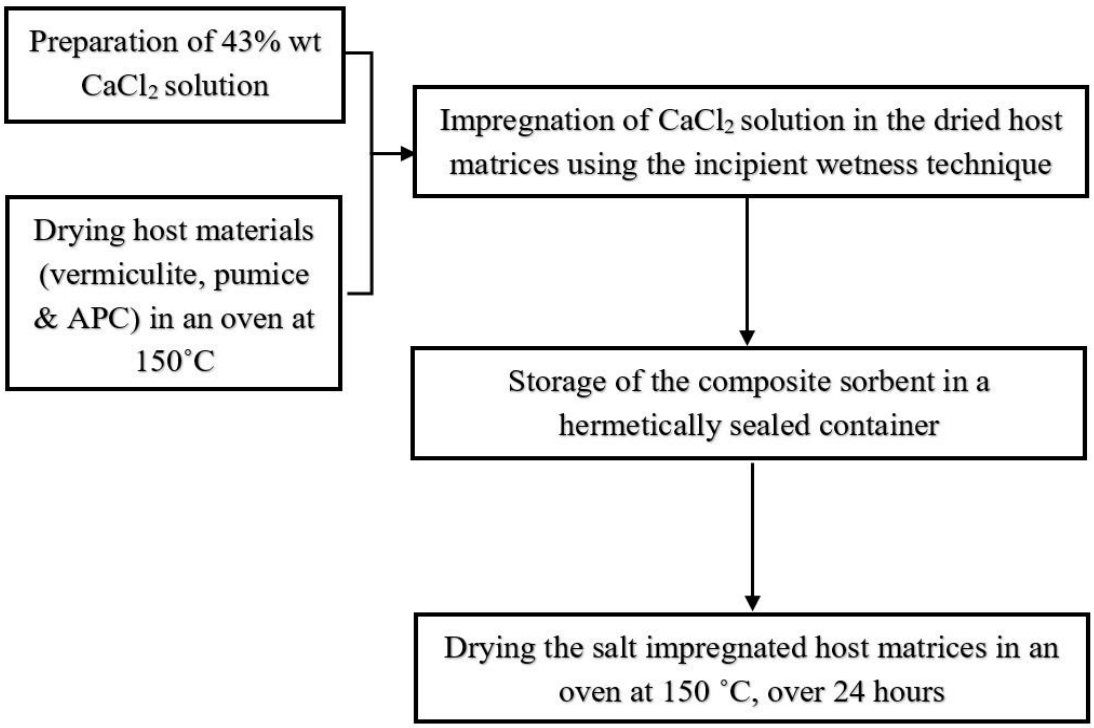

Figure 9: Flowchart showing the synthesis procedure for the composite sorbent.

3.2.1 Specifications of the Sorption Materials

Vermiculite-$CaCl_2/H_2O$

$CaCl_2$ is a salt hydrate widely used as a sorbent in THS systems. Despite its promising characteristics such as high heat storage capacity, low price and non-toxicity, it suffers mainly from unsteady sorption performance over the hydration phase. Due to this weakness, it shows a high sorption rate for a short period at the start of the discharging process and releases a high amount of thermal energy. However, the sorption rate and consequently the released heat, drops quickly in the following period. The chemical reaction of $CaCl_2$ and water is as follows:

$$CaCl_2.\ xH_2O(s) + \text{heat} \longleftrightarrow CaCl_2.\ (x\text{-}y)\ H_2O(s) + yH_2O\ (g) \qquad (24)$$

Using vermiculite as a porous host matrix in salt-based THS systems mainly resolves the deliquescence problem of these materials. Furthermore, it prevents salt leakage over the discharging phase of the full process. Vermiculite is one of the most preferable host matrices due to its low price and low charging temperature [7, 30].

Zeolite 13X/H_2O

The pair of zeolite 13X/H_2O has been used in this study due to its high sorbate uptake capacity and high reaction kinetics. The main constraint of using zeolite 13X in solar assisted THS systems is its high desorption temperature, which is between 200 and 250 ºC. In addition, similar to vermiculite-$CaCl_2/H_2O$, it is not able to provide a steady sorption performance [15, 35]. Zeolite 13X is composed of different materials as illustrated below:

$$Na_2O \times Al_2O_3 \times mSiO_2 \times nH_2O \qquad (m \leq 2.35) \qquad (25)$$

APC-$CaCl_2$/H_2O

Aerated porous concrete is a porous composite material that has been widely used in energy efficient buildings as an insulation material. In this study, APC impregnated with $CaCl_2$ has been used for the first time as a composite sorbent. This material has not been used previously in any THS system and thus, there is no any information available in the literature about its thermal and hygrothermal properties.

Pumice-$CaCl_2$/H_2O

Pumice stone is a natural lightweight aggregate formed by sudden cooling of molten volcanic matter. The main components of this stone are: SiO_2 (60 – 75 %), Al_2O_3 (13 – 17 %), and, Na_2O – K_2O (7 – 8 %).

Table 2: Properties of the sorbent materials used in this study [44, 58]

Material	ρ_{bulk}	λ	Cp	T_r	T_d	d_{pore}	Δm	cost
	g/cm^3	W/mK	kJ/kgK	ºC	ºC	-	kg/kg	$/kg
V – $CaCl_2$	0.5	0.0737	0.84 – 1.08	50 – 80	21	1.25µm	1.50	0.2 – 0.4
APC – $CaCl_2$	0.1	0.09 – 0.19	0.09 – 0.19	–	–	1 – 3mm	1.27	0.15 – 0.4
Zeolite 13X	0.6	0.0669	1.08	>200	20 – 40	1.21nm	0.5	1.6 – 2.2
P – $CaCl_2$	1.1	–	–	–	–	–	1.35	0.3 – 0.5

The experimental procedure carried out in this study is given in Figure 10. Prior to the testing stage, the composite materials were synthesized via IWT (see Figure 9).

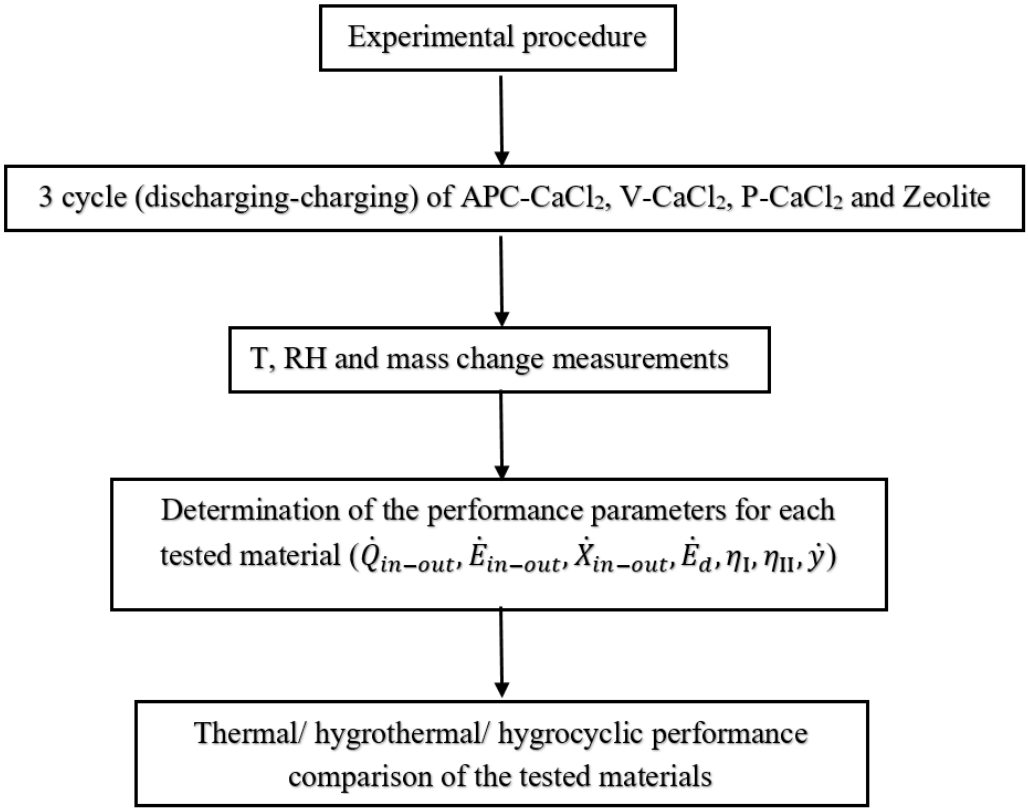

Figure 10: Experimental methodology applied in the study

The materials were tested for three consecutive cycles of discharging – charging. The discharging phase was performed under the conditions of $T_{a\text{-}in}$ = 20 – 21ºC, $RH_{a\text{-}in}$ = 85 – 90% and $m_{a\text{-}in}$ = 0.02 kg/s. Over the charging phase the conditions were, $T_{a\text{-}in}$ = 85 – 95 ºC and $m_{a\text{-}in}$ = 0.04 kg/s. *T*, *RH* and mass changes were measured over the entire duration of the measurements. Upon completion of the tests, energetic and exergetic performance parameters were calculated and thereby the thermal, hygrothermal and hygro-cyclic performances of the THS system were comparatively investigated for each tested material.

3.3 Results and Discussions

3.3.1 Discharging Analysis

The characteristics of V-$CaCl_2$, zeolite, P-$CaCl_2$ and APC-$CaCl_2$, for three discharging cycles, obtained from the analysis have been presented in this section. The duration of

each cycle was five hours (t_{dcr} = 300 min) and the air flow rate was constant ($\dot{m}_{dcr}$= 0.02 kg/s). The range of each measured parameter, its accuracies and the percentage errors due to the utilized measurement devices are listed in Table 3. Variation in of the temperature and RH measurements during the discharging and charging cycles is plotted in Figures 11, 12 and Figures 15 and 16, respectively. The uncertainties in the calculated parameters including the flow energy/exergy, discharging COP and energy/exergy efficiency of the heat storage processes were determined using the error propagation method as described in Section 3.1.3 above and their values are given in Tables 4 – 6.

Table 3: Standard uncertainty, error, and measuring range of instruments

Sensor	Measured parameter	Range	Accuracy	Error
Temperature (Sensirion-SHTC3)	Temperature	0 – 130 ºC	±0.2ºC	±1.2 %
Humidity (Sensirion-SHTC3)	Relative humidity	0 – 100%	±2%	±2.5 %
Anemometer (Pasco-Xplorer)	Air velocity	2 – 6 m/s	±0.1m/s	±3.0 %
Pyrometer and Radiation meter	Solar intensity	0 – 2800W/m^2	±3 W/m^2	±0.5 %

Temperature and RH variations

The air temperature profiles for the tested sorbents at the inlet and outlet of the reactor are shown in Figure 11. On average, the inlet temperature varies between 20 ºC and 21 ºC. All four sorbent materials are observed to experience a substantial temperature rise at the start time of each cycle due to the high adsorption rate of the sorbate during this short period. For all four materials, the average temperature difference is seen to decrease with the repeating cycles. Despite the highest temperature difference obtained with zeolite (ΔT_{avg} = 23.2 ºC) in the first cycle, it decreases sharply to 16.8 ºC and 10.6 ºC in the second and third cycles, respectively. On the other hand, ΔT_{avg} of V-$CaCl_2$

for the three cycles is observed to be in the range of 15 – 17 ºC, while for APC-$CaCl_2$, it is observed to be 18.1 ºC, 17.4 ºC and 16.2 ºC for the three successive cycles, respectively. P-$CaCl_2$ was the last tested composite and showed the best temperature performances over the three cycles, with temperature differences of 22.4 ºC, 19.9 ºC and 18.2 ºC, respectively. The considerable decrease of ΔT_{avg} for zeolite is due to an insufficient charging temperature of the material, which is in the range of 85 – 95 ºC (the proved charging temperature for zeolite was 200 – 250ºC).

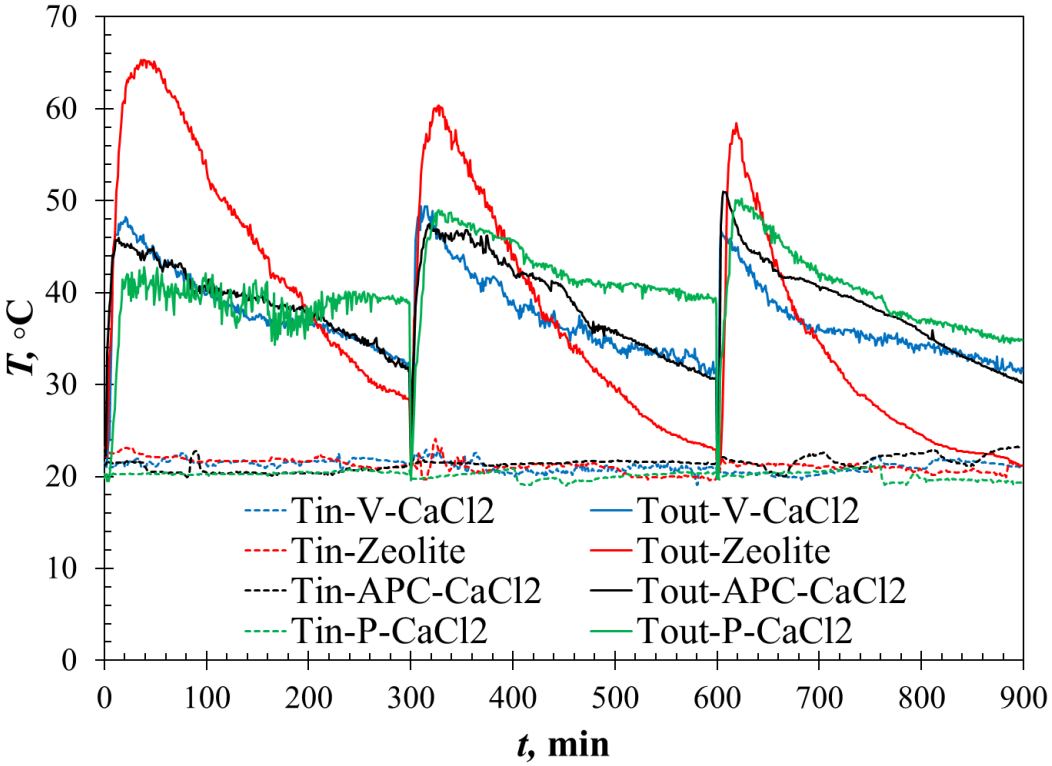

Figure 11: Temperature variation for V-$CaCl_2$, P-$CaCl_2$, zeolite, and APC-$CaCl_2$ composite materials

The *RH* of inlet-outlet air and its variation, Δ*RH*, over the duration of the discharging process is plotted in Figure 12. Over the discharging period, *RH* of air at the inlet of the reactor was in the range of 85 – 90% whereas the outlet air *RH* varied between 10 to 40%. Accordingly, Δ*RH* of air showed similar trends during the testing of all

materials, where it reached ~75% at the beginning of the experiments and gradually dropped ~50% over the testing duration.

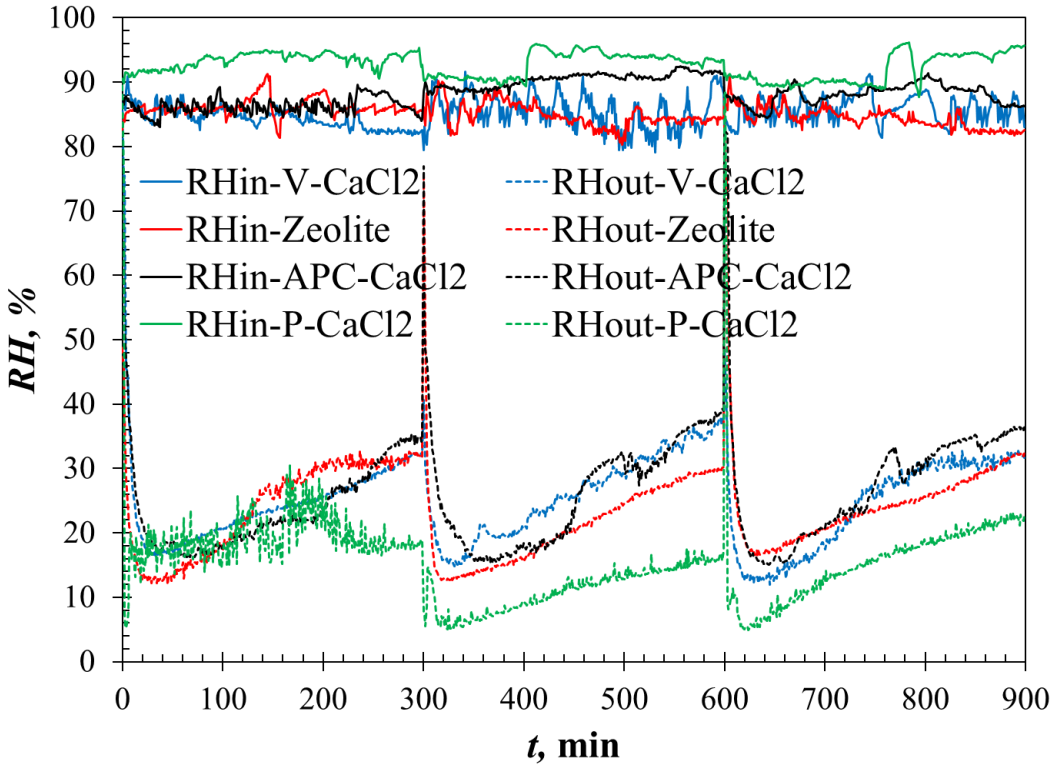

Figure 12: Relative humidity variations corresponding to$V\text{-}CaCl_2$, $P\text{-}CaCl_2$, zeolite and $APC\text{-}CaCl_2$ composites

Energy and exergy outputs

The energetic and exergetic characteristics of the THS system in the discharging phase are shown in Figure 13. The cumulative energy values for $APC\text{-}CaCl_2$ composite in each cycle are seen to decrease and the energy output values of 1.96, 1.88 and 1.76 kWh have been obtained in the successive cycles. Energy output of $V\text{-}CaCl_2$ is found to be 1.80, 1.78 and 1.64 kWh for the three cycles, respectively. The total energy output value of zeolite decreases considerably in each cycle and is, respectively 1.98, 1.82 and 1.61 kWh. This decrease is mainly due to the insufficient desorption of water in the charging phase. The charging temperature of zeolite was between 200 – 250 ºC;

however, the charging temperature of the tested THS system varied between 85 ºC and 95 ºC. The cumulative energy performance values of P-$CaCl_2$ have been observed to be the highest among the tested materials with output values of 22.41, 19.98 and 18.12 kWh, respectively during the three cycles.

As shown in Figure 13, the exergy output profiles for the tested materials show a substantial difference as compared to the energy output profiles. For V-$CaCl_2$, zeolite, APC-$CaCl_2$ and P-$CaCl_2$, the cumulative exergy outputs obtained are (0.034, 0.035, 0.026 kWh), (0.082, 0.043, 0.031 kWh), (0.017, 0.013, 0.016 kWh) and (0.023, 0.015, 0.013 kWh), respectively over the three repeating cycles. The main reason for the large difference could be due to the varying ambient temperatures during the testing of the materials. Besides, the gradual drop in ΔT_{avg} for all tested materials over repeating cycles influences the exergy outputs in a negative manner. For zeolite, V-$CaCl_2$, APC-$CaCl_2$ and P-$CaCl_2$ exergy outputs drop in the range of 0.082 kWh → 0.031kWh, 0.034 kWh → 0.026 kWh, 0.017 kWh → 0.013 kWh and 0.117 kWh → 0.068 kWh respectively. This outcome suggests that in terms of the exergy output, APC-$CaCl_2$ performs better as compared to the other tested materials.

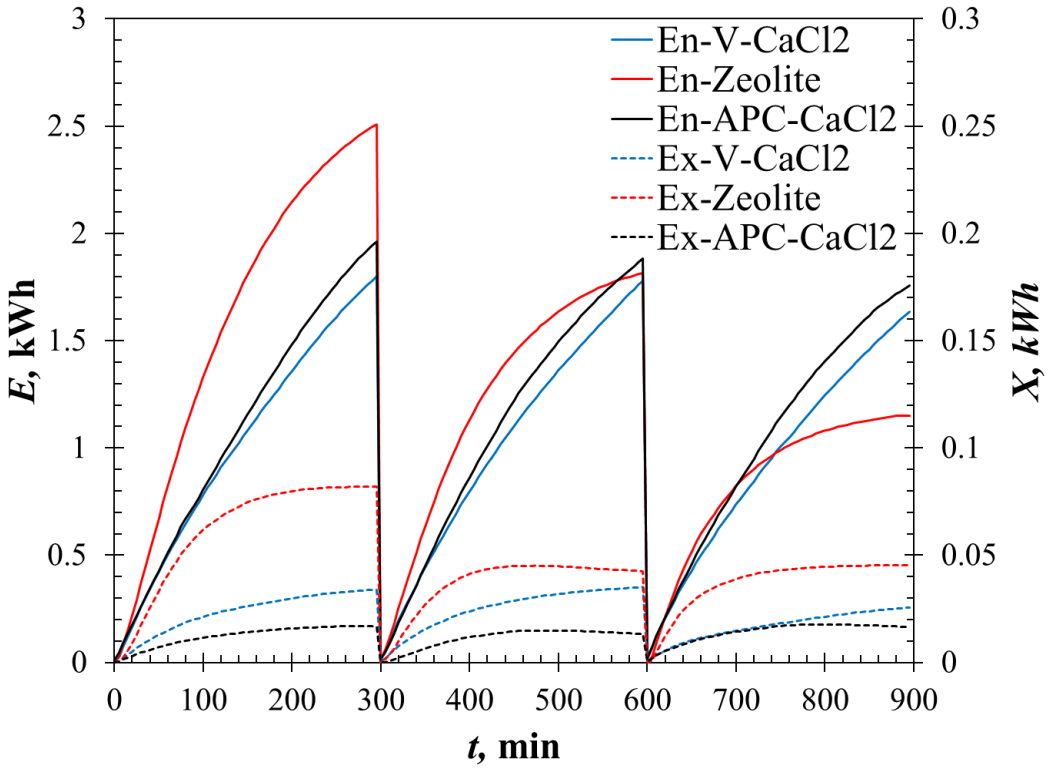

Figure 13: Variation of the energy and exergy values for V-$CaCl_2$, P-$CaCl_2$, zeolite, and APC-$CaCl_2$ composites

The discharging coefficient of performance (*COP*) in THS systems is defined as the ratio of the net useful heat output to the net electric work input to the system. In the discharging phase, the electricity-consuming units were the ultrasonic humidifier and the fan. *COP* of the tested materials is found to show a decreasing trend after reaching their maximum value (see Figure 14). Among all, the discharging *COP* for zeolite shows a very sharp drop, while V-$CaCl_2$, P-$CaCl_2$, and APC-$CaCl_2$ are found to be steadier.

Due to the high response time and fast sorption kinetics of zeolite, at the beginning of the discharging process, it absorbs a large amount of moisture, resulting in high heat output and *COP*. Later on, as that material gets saturated in a short period, its thermal performance dramatically drops, which is not a desired condition in practical

applications. On the other hand, salt composites show slower but steadier sorption kinetics resulting in more stable performance outputs (i.e., *COP*) during the discharging cycle. Based on the calculated average heat gains and electrical consumption of the system components, the average discharging *COP* of APC-$CaCl_2$, V-$CaCl_2$, P-$CaCl_2$ and zeolite over the three repeating cycles has been determined to be 7.46, 6.95, 8.23 and 7.30, respectively.

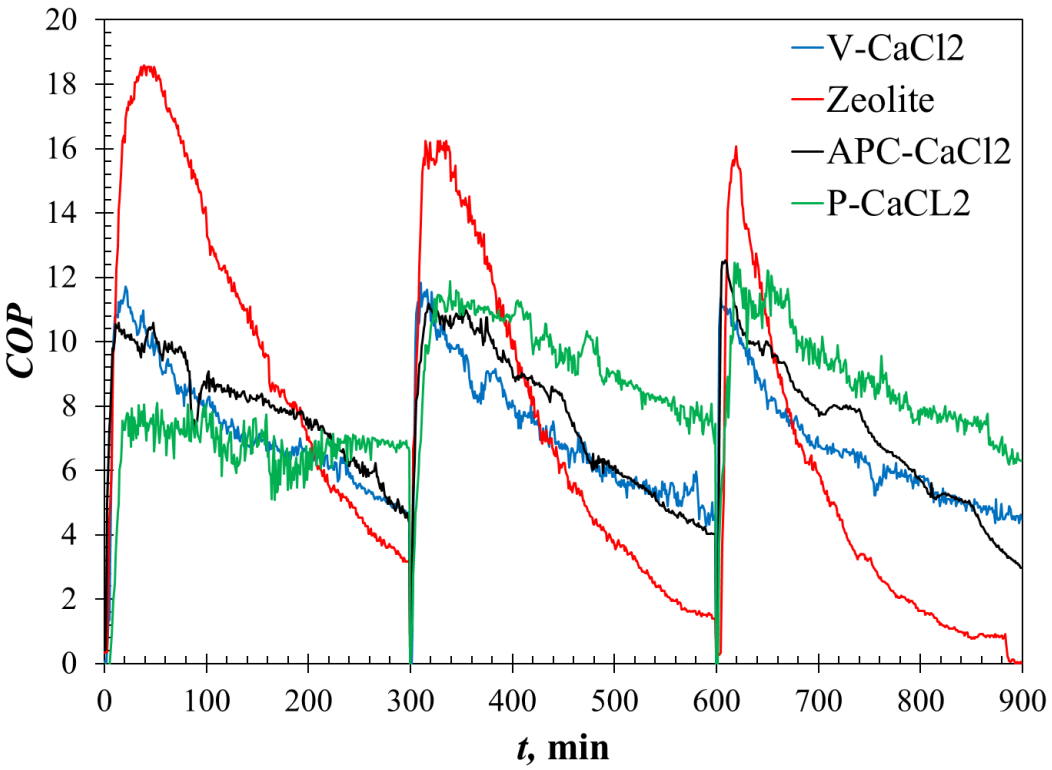

Figure 14: Variation of discharging COP for V-$CaCl_2$, P-$CaCl_2$, Zeolite, and APC-$CaCl_2$ composites

3.3.2 Charging Analysis

The three-cycle charging performance of APC-$CaCl_2$, V-$CaCl_2$, P-$CaCl_2$, and zeolite, with t_{cr} = 180 min and $\dot{m}_{dcr}$ = 0.04 kg/s, has been discussed in this section.

Temperature and RH variations

During the charging cycles, the air temperature at the inlet of the reactor was in the range of 85 – 95 ºC. ΔT_{avg} for APC-$CaCl_2$, V-$CaCl_2$, P-$CaCl_2$ and zeolite were 18.6 ºC, 18.6 ºC, 19.1 ºC and 22.3 ºC, respectively. As shown in Figure 15, T_{out} for APC-$CaCl_2$ has a gradually increasing trend. This indicates that APC-$CaCl_2$ releases moisture at a steady rate and there is no step-wise desorption kinetics for this material. As can be seen from Figure 15, at the end of the charging cycle, T_{out} is still lower than the inlet temperature (70 – 80 ºC) and moisture desorption is continuing. Thus, it can be concluded that APC-$CaCl_2$ has the potential to be regenerated at the applied temperature, however, due to its low desorption rate, a long charging duration is required at the applied regeneration temperature. On the other hand, P-$CaCl_2$ and V-$CaCl_2$ show quite a similar thermal behavior in the charging phase. T_{out} remains steady between 40 – 60 ºC over ~ 40 min, indicating that a substantial amount of moisture is desorbed in this period. Later on, a gradual increase up to 80 – 90 ºC is observed in P-$CaCl_2$ and V-$CaCl_2$ charging. In that period, moisture desorption continued, but it was at a lower rate as compared to the initial part of the cycle. Zeolite is observed to reach its maximum T_{out} in approximately 60 min and after that stays at that temperature till the end of the cycle. As the desorption rate is slow at the applied temperature, latent heat consumption for the water desorption is lower in zeolite charging as compared to other materials. Therefore, the outlet temperature rapidly reaches its peak value and stays at that point. The results obtained demonstrate that higher charging temperatures are required for observing a step-wise temperature variation in zeolite charging. During the charging of materials, ΔRH_{avg} of V-$CaCl_2$ was found to be 16%, which is the highest among all tested materials and implies that V-$CaCl_2$ has the highest

desorption ability. On the other hand, ΔRH_{avg} of P-$CaCl_2$, APC-$CaCl_2$ and zeolite were 10.3%, 8.16% and 6.85% for the three charging cycles (see Figure 16).

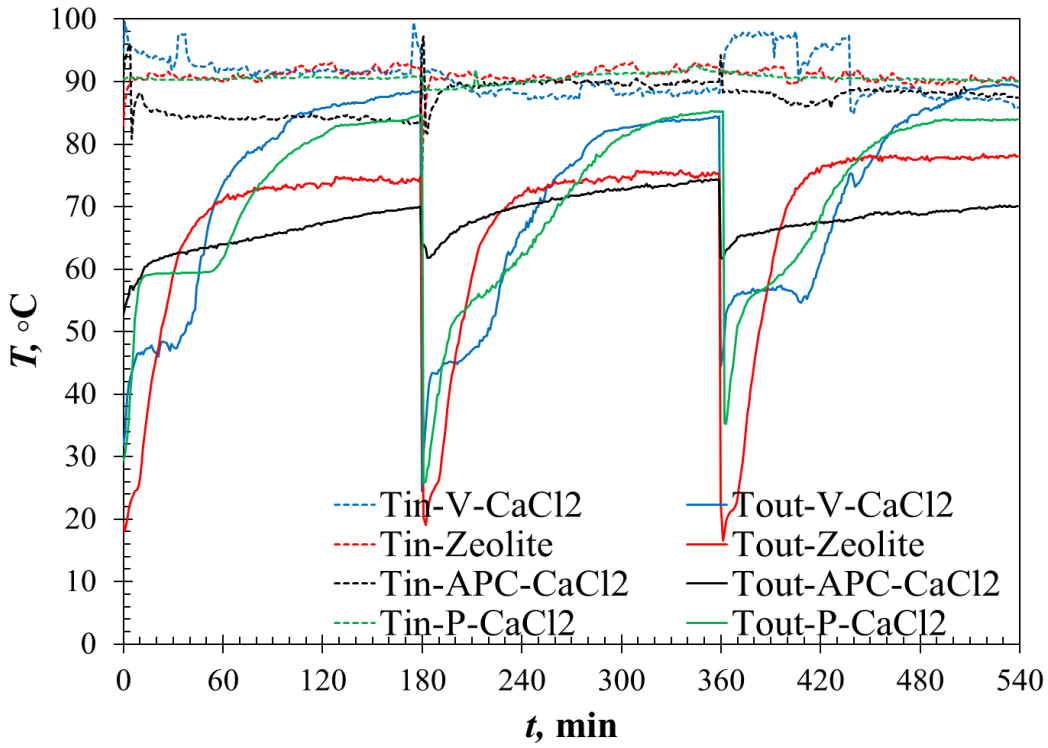

Figure 15: Temperature variation during the charging process for V-$CaCl_2$, P-$CaCl_2$, zeolite, and APC-$CaCl_2$ composites

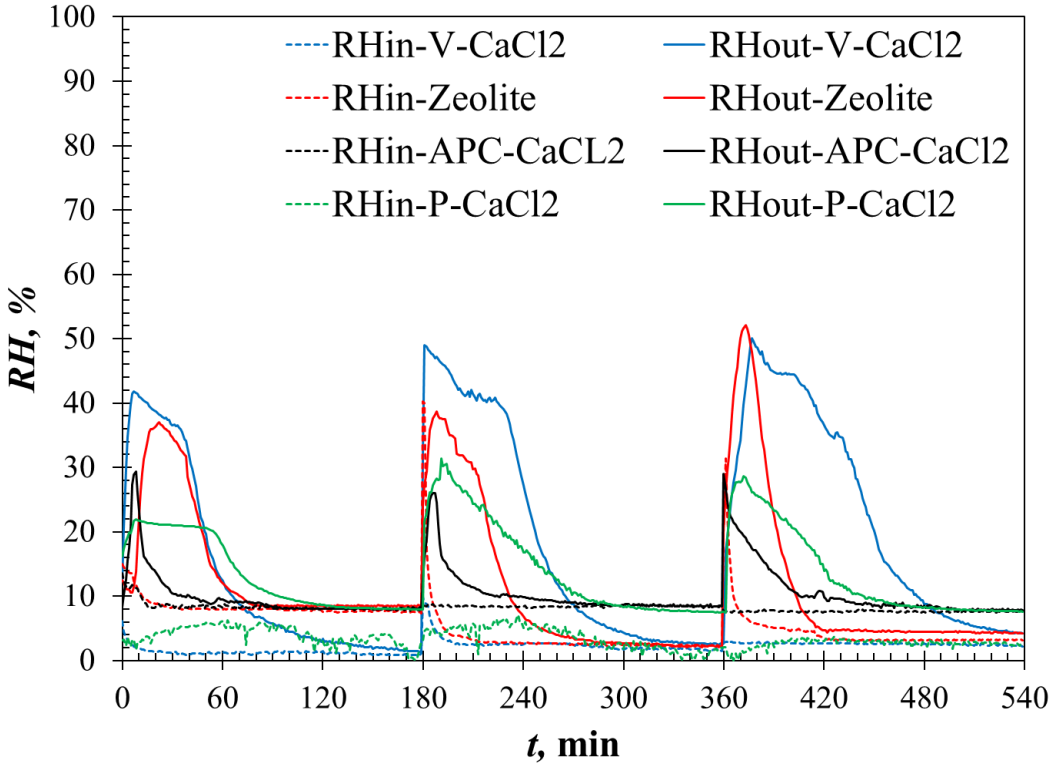

Figure 16: Variation of the relative humidity for V-$CaCl_2$, P-$CaCl_2$, zeolite, and APC-$CaCl_2$ composites

Energy and exergy inputs

The energy and exergy profiles of the THS system for zeolite, P-$CaCl_2$, V-$CaCl_2$ and APC-$CaCl_2$ for the charging cycle are shown in Figure 17. As can be seen from the figure, due to its high specific heat and high desorption temperature requirement, zeolite consumes a substantial amount of energy during the desorption phase. From the analysis, the total energy consumption in zeolite charging cycles was found to vary in the range of 3.3 kWh and 2.7 kWh. On the other hand, V-$CaCl_2$ and APC-$CaCl_2$ show similar trends over the charging cycle, showing an energy consumption between 2.5 kWh and 2.3 kWh. P-$CaCl_2$ shows the lowest energy consumption in the regeneration phase, 2 kWh, 2.2 kWh, and 1.7 kWh over three cycles, respectively. The average cumulative energy consumption for zeolite, APC-$CaCl_2$, V-$CaCl_2$, and P-$CaCl_2$ was found to be 3.04 kWh, 2.44 kWh, 2.43 kWh, and 2.25 kWh respectively.

The cumulative exergy consumption of the THS system for APC-$CaCl_2$, zeolite, V-$CaCl_2$, and P-$CaCl_2$ was estimated to be 0.31 kWh, 0.38 kWh, 0.35 kWh and 0.33 kWh, respectively. From the performed exergetic analysis for the discharging and charging cycles, the exergy consumption in charging cycles was found to be >10 times of the exergy gain during the discharging cycles. Further, the quantity of the energy output-input in discharging-charging cycles is not substantially different in THS processes, the amount of energy supplied during charging is much higher as compared to the amount of energy obtained during discharging. This is due to a considerable difference between the required charging temperature and obtained discharging temperature. In the charging cycle, inlet air temperature was 85 – 95 ºC, while in the discharging cycle, the average outlet air temperature was 30 – 35 ºC. This condition demonstrates an important fact: in order to obtain a high exergetic cyclic performance, it is crucial to develop new THS materials that could be charged at low-temperature ranges. This could also be a step-forward toward utilizing solar air heating units for sorbent regeneration. In the current condition, it seems highly unlikely to realize solar-driven THS systems due to the high energy (high regeneration temperature) requirement of conventional sorbents.

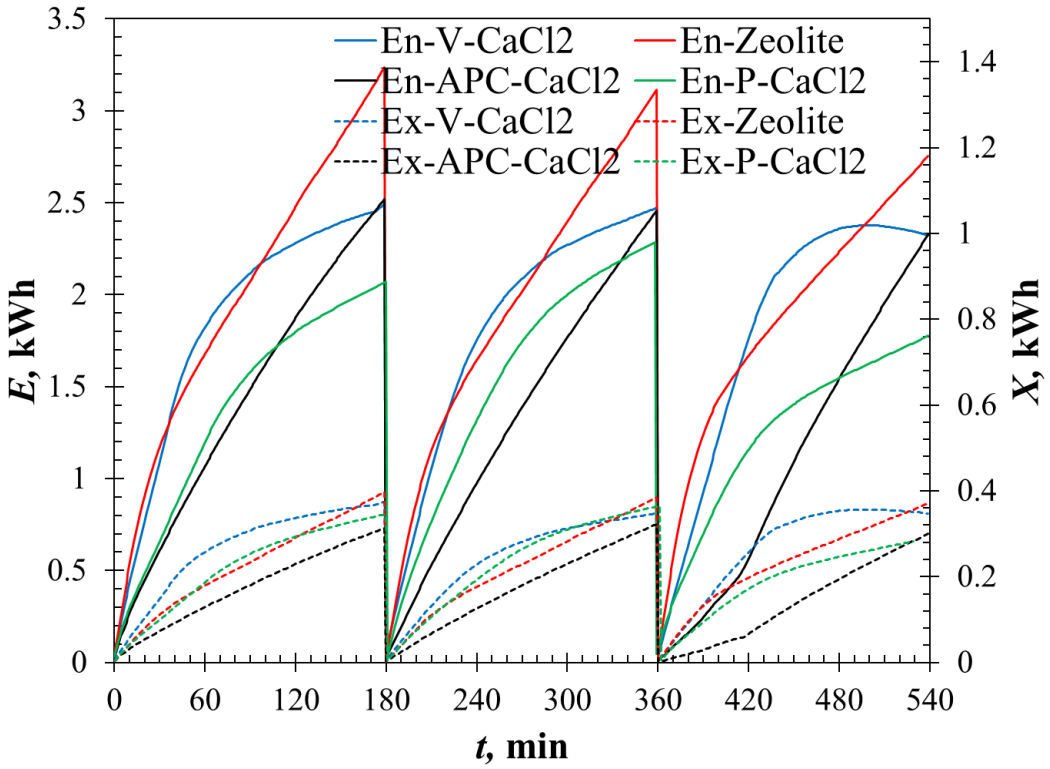

Figure 17: Variation of the energy and exergy values for V-$CaCl_2$, P-$CaCl_2$, zeolite and APC-$CaCl_2$ composites

3.3.3 Overall Cyclic Analysis

Images of the sorption materials before and after the discharging cycles are shown in Figure 18. All the materials were in a dehydrated form prior to the discharge process, whereas, after hydration, they were fully saturated with water. As can be seen from the images, there is no structural degradation of the materials after the charging and discharging processes. Therefore, it can be concluded that all tested materials have physical stability as long as they are not over-saturated. For the case in which P-$CaCl_2$, APC-$CaCl_2$, and V-$CaCl_2$ get over-saturated with water, it was observed that a structural deformation occurs and the materials become mushy, which is not a desired property. On the other hand, for zeolite, cracking was observed with the supply of an excessive amount of moisture.

Figure 18: Images showing the tested materials after discharging (a) and after charging (b)

The values of the different performance parameters obtained from the tests conducted during the discharging and charging process are given in Tables 4 and 5, respectively. The testing of each material was done after completely drying the material in an electrical furnace at a temperature of 150 ºC. After this stage, the discharging–charging

tests were performed consecutively for the three cycles of each phase. The first law efficiency (η_I), second law efficiency (η_{II}) and hygrothermal efficiency (η_{hyg}) of each material for each cycle is given in Table 6.

Table 4: Overall summary of the results of discharging for four materials

Material	Cycle	T_{out}	ΔT_{avg}	$\Delta\dot{Q}$	E	$\dot{X}$	X	$M_{w\text{-}abs}$	E_d	y
		(ºC)	(ºC)	(kW)	(kWh)	(kW)	(kWh)	(g)	(kWh/m^3)	(g/min)
		±1.2%	±1.2%	±1.6%	±2.1%	±1.6%	±2.1%	±2.0%	±2.9%	±3.1%
V-$CaCl_2$	1	38.2	16.6	0.360	1.803	0.007	0.034	2388	180	7.939
	2	37.4	16.4	0.356	1.783	0.007	0.035	2517	178	8.369
	3	36.0	15.1	0.327	1.639	0.005	0.026	2668	163	8.868
Zeolite	1	44.9	23.1	0.501	1.986	0.016	0.082	2683	251	8.916
	2	37.5	16.7	0.362	1.817	0.008	0.043	2196	181	7.301
	3	31.5	10.6	0.229	1.612	0.009	0.031	2388	114	7.939
APC-$CaCl_2$	1	38.8	18.1	0.392	1.965	0.003	0.017	2193	196	7.292
	2	38.9	17.4	0.376	1.885	0.003	0.013	2324	188	7.730
	3	38.1	16.2	0.351	1.758	0.003	0.016	2155	175	7.161
P-$CaCl_2$	1	42.4	22.4	0.467	2.345	0.023	0.117	3397	234	11.289
	2	40.0	19.9	0.437	2.141	0.015	0.075	3071	214	10.447
	3	38.4	18.1	0.330	1.655	0.013	0.068	2206	165	7.329

Table 5: Overall summary of the results of charging for four materials

Material	Cycle	T_{out}	ΔT_{avg}	$\Delta \dot{Q}$	E	$\dot{X}$	X	$M_{w\text{-}des}$	E_d	y
		(°C)	(°C)	(kW)	(kWh)	(kW)	(kWh)	(g)	(kWh/m^3)	(g/min)
		±1.2%	±1.2%	±1.6%	±2.1%	±1.6%	±2.1%	±2.0%	±2.9%	±3.1%
V-$CaCl_2$	1	73.4	19.1	0.827	2.494	0.124	0.375	2025	249	11.239
	2	69.6	18.9	0.820	2.474	0.115	0.348	2060	247	17.459
	3	73.4	17.8	0.769	2.320	0.115	0.347	2006	232	11.123
Zeolite	1	66.3	24.9	1.076	3.247	0.132	0.399	873	324	4.812
	2	67.1	20.8	1.036	3.126	0.128	0.386	674	312	3.745
	3	69.4	21.1	0.915	2.761	0.123	0.372	843	276	4.640
APC-$CaCl_2$	1	65.2	19.3	0.838	2.527	0.104	0.314	1962	252	10.862
	2	70.6	18.9	0.818	2.468	0.107	0.324	1718	246	9.483
	3	68.0	17.5	0.757	2.339	0.100	0.302	1663	233	9.174
P-$CaCl_2$	1	71.5	19.0	0.686	2.700	0.114	0.345	2913	207	16.184
	2	69.3	21.1	0.762	2.297	0.121	0.365	2456	230	15.921
	3	73.2	17.2	0.589	1.776	0.097	0.292	1853	211	10.290

Table 6: Energetic, exergetic, and hygrothermal efficiencies of the THS system

Material	Cycle	η_I ±3.3%	η_{II} ±2.7%	η_{hyg} ±2.3%
V-$CaCl_2$	1	0.723	0.091	0.848
	2	0.721	0.101	0.819
	3	0.706	0.074	0.752
Zeolite	1	0.612	0.205	0.326
	2	0.581	0.110	0.307
	3	0.584	0.083	0.353
APC-$CaCl_2$	1	0.777	0.053	0.895
	2	0.764	0.041	0.739
	3	0.754	0.052	0.774
P-$CaCl_2$	1	0.868	0.339	0.857
	2	0.932	0.207	0.799
	3	0.931	0.231	0.840

The first law and second law efficiencies (η_I, η_{II}) of the THS system for the four tested materials are plotted in Figure 19. The average η_I for APC-$CaCl_2$, V-$CaCl_2$, zeolite and P-$CaCl_2$ is found to be 76.5%, 71.6%, 59.2% and 0.91%, respectively while the η_{II} for these materials is found to be 4.8%, 8.8%, 13.2%, and 25.9%. The measured mass changes of the tested materials after discharging and charging cycles is shown in Figure 20. In the figure, positive and negative mass changes indicate the amount of water adsorbed and desorbed, respectively. The composite materials V-$CaCl_2$ and APC-$CaCl_2$ show an almost constant moisture adsorption trend, whereas zeolite and P-$CaCl_2$ show a decreasing trend after the first cycle. This is mainly due to the limited amount of moisture desorption from that material during the charging cycles. For V-$CaCl_2$ and APC-$CaCl_2$, desorption capacities are between 1500 – 2000 g, while for zeolite, it is in the range of 500 – 1000 g and for P-$CaCl_2$, between 1800 – 2800 g over the three repeating charging cycles. In order to provide a more accurate comparison of the adsorption/desorption characteristics of the materials, the hygro-cyclic efficiency (η_{hyg}), which is the ratio of the amount of desorbed sorbate to the amount of adsorbed sorbate, was also calculated.

The $\eta_{hyg\text{-}\,avg}$ for APC-$CaCl_2$, V-$CaCl_2$, zeolite, and P-$CaCl_2$ were found to be 0.802, 0.806, 0.328 and 0.832, respectively (see Figure 21). This outcome indicates that at temperatures between 85 – 90 ºC, ~80% of the moisture could be desorbed from the salt-based composites; however, only ~33% of the adsorbed moisture could be desorbed from zeolite. Therefore, a gradual drop in zeolite performance over further repeated cycles is expected. The energetic and hygro-cyclic efficiencies of V-$CaCl_2$, P-$CaCl_2$, and APC-$CaCl_2$ were found to be in close approximation, whereas zeolite showed a poor performance due to its low charging capacity at the applied regeneration

temperature. On the other hand, zeolite's exergetic efficiency was found to be superior as compared to APC-$CaCl_2$ and V-$CaCl_2$ but less than P-$CaCl_2$. This is mainly due to the higher peak discharge temperatures obtained with that material. Despite the high initial heat output rate of zeolite, over repeated cycles, its performance shows a sharp drop. This could possibly be due to the blockage of the pores with water vapor because of a drop in the sorption rate. Similarly, in the charging cycle, due to the very small size of the pores, high-temperature heat is required for moisture desorption. These are all negative aspects of using zeolite, particularly in the domestic scale solar thermal heat storage applications. In this context, $CaCl_2$ impregnated vermiculite, pumice, and APC based composites synthesized in this work are promising candidate materials for THS due to their high heat storage efficiency and heat storage densities at regeneration temperatures <100 ºC.

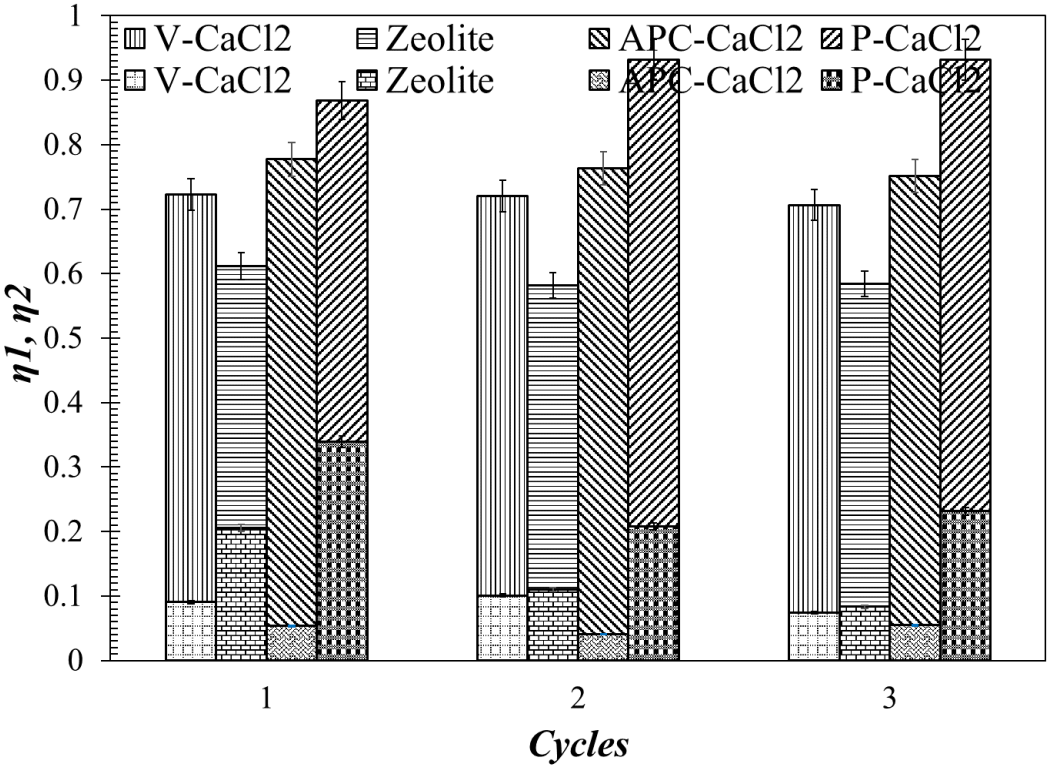

Figure 19: Energetic and exergetic efficiencies of the tested materials

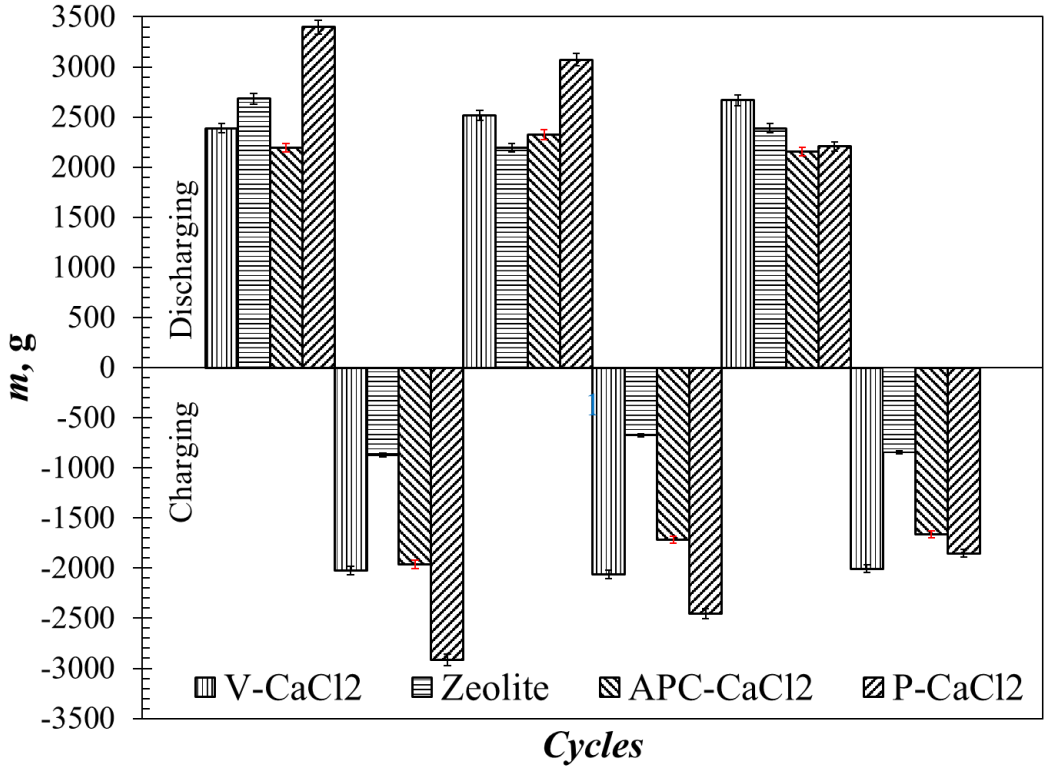

Figure 20: Total amount of absorbed/desorbed water vapor over repeating cycles

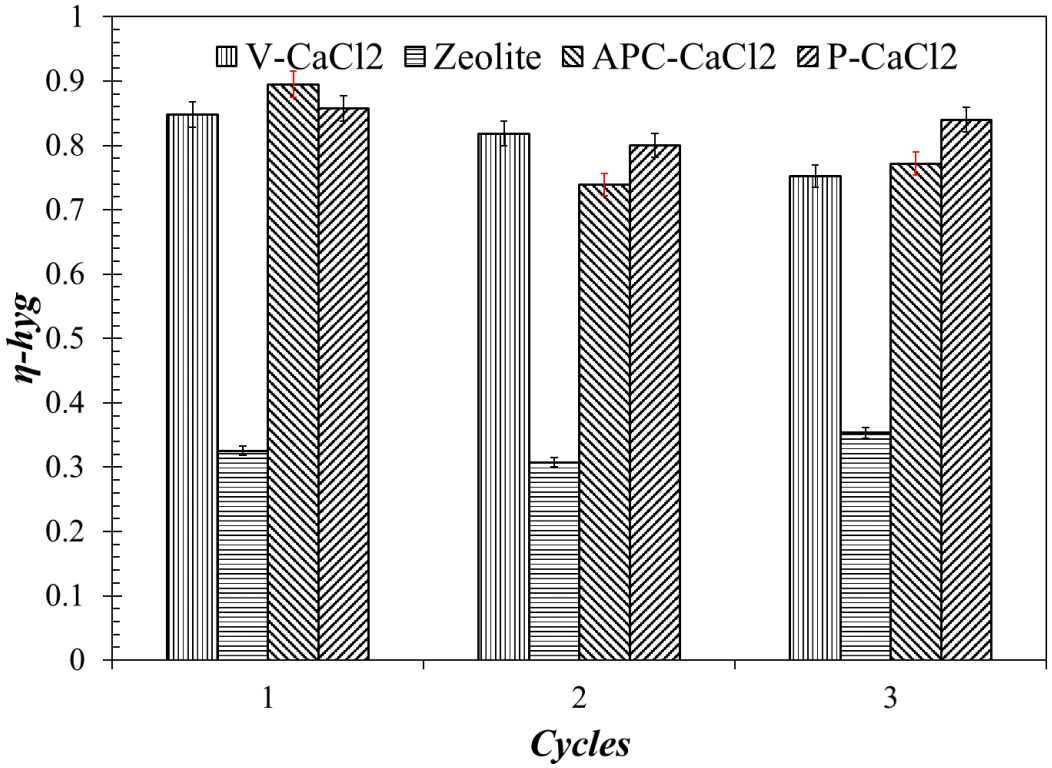

Figure 21: Hygrothermal efficiencies of the tested materials

In spite of several salts that have been considered for THS applications, only a limited number of candidate porous matrices have been investigated previously. A porous host matrix is a key component in the THS process as it plays a vital role in an efficient heat and mass transfer between the sorbate and the sorbent during the charging and discharging cycles. Table 7 summarizes past studies investigating different sorption materials for their use in THS. As can be seen from the table that host matrices including vermiculite, pumice, expanded clay, silica gel and mesoporous ceramic (WSS) have been utilized for salt impregnation. In this study, a new composite THS material has been developed by using APC as the host matrix and $CaCl_2$ as the sorbent material.

The main objective of the study was to do a comparative investigation of APC-$CaCl_2$ performance along with three different sorbents (V-$CaCl_2$, P-$CaCl_2$, and zeolite) to validate its suitability for THS applications. With this aim, several performance parameters such as cyclic stabilities, charging characteristics and full-cycle energetic/exergetic performances of the tested materials were measured. From the analysis, APC-$CaCl_2$ is observed to show a competitive performance to V-$CaCl_2$ over repeating cycles, while the performance of zeolite shows a sharp decrease after the initial cycle. P-$CaCl_2$ is observed to be the best candidate in terms of energetic and exergetic efficiency and also shows the highest average energy density (E_d).

In previous research studies, different types of zeolites (4A, MSX, 13A) have been investigated and energy densities in the range of 136 – 154 kWh/m^3 have been obtained for regeneration temperatures between 180 – 230 ºC. In the present study, the energy density of zeolite 13X was found to be 251 kWh/m^3 in its fully dehydrated state, whereas, it dropped to 114 kWh/m^3 when regenerated at 90 ºC. To our best knowledge

in no other study, low regeneration temperatures have been used to investigate the behavior of zeolite in its partially hydrated form. This study demonstrates that insufficient regeneration temperature of zeolite results in a sharp drop in the discharging heat output and thus, low energy densities (<50% of the fully dehydrated condition). On the other hand, several salt-impregnated matrices have been investigated previously. The performance of V-$CaCl_2$ investigated in this study was found to be in close approximation with the study of Casey et al., [9] (as presented in Table 7). In several different investigations where pumice, expanded clay, and WSS were used as host matrices, much lower energy densities were obtained due to the low pore volume of these materials. In the study performed by Courbon et al., [59], the energy density of silica gel-$CaCl_2$ composite was obtained as 211 kWh/m^3 at 80 ºC regeneration temperature, which is close to the results obtained in the present study. To summarize, the energy density of the newly developed APC-$CaCl_2$ composite has been found to be promising (196 – 175 kWh/m^3) as compared to the previously developed materials and shows good potential to be used in future THS applications.

Table 7: Comparison of the previous studies performed on different THS materials

Reference	**Year**	**Working material**	**Description**	**Operating conditions**	**E_d**
Casey et al. [9]	2015	Vermiculite+$CaCl_2$+H_2O	Experimental, open system	T_{cr} = 70–120 $T_{dcr,max}$ = 40 ºC	164 kWh/m^3
Mehrabadi & Farid[60]	2018	Pumice+$SrBr_2$+H_2O Expanded Clay+$SrBr_2$+H_2O	Experimental, open system	T_{cr} = 90–130 ºC	29 kWh/m^3 7.3 kWh/m^3
Courbon et al. [59]	2018	Silica gel+$CaCl_2$+H_2O		T_{cr} = 80 ºC P_v = 12.5 mbar	211 kWh/m^3
Liu et al. [29]	2013	WWS+$CaCl_2$+H_2O	Experimental, open system	T_{cr} = 80–100 ºC	75.5 kWh/m^3
Zettl et al. [50]	2014	Zeolite 4A+H_2O Zeolite MSX+H_2O	Experimental, open system	T_{cr} = 230 ºC $T_{dcr,max}$ ~ 61 ºC	148 kWh/m^3 154 kWh/m^3
Van Alebeek et al. [38]	2018	Zeolite 13X+H_2O	Experimental, open system	T_{cr} = 180 ºC	136 kWh/m^3
Present study	–	Vermiculite+$CaCl_2$+H_2O Zeolite 13X+H_2O APC+$CaCl_2$+H_2O P+$CaCl_2$+H_2O	Experimental, open system	T_{cr} = 85–95 ºC	180→163 kWh/m^3 251→114 kWh/m^3 196→175 kWh/m^3 234→165 kWh/m^3

Chapter 4

DESIGN AND DEVELOPMENT OF AN ADSORPTIVE SOLAR THERMAL ENERGY STORAGE UNIT

As discussed in Chapter 2, in addition to off-peak electricity, a THS unit can utilize solar energy in the desorption phase to separate the sorbate from a sorbent. Based on the available literature, only a few studies have been conducted on the designing and manufacturing of a solar-driven THS system. This chapter presents the design and construction details of a novel adsorptive solar thermal energy storage unit. The performance of the system and the experimental results have been discussed in this chapter.

4.1 Design, Manufacturing and Thermal Analysis of the THS System

A photograph and a schematic view of the manufactured THS system are shown in Figures 22 and 23, respectively. The proposed THS system is comprised of two main components: a parabolic solar concentrator and a sorption pipe reactor. A radial fan has been used to provide sufficient airflow to the reactor. In the sorption phase, two household humidifiers were used to increase the humidity of the supplied airflow to the reactor. A manufactured parabolic concentrator and a sorption pipe reactor were fitted on a metallic frame mounted at an angle of 45˚ from the ground (see Figure 23). In order to measure the temperature and humidity of the inlet and outlet airflow and the ambient air, three SHTC3 Sensiron type sensors were installed in the system. A PASCO-GLX airflow meter was used to measure the airflow speed at the outlet of the reactor.

Figure 22: Photograph of the designed THS system.

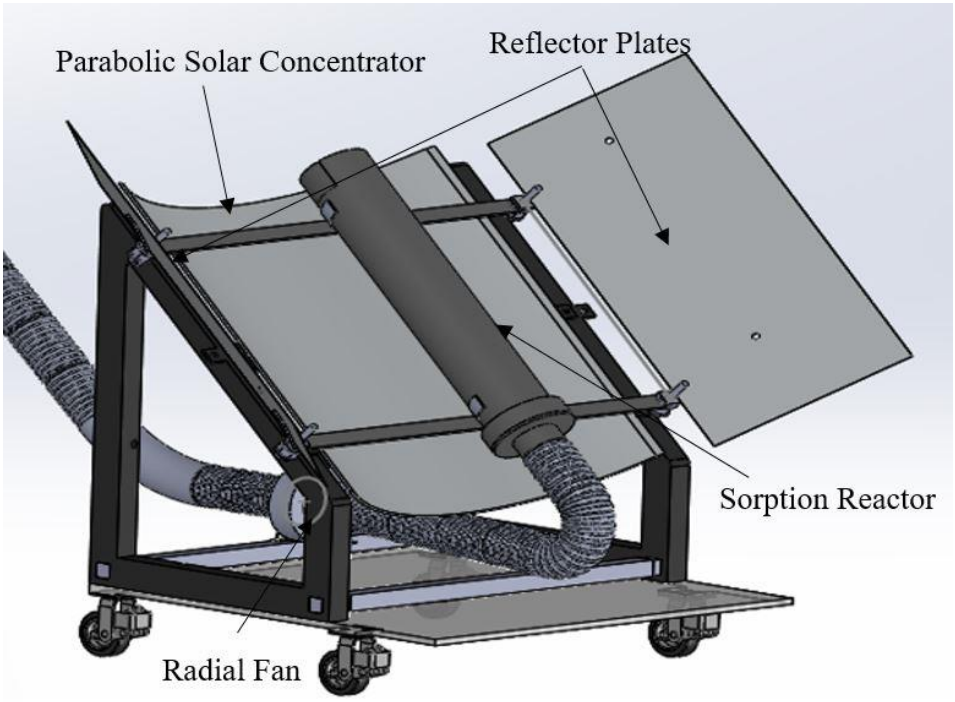

Figure 23: Schematic of the designed THS system.

4.1.1 Sorption Pipe Reactor

A schematic of the sorption pipe is shown in Figure 24 The sorption pipe reactor is made up of a black-painted cylindrical shell and a perforated conical duct. A view of the conical duct is shown in Figure 25. Over the discharging and charging phases, the volumetric flow rate of air was 0.03 m^3/s and 20 liters (~10 kg) of V-$CaCl_2$ composite material was filled into the reactor. The idea behind using a perforated conical duct was to establish a uniform airflow to diffuse inside the filled material. Due to this, the sorption material was moisturized or dried uniformly during the sorption and desorption stages. The geometrical parameters of the sorption pipe reactor are given in Table 8.

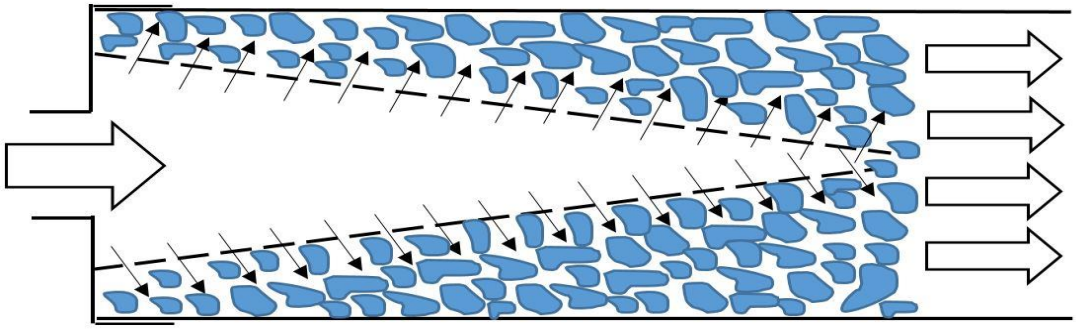

Figure 24: Schematic of the sorption pipe reactor

Figure 25: Picture of the conical sorption pipe

Table 8: Geometrical parameters of the sorption pipe reactor

	Length (mm)	Diameter (mm)	material
Cylindrical shell	1000	200	Galvanized steel
Conical duct	950	100 → 0	Galvanized steel

4.1.2 Parabolic Solar Concentrator

A parabolic solar concentrator was designed and manufactured in order to utilize the solar thermal energy in the charging process of the THS system. A stainless steel sheet having dimensions of 1160 mm × 1250 mm × 24 mm was used to manufacture the parabolic concentrator. A drawing showing a cross – sectional view of the parabolic concentrator is given in Figure 26. The concentrator was designed based on simple parabolic equations (Equations 26 and 27). The geometrical parameters of the parabolic solar concentrator are given in Table 9.

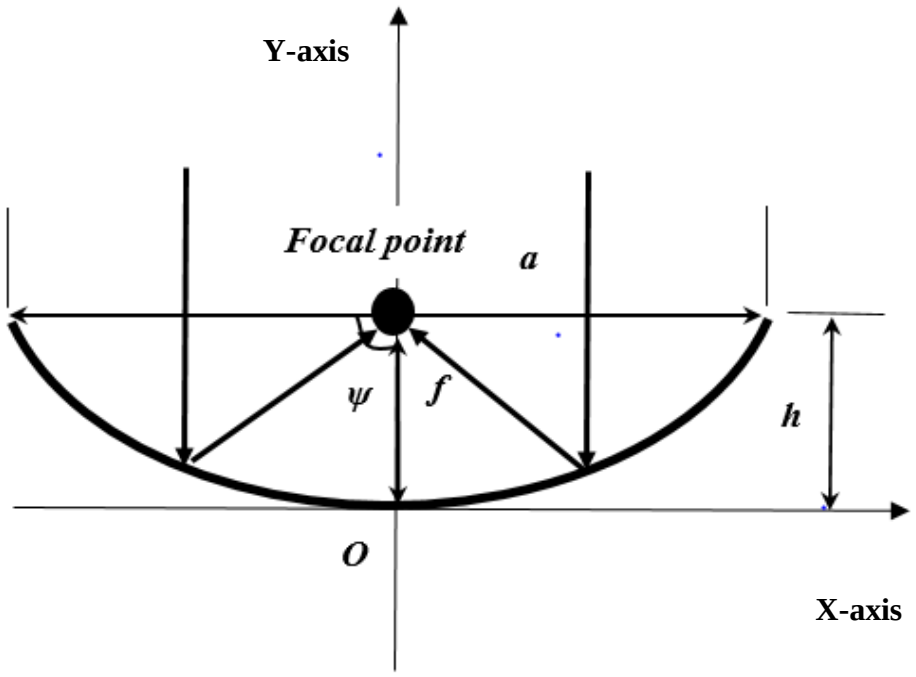

Figure 26: A cross-sectional view of the parabolic concentrator.

The parabola equation in the Cartesian coordinate is:

$$x^2 = 4fy \tag{26}$$

The height (h) of the parabola in terms of the aperture diameter (a) and focal length (f) can be derived from Equation 26 as,

$$h = \frac{a^2}{16f} \tag{27}$$

Table 9: The geometrical data of the designed parabolic concentrator

Item	Symbol	value
Length	L	1250 mm
Aperture	a	1180 mm
Focal length	f	400 mm
Height	h	220 mm

4.1.3 Experimental measurement and thermodynamic analysis

The operation of the THS system can be described in the "charging – discharging" cyclic order. The tests were performed between 25th May and 10th June of 2019. All the discharging tests were done during the evenings and hence, solar heat had no effect on the discharging tests. Over the discharging phase, the humidity in the inlet air was increased up to 80 – 90% RH and blown into the reactor. Due to the conical perforated inlet channel and cylindrical shape of the outer shell of the reactor, the blown moisturized air uniformly passes through the composite sorbent material. An exothermic reaction between the sorbent material and absorbed water causes heat generation and finally, hot air with lower humidity leaves the reactor bed.

During the charging phase, the incident solar radiation, after reflecting from the surface of the parabolic concentrator, gets collected on the surface of the reactor. Furthermore, the upper surface of the reactor directly attracts solar radiation. The hot cylindrical shell transfers its heat to the wet material and consequently, the water desorbs from the composite sorbent and is released in the air that was blown through the reactor by the fan. The reactor outlet air has a higher temperature and humidity than the ambient air at the inlet.

The performance of the solar-driven THS system has been investigated by measuring the different performance parameters using the installed sensors. The thermodynamic equations, discussed in detail in Section 3.1.2 have been used to calculate the thermodynamic parameters. In addition, uncertainty analysis has been done based on the same method as the one described in Section 3.1.3.

4.2 Material Synthesis and Experimental Methodology

Due to its availability, high sorption property and low regeneration temperature, which are the key parameters for selecting a working material in solar – driven THS systems, V-$CaCl_2$ composite was selected as the working material in testing the newly designed THS system. The method and procedure used for synthesizing the V-$CaCl_2$ composite has been discussed in detail in Section 3.2 and Figure 9. The same procedure as that followed in the testing of the candidate materials, in the developed laboratory-scale THS system (see Figure 10), has been used during these tests. The accuracy range and percentage error of the measurement devices is given in Table 3.

4.3 Results and Discussion

4.3.1 Discharging Analysis

The performance of the developed system and the characterization of the V-$CaCl_2$ composite for the three discharging cycles have been discussed in this section. Each cycle was completed in five hours (t_{dcr} = 300 min).

Temperature and RH variations

Figure 27 presents the airflow temperature at the inlet and outlet of the reactor. The reactor's inlet temperature varies between 21 – 24 ºC. As previously observed in the performed lab tests (see Section 3.1.1 and Figure 11), due to the high absorption rate in the beginning, a substantial temperature increase occurs at the start of each cycle. The average values of the measured airflow temperature at the reactor outlet for each cycle are 43.2, 42.5 and 37.9 ºC, respectively while those at the reactor's inlet are 23.6, 24.4, and 20.8 ºC, respectively.

The variation of the relative humidity at the inlet and outlet of the reactor is shown in Figure 28. RH at the inlet of the reactor was in the range of 80 – 90% whereas the outlet RH with increasing slope varied between 9% and 32%.

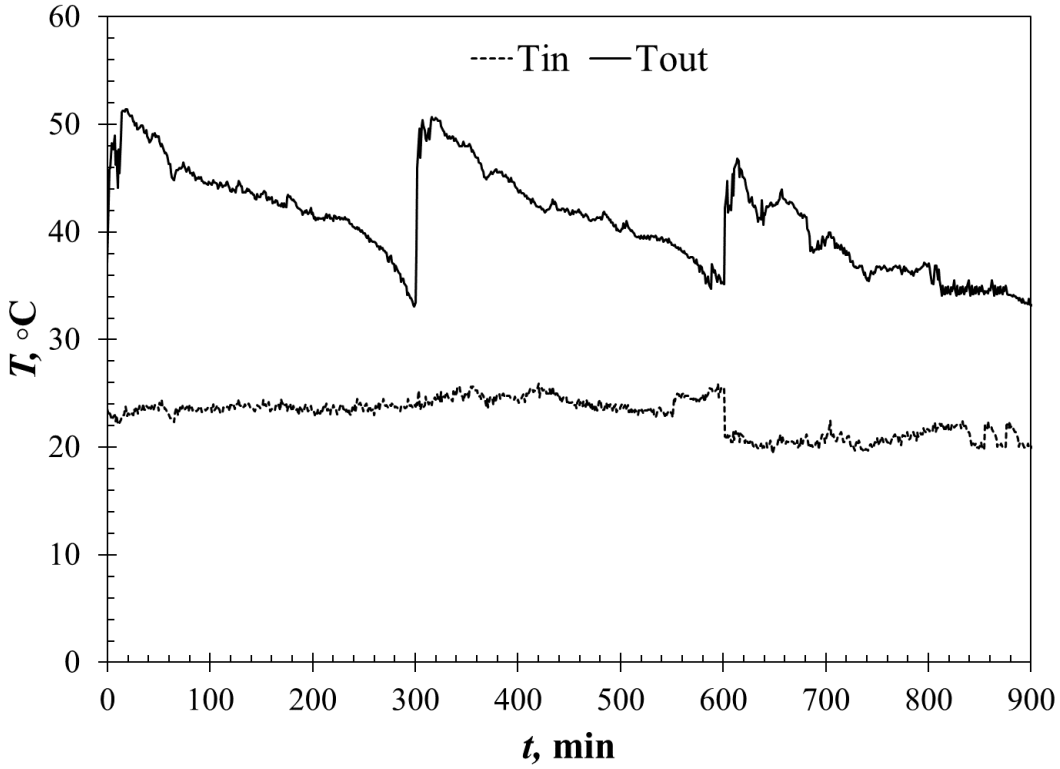

Figure 27: Variation of the V-$CaCl_2$ temperature during the discharging process

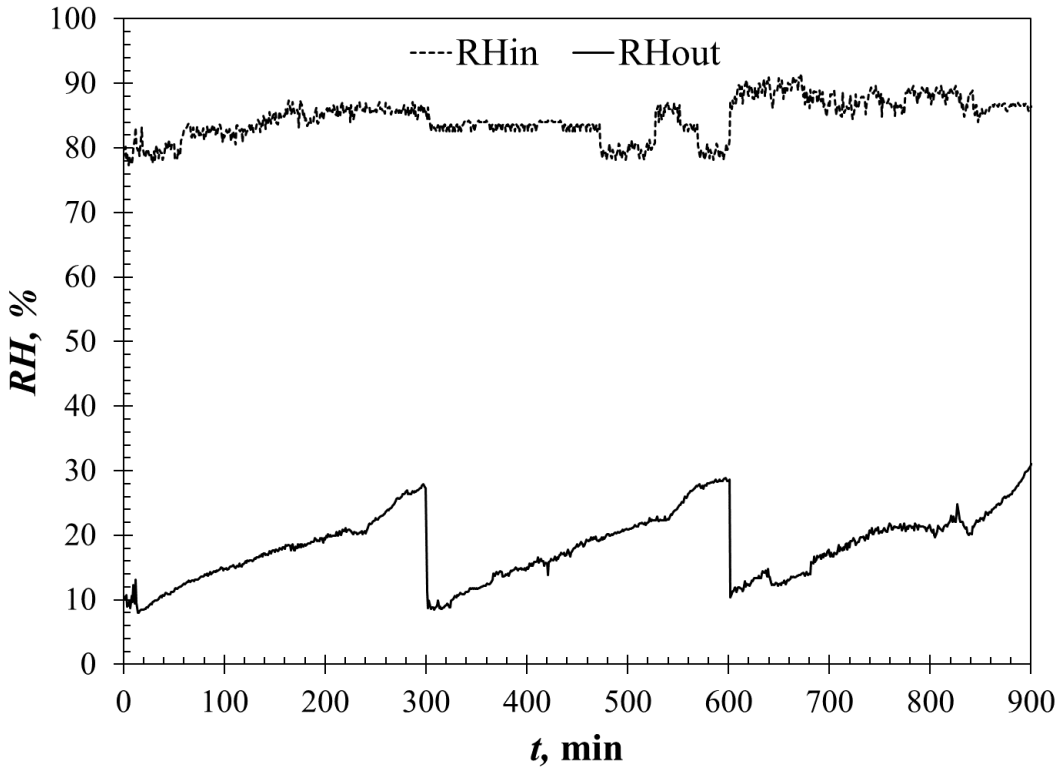

Figure 28: Variation of the relative humidity of V-$CaCl_2$ during the discharging process

Energy and exergy outputs

Figure 29 presents the cumulative energy and exergy characteristics of the novel THS system for the three discharging tests carried out on the V-$CaCl_2$ composite. The cumulative energy performance of each cycle shows a decreasing trend as compared to the previous cycle. As discussed in Section 3.1.1, this is mainly due to the incomplete desorption of the sorbate during the charging phase. The energy output of the system for each cycle was 2.26, 2.09 and 1.97 kWh, respectively. As can be seen from Figure 29, the cumulative exergy of the system was almost constant over the three discharging cycles, with values of 0.038, 0.038 and 0.037 kWh, respectively at the end of each cycle. From the analysis results, the exergy output obtained is found to be much lower as compared to the energy output. This is because the operating temperature of the THS is low (40 – 50 ºC) and therefore, the work potential of the useful output energy is limited, resulting in low exergy values. However, when comparing these values with those found in the literature [9, 31], the energy and exergy values are found to be in good agreement with previous studies.

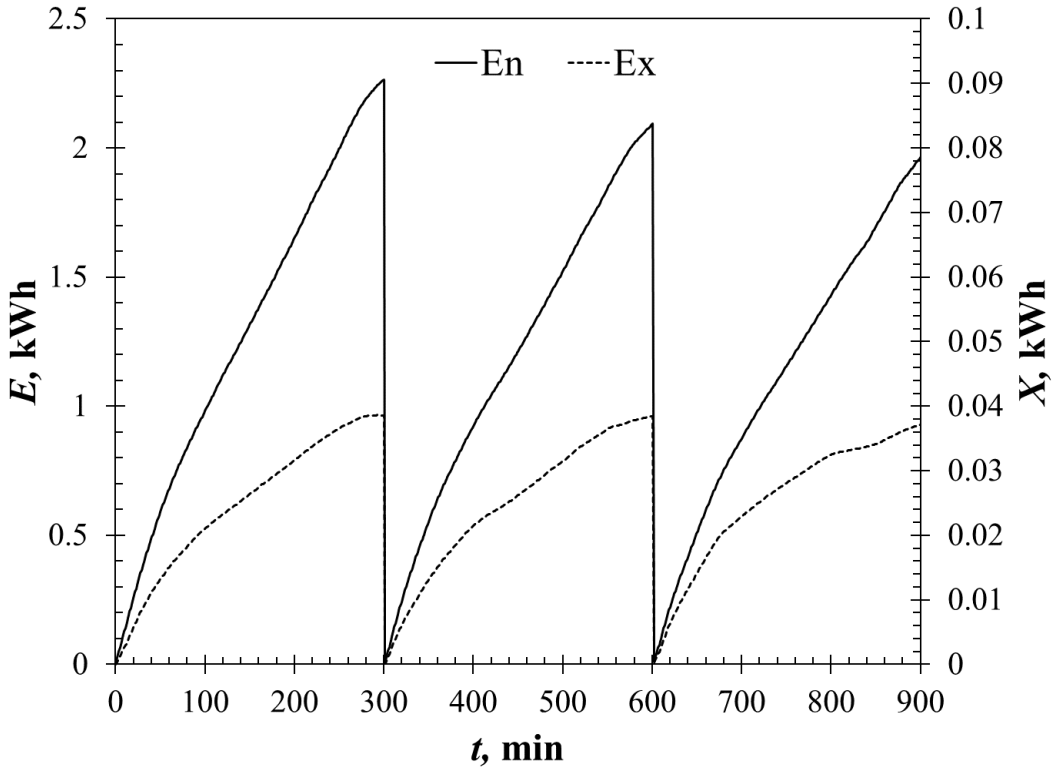

Figure 29: Variation of the energy and exergy values of V-$CaCl_2$ during the discharging process

In addition to the overall heat storage efficiency analysis described in the following section, the discharging *COP* is also important that must be determined in order to evaluate the heat storage performance during the discharging process. The discharging *COP* of the new system developed in this work is shown in Figure 30. As stated previously, it is the ratio of the useful heat output to the summation of electrical energy used by the system. As can be seen from the figure, after reaching the maximum value, the *COP* starts to decrease and from nearly the midpoint duration of each cycle, becomes approximately constant. The average value of the *COP* for the discharging cycles is 9.0, 8.4, and 7.9, respectively. As expected, the *COP* of the first cycle is the highest and it reduces in the following cycles. This is due to the decrease of the useful heat output from the first to the third cycle. However, it should be noted that the percentage drop of *COP* between the first and third cycles is only 5.5%, which

indicates that the charging performance of the solar THS unit developed in the present work is efficient. However, further auxiliary heating could be needed in order to achieve completely steady performances between the repeating cycles.

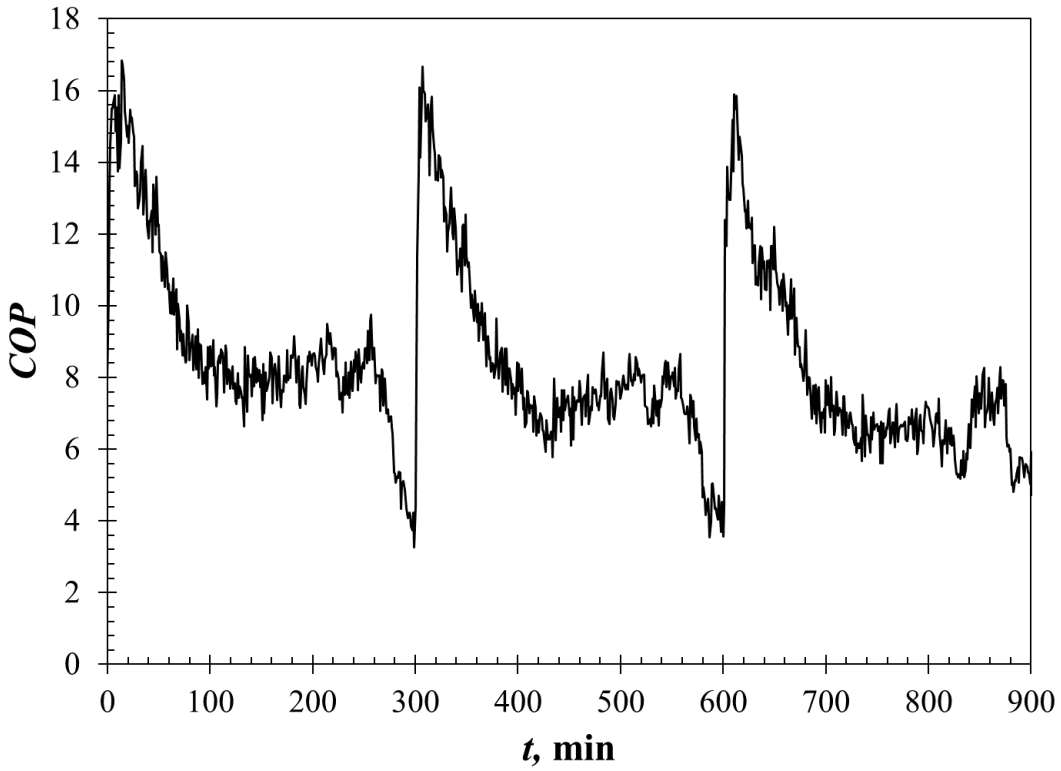

Figure 30: Variation of the COP of V-$CaCl_2$ during the discharging process

4.3.2 Charging Analysis

The variation of the intensity of solar radiation entering the THS system during the charging tests is shown in Figure 31. The charging performance depends heavily on the solar radiation absorbed by the system. In order to receive the highest radiation energy, the position of the system was changed manually during the charging tests. The solar irradiance measurements were performed every 20 minutes. The average of the solar irradiance for the three charging cycles was 850, 842 and 857 W/m^2.

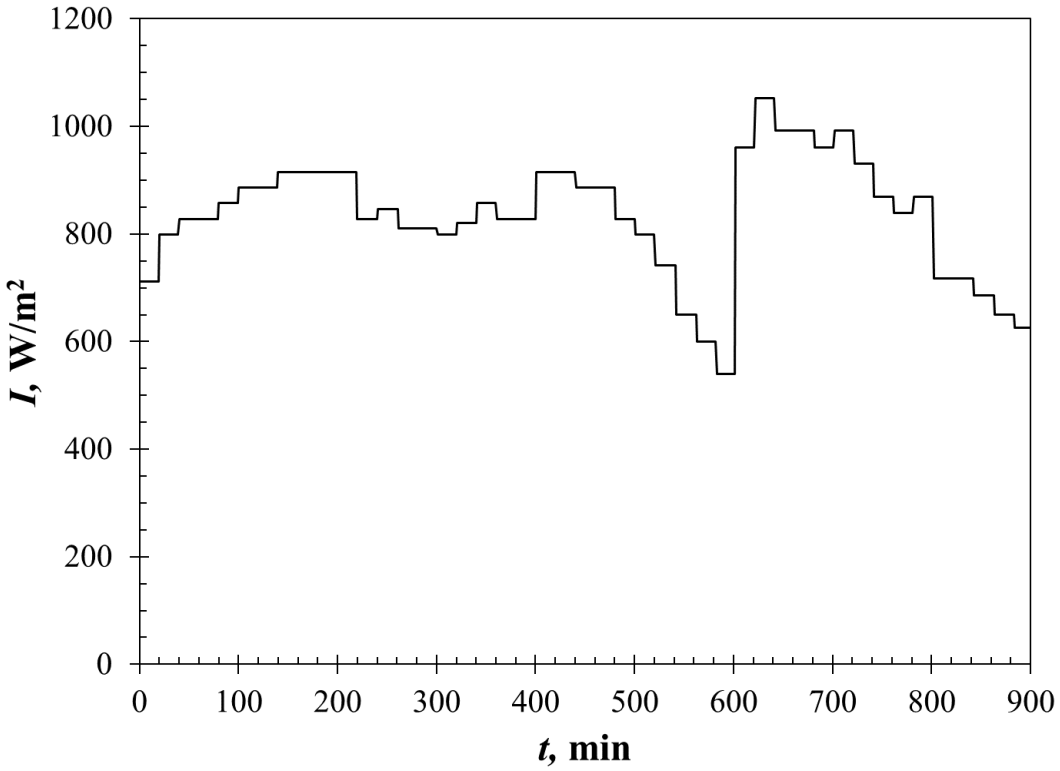

Figure 31: Variation in the intensity of solar radiation entering the THS system

Temperature and relative humidity variations

The variation of the ambient, outlet, material and reactor surface temperatures are shown in Figure 32. The average surface temperature ($T_{s,avg}$) of the reactor for all the cycles was in the range of 78 – 83 ºC. The average ambient temperature ($T_{amb,avg}$) of the cycles was 36.1, 35.0 and 34.4 ºC, respectively. The temperature of the material inside the reactor depends on the temperature on the reactor surface and the ambient temperature. The average material temperatures for the three cycles were 56.6, 55.3 and 57.2 ºC, respectively. The average outlet temperatures of the three charging cycles were 48.0, 47.1 and 46.3 ºC. Over the charging process, the solar heat energy enters the reactor via the cylinder shell and causes desorption of moisture in the sorption material to the airflow. Consequently, due to the addition of solar heat, the temperature of the airflow at the outlet of the reactor is higher than that at the inlet. As shown in

Figure 32, the outlet temperature has an increasing trend and at the end of the tests, it becomes approximately equal to the material temperature.

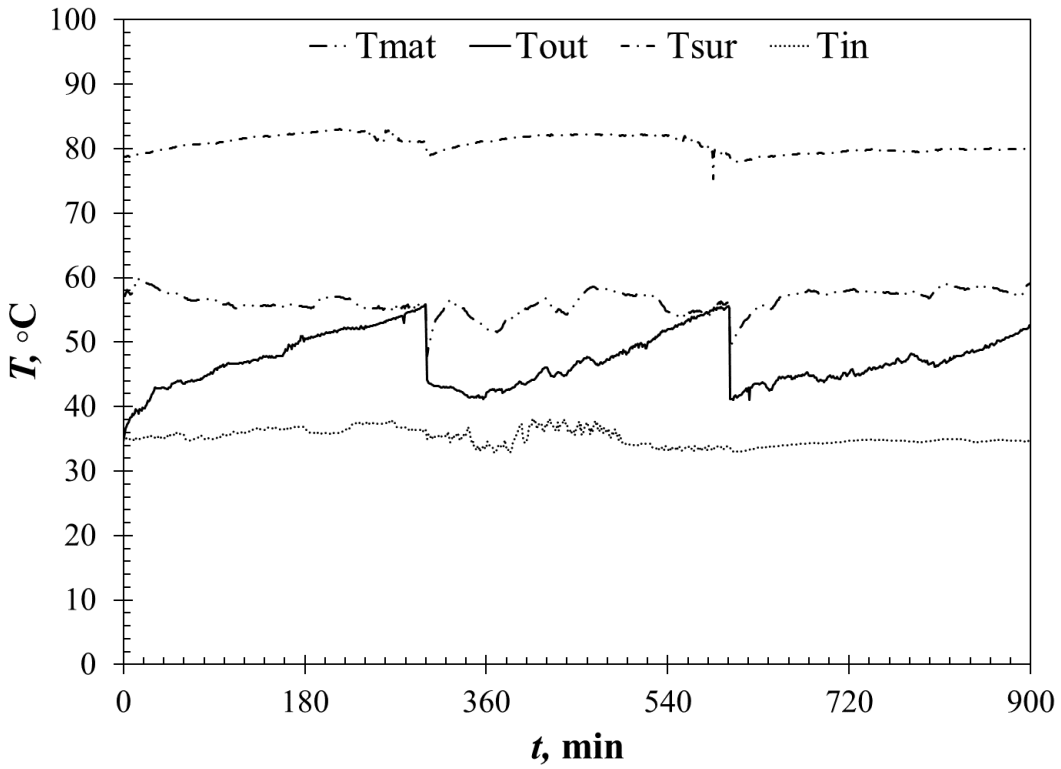

Figure 32: Variation of temperature during the charging process

The variation of the ambient and the outlet relative humidity are presented in Figure 33. The average of the ambient relative humidity for the three cycles is 45.0%, 46.3%, and 47.4 %, respectively, whereas, the average outlet relative humidity is 28.1%, 30.0%, and 30.5%, respectively.

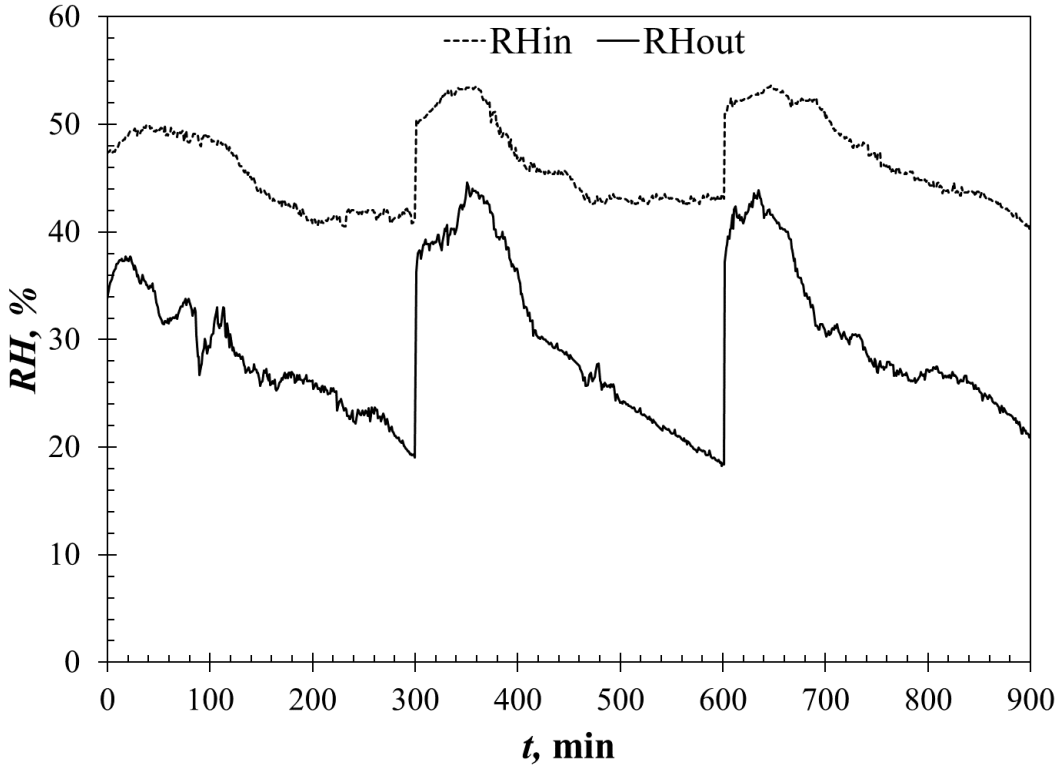

Figure 33: Variation of the relative humidity during the charging process

Energy inputs and outputs

The variation of the solar energy that entered inside the THS system during the charging cycle is shown in Figure 34. The solar energy input to the system was calculated by multiplying the concentrator aperture area (A_a) by the solar irradiance (I),

$$Q_{solar} = I.A_a \quad (28)$$

The average of the input solar energy for the three cycles is 1.02, 1.11 and 1.20 kW, respectively.

The useful energy and solar energy over the charging cycles are presented in Figure 35. Useful energy is defined as the energy difference between the outlet and the inlet airflow.

$$\dot{Q}_{useful} = \dot{m_{cr}}(h_{out} - h_{in}) \quad (29)$$

From the analysis results, the cumulative solar energy that enters inside the THS system for the three charging cycles was found to be 5.11, 5.57 and 6.01 kWh, respectively and total useful energy for the cycles was found to be 4.36, 3.80 and 3.67 kWh, respectively. As it is illustrated in Figure 35, despite the cumulative solar energy entered to the system increased from cycle 1 to cycle 3, the useful energy has decreased in the proceeding cycles and this is mainly due to reason that the sorbent composite material was not completely dried in each cycle and the amount of moisture remained inside the material increased in each cycle.

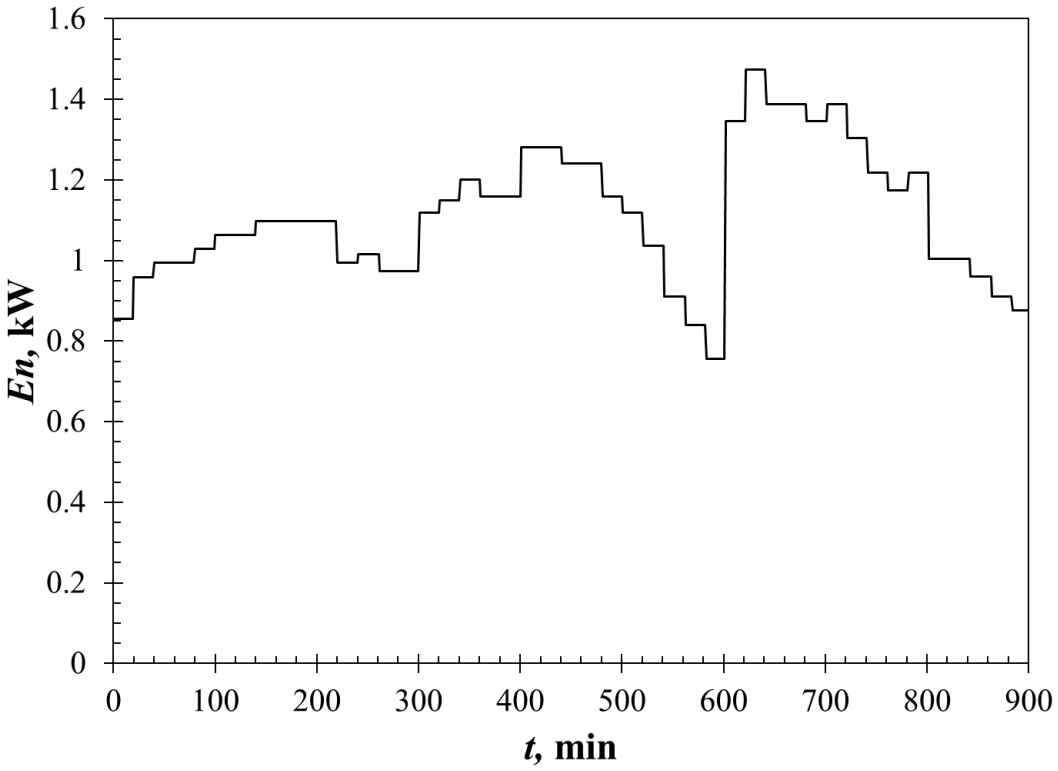

Figure 34: Variation of the input solar energy

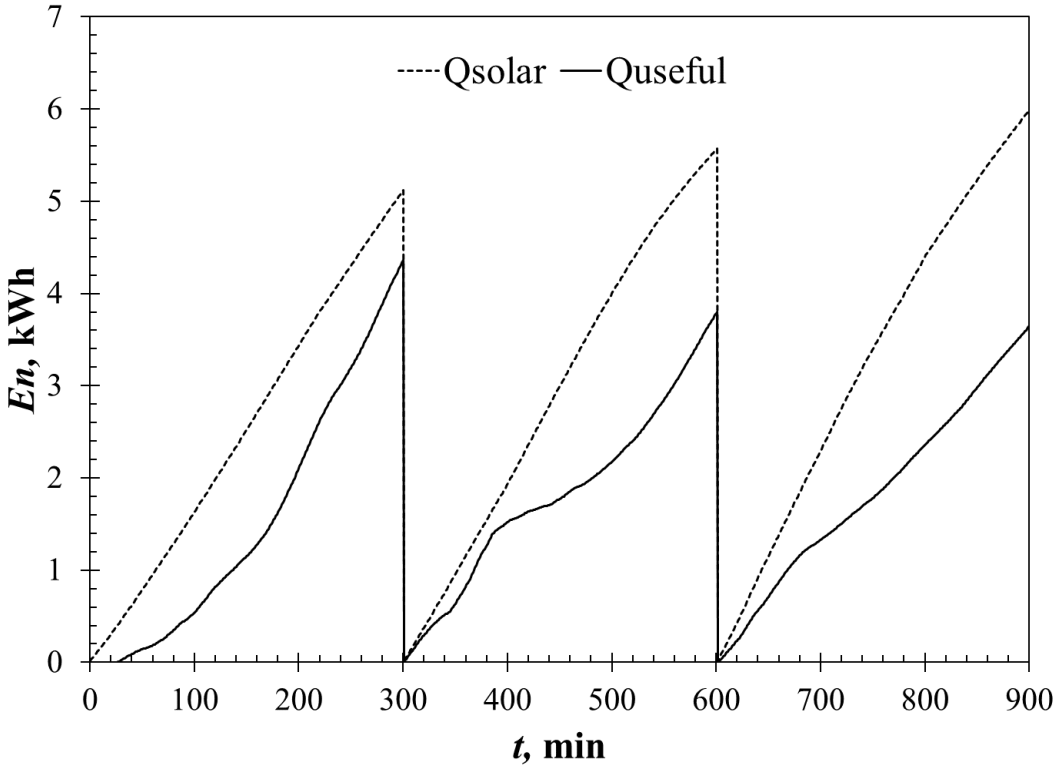

Figure 35: Variation of the cumulative solar energy and cumulative useful energy

4.3.3 Overall Cyclic Analysis

The discharging-charging cycles were started after completely drying the V-$CaCl_2$ composite material at 150 ºC in an electrical furnace. Numerical values of the different performance parameters obtained from the tests performed during the discharging and charging stages are given in Tables 10 and 11, respectively.

The charging efficiency (η_{cr}) and overall efficiency $(\eta_{overall})$ are defined as:

$$\eta_{cr} = \frac{Q_{useful}}{Q_{solar}} \tag{30}$$

$$\eta_{overall} = \frac{Q_{dcr}}{Q_{solar}} \tag{31}$$

Values of η_{cr}, $\eta_{overall}$ and the hygrothermal efficiency (η_{hyg}) are given in Table 12.

Table 10: Numerical values of the different performance parameters obtained from the test carried out during the discharging stage

Material	Cycle	T_{out} (ºC) ±1.2%	ΔT_{avg} (ºC) ±1.2%	$\Delta \dot{Q}$ (kW) ±1.6%	E (kWh) ±2.1%	$\dot{X}$ (kW) ±1.6%	X (kWh) ±2.1%	$M_{w\text{-}abs}$ (g) ±2.0%	E_d (kWh/m^3) ±2.9%	y (g/min) ±3.1%
V-$CaCl_2$	1	43.2	19.6	0.451	2.265	0.007	0.038	2974	168	9.879
	2	42.4	18.1	0.417	2.094	0.007	0.038	3150	155	10.468
	3	37.9	17.0	0.393	1.972	0.007	0.037	2802	146	9.324

Table 11: Numerical values of the performance parameters obtained from the test carried out during the charging stage

Material	Cycle	T_{out} (ºC) ±1.2%	ΔT_{avg} (ºC) ±1.2%	T_s (ºC) ±1.2%	T_m (ºC) ±1.2%	E_{useful} (kWh) ±2.1%	E_{solar} (kWh) ±2.1%	$M_{w\text{-}des}$ (g) ±2.0%	I_{avg} (W/m^2) ±2.5%	y (g/min) ±3.1%
V-$CaCl_2$	1	48.0	11.9	81.3	56.4	4.36	5.12	1909	850	6.343
	2	47.1	12.2	81.3	55.3	3.68	5.57	1988	841	6.605
	3	46.4	11.9	79.3	57.2	3.80	6.01	1972	857	6.552

Table 12: Charging, overall and hygrothermal efficiencies

Material	Cycle	η_{cr} ±2.4%	η_{overal} ±3.0%	η_{hyg} ±2.3%
V-$CaCl_2$	1	0.852	0.442	0.642
	2	0.661	0.376	0.631
	3	0.632	0.328	0.704

The charging efficiency (η_{cr}) of the system, which the ratio of the useful energy to the input solar energy, has been plotted as a function of cycles in Figure 36. Due to the incomplete charging process, some moisture remains inside the material and thus, the charging efficiency of the system decreases from the first to the last cycle. The average η_{cr} for the charging cycles is 0.85, 0.66 and 0.63, respectively.

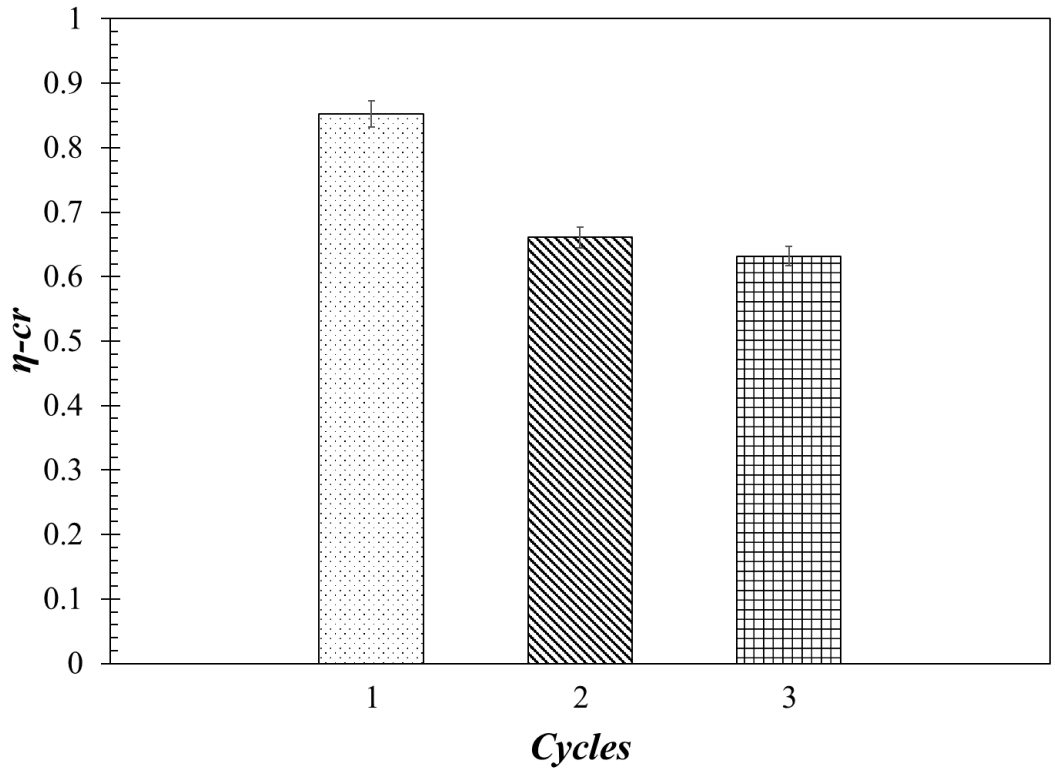

Figure 36: Charging efficiency of the THS system

The overall efficiency ($\eta_{overall}$) of the system for every discharging–charging cycle is presented in Figure 37. It is defined as the ratio of the cumulative discharging energy to the cumulative input solar energy. The average values of $\eta_{overall}$ of the system are 0.44, 0.38 and 0.33 for the three cycles. As mentioned before, due to insufficient desorption, some moisture remains inside the sorption material and consequently, the discharging energy decreases over the cycles. Therefore, despite the increase in the cumulative solar energy in the cycles (see Table 12), $\eta_{overall}$ is reduced in the subsequent cycles.

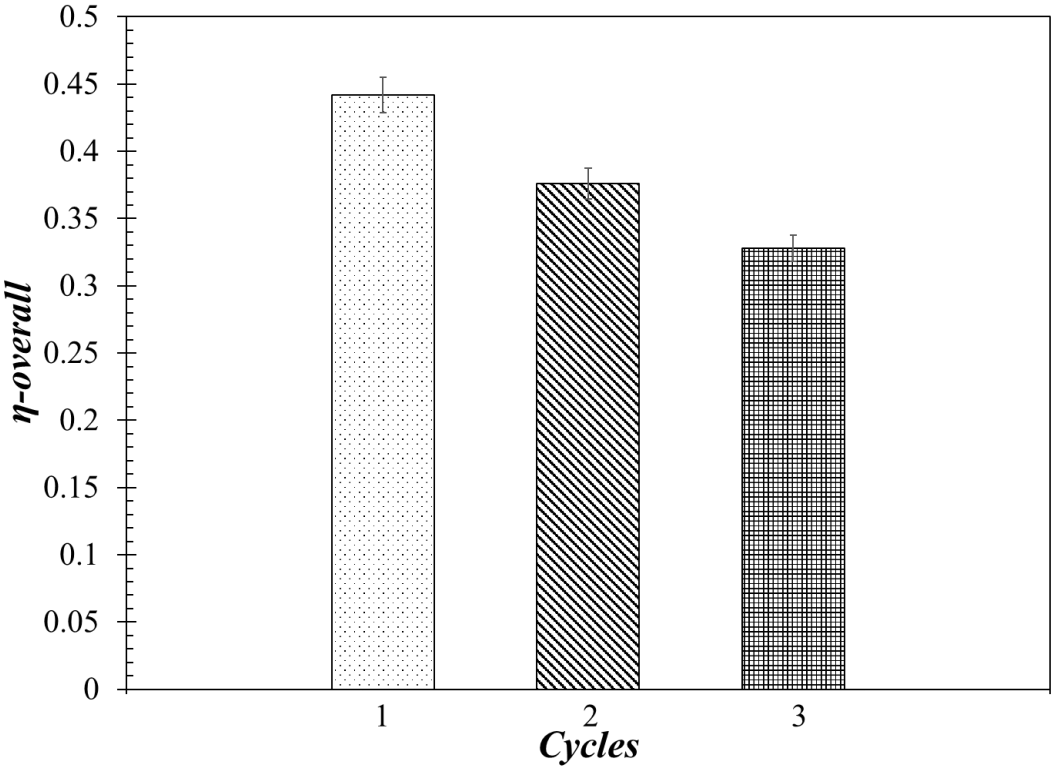

Figure 37: Charging efficiency of the THS system

The hygrothermal efficiency (η_{hyg}) is shown in Figure 38. The average values of the hygrothermal efficiency for the three cycles are 0.64, 0.63 and 0.70, respectively. This result shows that with volumetric air flow rate of 0.03 m^3/s and the average input solar energy of 1.1 kW, proposed solar driven THS system has a steady desorption performance. Despite the V-$CaCl_2$ couldn't fully regenerated at the applied solar charging temperature, the overall hygrothermal performance of it over repeating cycles was found stable with a hygrothermal efficiency in the range of 60 – 70%. Accordingly obtained experimental results concluded that, in the proposed design, V-$CaCl_2$ could be utilized for short term or seasonal heat storage with good cyclic performance.

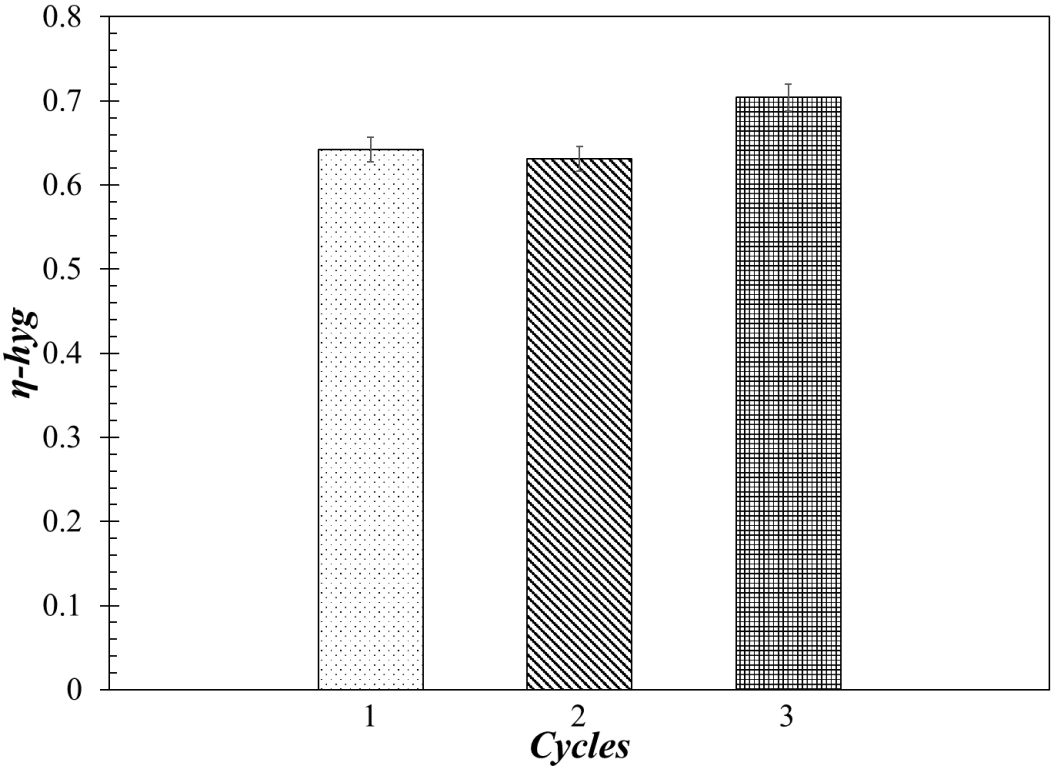

Figure 38: Hygrothermal efficiency of the THS system

A plot showing the amount of the adsorption and desorption of water over the discharging and charging phases is given in Figure 39. As illustrated, the desorption amount is less than the sorption amount for every discharging–charging cycle. This is mainly due to the insufficient amount of desorption over the charging phases. The primary reason for the incomplete drying of the material during the charging process was the high moisture content of the inlet air.

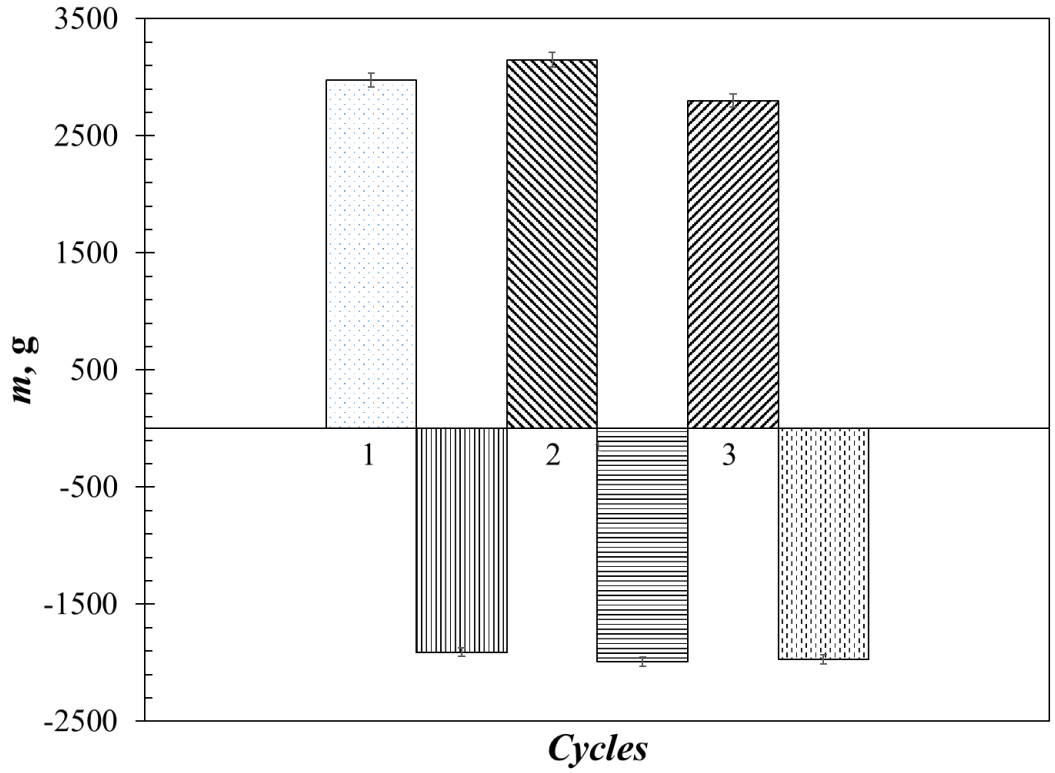

Figure 39: Total amount of absorbed/desorbed water mass over repeating cycles

4.4 Economic Analysis of the New THS System

In order to evaluate the economic and technical performance of the new THS system developed in this work, the annual heating load of a residential building was simulated under North Cyprus climatic conditions. DesignBuilder software was used to simulate the energy consumption and environmental effects on the designed building. A schematic of the simulated building is shown in Figure 40. The simulated dwelling is a single floor building having an area of A = 90 m^2 and consists of a bedroom, a kitchen-living saloon, and a bathroom.

Because that the weather data for Famagusta is not included in DesignBuilder software, Larnaca, which is the closest available location to Famagusta in Cyprus, has

been selected as the test location. As the distance between these cities is very short, year round climatic conditions of Larnaca and Famagusta is considered as same.

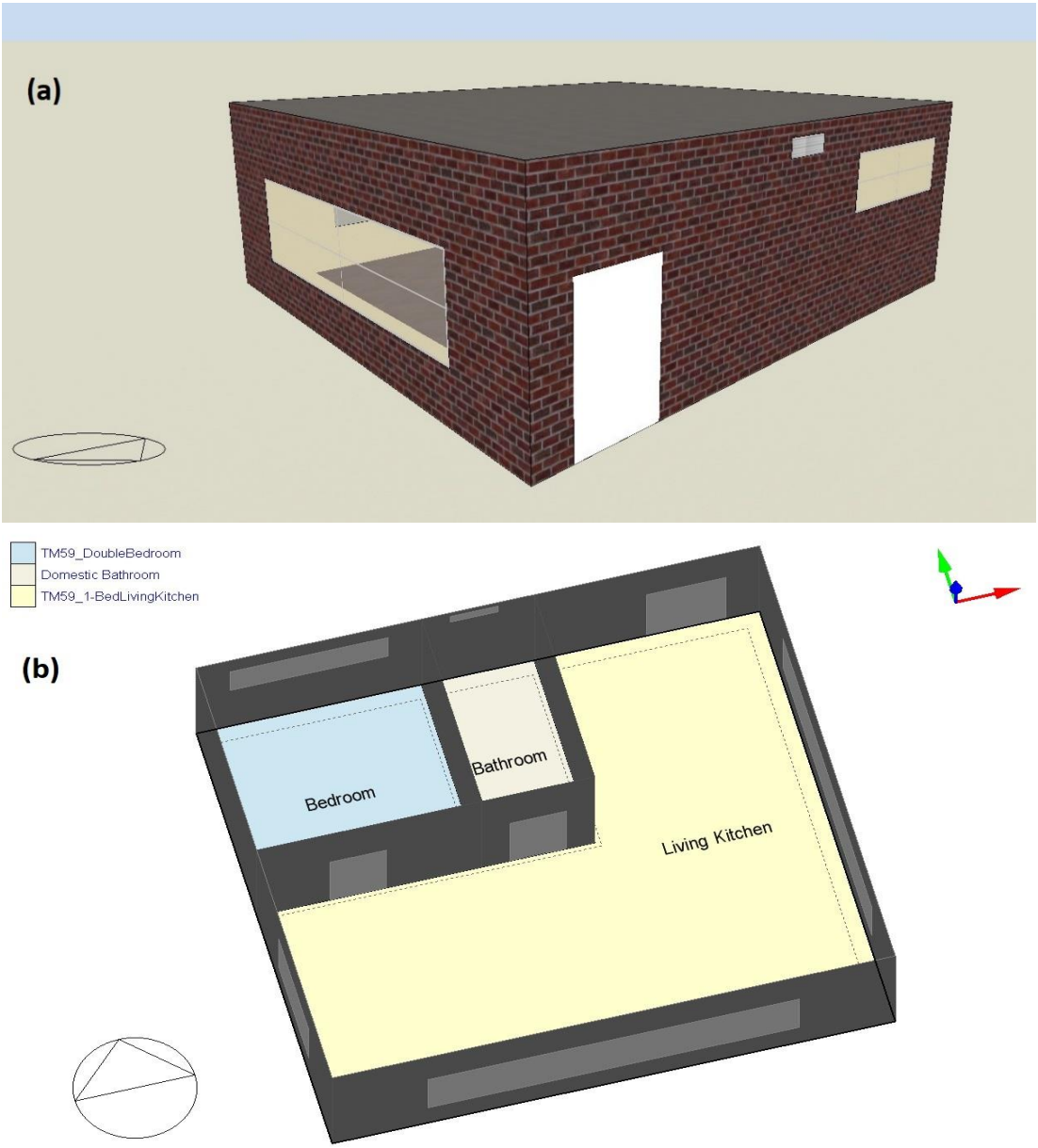

Figure 40: (a) 3-D schematic view and (b) plan view of the simulated building

The parameters of the HVAC system that were used in the DesignBuilder software for calculating the heating load are given in Table 13 while Table 14 gives the numerical values of the rate of heat transfer of the simulated building components.

Table 13: Parameters of the HVAC system used for the simulation of the building

Parameter	Unit	Value
HVAC system	NA	Split no fresh air
Heating set point temperatures	ºC	Heating → 21
		Heating set back → 12
Fuel	NA	Electricity from grid
COP	W/W	2.35
Air velocity for comfort calculations	m/s	0.1370
Design margin in system sizing	NA	1.25
Maximum supply air temperature	ºC	35
Maximum supply air humidity ratio	g/g	0.0156

Table 14: Rate of the heat transfer (U) of the building components

Surface	U ($W/m^2.K$)
Wall	0.353
Roof	0.250
Floor	0.253
Window	2.665
Door	5.429

From the simulation results, it is found that the electrical energy required to supply heat inside the building for one year is 581.507 kWh which corresponds to 1366 kWh thermal energy. The test results of the new sorption unit and laboratory-scale THS unit, developed in this study, gave the average energy density (E_d) of V-$CaCl_2$ as 156 kWh/m^3. The volume of the solar-driven THS system that can provide this amount of thermal energy was calculated to be V_s = 8.75 m^3.

In order to assess the potential of the proposed THS system, a simplified economic feasibility analysis has been performed. The attractiveness of a solar-driven THS system depends on the initial investment, annual fuel-saving, discount rate, and annual maintenance cost. The proposed THS system has been compared with an equivalent split unit heat pump system. The electricity tariff in North Cyprus based on the time of consumption is different and hence, US$ 0.12 was considered as the average tariff in this study. In North Cyprus, the heat pump mode of a split air conditioner is generally used for heating purposes. The equations used for determining the net present value (*NPV*), saving to investment ratio (*SIR*), simple payback period (*SPP*) and internal rate of return (*IRR*) in the economic feasibility analysis are as follows:

$$NPV = \Sigma PV_{AS} - \Sigma PV_{LCI} \quad (32)$$

where PV_{LCI} is the present value life cycle investment and PV_{AS} is the present value annual saving.

$$SIR = \frac{\Sigma PV_{AS}}{\Sigma PV_{LCI}} \quad (33)$$

$$SPP = \frac{Initial\ investment}{Annual\ saving} \quad (34)$$

IRR can be obtained when *SIR=1,* or NPV=0. (35)

A project could be considered economically feasible if SIR > 1, NPV > 0 and IRR > discount rate.

Table 15 gives the costs of the different components and the sorption material that were utilized in the THS system developed and tested in this work. The installation of the proposed sorption THS system, which can produce 1366 kWh thermal energy, costs $772, which is considered as the capital investment of the project. Increasing electricity consumption for thermal usage in the building causes a decrease of the payback period and this results in a corresponding increase in the size of the THS

system. Based on the results of the analysis performed for a 10-years simulated duration, the usage of the THS system is found to be economically feasible as compared to a heat pump split unit. The values of the different parameters considered in the economic feasibility analysis are as follows: NPV = $381, SIR = 1.6, IRR = 12% and SPP = 6.4 years and indicate that the THS system developed in this work is an economically feasible system.

Table 15: Cost of the components used in the THS system

Item	Cost ($)
Concentrator and frame	140.4
Sorption pipe unit	175.5
Construction, ducting	87.7
Fan and humidifiers	87.7
Sorption material	280.7

To summarize, in this chapter, a detailed description of the performance of the new solar-driven THS system, developed in the present work, under Northern Cyprus climatic conditions was presented. By considering the discharging-charging results, it can be anticipated that the proposed system can reach higher sorption performance in a low humidity climate. Due to the high moisture content of air in North Cyprus, the desorption performance was below the value that could be reached for V-$CaCl_2$ in the laboratory-scale tests.

Chapter 5

CONCLUSIONS

5.1 Synthesis and Experimentation of Novel Composite Sorbents

In this study, a novel composite THS material using APC as the host matrix and $CaCl_2$ as the sorbent has been synthesized and experimentally investigated in a laboratory-scale fixed-bed open THS system. In the study, a comparative investigation of the hygro-thermal performance of APC-$CaCl_2$, V-$CaCl_2$, P-$CaCl_2$, and zeolite was performed and the following conclusions were drawn:

- Based on the experimental measurements carried out for 3 h charging between T_i = 85 – 95 ºC and $\dot{m}_{cr}$ = 0.04 kg/s, zeolite was found to show poor desorption kinetics as compared to salt-based composites. For V-$CaCl_2$, P-$CaCl_2$, and APC-$CaCl_2$, η_{hyg} was 0.8, whereas, it was 0.33 for zeolite.
- Discharging cycles were performed over 5 h under the operating conditions of $\dot{m}_{dcr}$ = 0.02 kg/s, T_i = 20 –21 ºC and RH = 85–90%. For three consecutive cycles, ΔT_{avg} in the range of 16 → 15 ºC, 23 → 10 ºC, 18 → 16 ºC, and 22.4 → 18.1 ºC were obtained for V – $CaCl_2$, zeolite, APC – $CaCl_2$, and P – $CaCl_2$, respectively. Similarly, the values of E_d varied between 180 → 163 kWh/m^3, 251 → 114 kWh/m^3, 196 → 175 kWh/m^3, and 234 → 165 kWh/m^3, respectively for the same order of the materials. Accordingly, more than 50% drop in E_d was observed for zeolite from the first to the third cycle. On the contrary, E_d of V-$CaCl_2$, APC-$CaCl_2$, and P-$CaCl_2$ were steadier over the repeating cycles. Energy storage densities of V-$CaCl_2$, zeolite, APC-$CaCl_2$ and

P-$CaCl_2$ per unit mass of water absorption, have been determined to be 0.75 → 0.61 Wh/g, 0.82 → 0.67 Wh/g, 0.89 → 0.81 Wh/g and 0.69 → 0.75 Wh/g, respectively.

In contrast to the previous research studies on THS, in this study, four different candidate materials (APC-$CaCl_2$, V-$CaCl_2$, P-$CaCl_2$, zeolite 13X) were comparatively investigated via the full cycle analyses. In addition, the experimental results obtained were compared with previous studies available in the literature. In line with the objectives of this study, a low cost (< $ 0.5/kg) sorbent (APC-$CaCl_2$) with an energy density of >150 kWh/m^3 (at T_{cr} = 90 °C) was realized and its performance was found to be superior as compared to the previously developed sorbents.

Outcomes from the performed research demonstrate that new salt-based composites could be promising alternatives that could be used in the future advancement of solar/waste heat driven THS applications. The developed APC-$CaCl_2$ composite is seen to exhibit structural, thermal and hygroscopic stability over the repeating cycles. Its overall performance was found to be comparable with V-$CaCl_2$ and P-$CaCl_2$. In addition, its rigid structure was observed to be more advantageous, as compared to V-$CaCl_2$'s spongy structure, in terms of providing physical stability to the sorption bed, minimizing the drop in air pressure and enabling a uniform heat and mass transfer across the sorption bed. Future research direction could be the detailed characterization and optimization of APC-$CaCl_2$ for further advancement in its sorption kinetics, the efficiency of heat/mass transfer and structural stability. Such a material could find applications not only in THS processes but also in air dehumidification/purification units and in desiccant cooling systems.

5.2 Design and Development of an Adsorptive Solar Thermal Energy Storage Unit

The performance of the new solar-driven THS system developed in the present work was examined under North Cyprus climatic conditions. In addition, an economic feasibility comparison between the developed THS system and a typical heat pump split unit was performed for a house simulated using the DesignBuilder software package. Based on the analysis results, the important conclusions are listed below:

- Three discharging- charging cycles utilizing V-$CaCl_2$ as the sorption material were conducted in the new THS system developed in this work. Over five hours of discharging at T_i = 21 – 24 °C and $\dot{m}_{cr}$= 0.03 m^3/s, the $\eta_{overall}$ value was 0.38 while η_{hyg} was 0.66. The E_d values varied between 180 → 163 kWh/m^3 and the energy storage density per unit mass of water absorption was 0.76 → 0.70 Wh/g.
- Over five hours of the charging process of V-$CaCl_2$, the average charging efficiency (η_{cr}) varied between 0.85 → 0.63. In addition, the average desorption rate of moisture (y_{des}) was found to be 6.5 g/min.
- The annual heating load of a residential building with a surface area of 90 m^2 was simulated using the DesignBuilder software. An economic feasibility comparison between the proposed solar-driven THS system and a heat pump used in the simulated house was performed. From the results obtained, it was found that a THS system with 8.75 m^3 is required to meet the heating load of the building. Based on the economic feasibility analysis, the following values were obtained: NPV = $381, SIR = 1.6, IRR = 12% and SPP = 6.4 years. Therefore, the THS system was found to be economically feasible for using in residential buildings in North Cyprus.

5.3 Future Work and Recommendations

Taking into consideration the study performed in this work, further studies could be conducted as follows:

- Synthesis of new composites with a lower regeneration temperature and strong physical stability,
- Development of new solar-driven THS systems with higher charging, overall and hygrothermal efficiencies,
- Using fins and heat pipes for enhancing the heat transfer inside the reactor,
- Development of modular reactors for simplifying the heat/mass transfer process and operational control,
- Development of real-life pilot projects for the dissemination of solar thermal storage and industrial waste heat recovery with thermochemical materials and
- Coupling of THS systems to other conventional heating or cooling systems for improving the energetic and exergetic efficiencies of the whole system.

REFERENCES

[1] I. e. agency., "International energy agency. https://www.iea.org/wei2019/overview/."

[2] I. e. agency., " renewables 2018. https://www.iea.org/renewables2018/."

[3] I. e. agency., "renewables 2018/heat. https://www.iea.org/renewables2018/heat/."

[4] G. Alva, L. Liu, X. Huang, and G. Fang, "Thermal energy storage materials and systems for solar energy applications," *Renewable and Sustainable Energy Reviews*, vol. 68, pp. 693-706, 2017/02/01/ 2017.

[5] D. Gondre, K. Johannes, and F. Kuznik, "Specification requirements for inter-seasonal heat storage systems in a low energy residential house," *Energy Conversion and Management*, vol. 77, pp. 628-636, 2014/01/01/ 2014.

[6] X. Zhang, M. Li, W. Shi, B. Wang, and X. Li, "Experimental investigation on charging and discharging performance of absorption thermal energy storage system," *Energy Conversion and Management*, vol. 85, pp. 425-434, 2014/09/01/ 2014.

[7] H. Jarimi *et al.*, "Materials characterization of innovative composite materials for solar-driven thermochemical heat storage (THS) suitable for building

application," *International Journal of Low-Carbon Technologies,* vol. 13, no. 1, pp. 30-42, 2018.

[8] S. Katulić, M. Čehil, and Ž. Bogdan, "A novel method for finding the optimal heat storage tank capacity for a cogeneration power plant," *Applied Thermal Engineering,* vol. 65, no. 1, pp. 530-538, 2014/04/01/ 2014.

[9] S. P. Casey, D. Aydin, S. Riffat, and J. Elvins, "Salt impregnated desiccant matrices for 'open' thermochemical energy storage—Hygrothermal cyclic behaviour and energetic analysis by physical experimentation," *Energy and Buildings,* vol. 92, pp. 128-139, 2015/04/01/ 2015.

[10] Z. J. Huang F, Baleynaud JM, Lu J, "Heat recovery potentials and technologies in industrial zones. Journal of the Energy Institute," *Journal of the Energy Institute,* vol. 90, pp. 951-961, 2017.

[11] E. J. L. Energy, UK: Department of Energy and C. Change, "The potential for recovering and using surplus heat from industry," 2014.

[12] W. Institute, "State of The World Confronting Climate Change 2009," *Earthscan Publishing,* 2009.

[13] I. BCS, US Department of Energy, Industrial Technologies Program, "Waste Heat Recovery: Technology and Opportunities in U.S. Industry," 2008.

[14] K. E. N'tsoukpoe, H. Liu, N. Le Pierrès, L. J. R. Luo, and S. E. Reviews, "A review on long-term sorption solar energy storage," vol. 13, no. 9, pp. 2385-2396, 2009.

[15] D. Aydin, S. P. Casey, S. J. R. Riffat, and S. E. Reviews, "The latest advancements on thermochemical heat storage systems," vol. 41, pp. 356-367, 2015.

[16] N. Yu, R. Wang, L. J. P. i. E. Wang, and C. Science, "Sorption thermal storage for solar energy," vol. 39, no. 5, pp. 489-514, 2013.

[17] Y. I. J. J. o. C. E. o. J. ARISTOV, "Novel materials for adsorptive heat pumping and storage: screening and nanotailoring of sorption properties," pp. 0710050048-0710050048, 2007.

[18] L. Gordeeva and Y. I. J. I. J. o. L.-C. T. Aristov, "Composites 'salt inside porous matrix' for adsorption heat transformation: a current state-of-the-art and new trends," vol. 7, no. 4, pp. 288-302, 2012.

[19] I. Ponomarenko, I. Glaznev, A. Gubar, Y. I. Aristov, S. J. M. Kirik, and m. materials, "Synthesis and water sorption properties of a new composite "CaCl2 confined into SBA-15 pores"," vol. 129, no. 1-2, pp. 243-250, 2010.

[20] J. Veselovskaya, R. Critoph, R. Thorpe, S. Metcalf, M. Tokarev, and Y. I. J. A. t. e. Aristov, "Novel ammonia sorbents "porous matrix modified by active salt" for adsorptive heat transformation: 3. Testing of "BaCl2/vermiculite"

composite in a lab-scale adsorption chiller," vol. 30, no. 10, pp. 1188-1192, 2010.

[21] Y. I. Aristov, G. Di Marco, M. Tokarev, V. J. R. K. Parmon, and C. Letters, "Selective water sorbents for multiple applications, 3. CaCl 2 solution confined in micro-and mesoporous silica gels: Pore size effect on the “solidification-melting” diagram," vol. 61, no. 1, pp. 147-154, 1997.

[22] Y. I. Aristov, G. Restuccia, G. Cacciola, and V. J. A. T. E. Parmon, "A family of new working materials for solid sorption air conditioning systems," vol. 22, no. 2, pp. 191-204, 2002.

[23] Y. I. Aristov, G. Restuccia, M. Tokarev, G. J. R. K. Cacciola, and C. Letters, "Selective water sorbents for multiple applications, 10. Energy storage ability," vol. 69, no. 2, pp. 345-353, 2000.

[24] Y. I. Aristov, M. Tokarev, G. Cacciola, G. J. R. K. Restuccia, and C. Letters, "Selective water sorbents for multiple applications, 1. CaCl 2 confined in mesopores of silica gel: sorption properties," vol. 59, no. 2, pp. 325-333, 1996.

[25] Y. I. Aristov, M. Tokarev, G. Restuccia, G. J. R. K. Cacciola, and C. Letters, "Selective water sorbents for multiple applications, 2. CaCl 2 confined in micropores of silica gel: Sorption properties," vol. 59, no. 2, pp. 335-342, 1996.

[26] B. Okunev, A. Gromov, L. Heifets, Y. I. J. I. J. o. H. Aristov, and M. Transfer, "A new methodology of studying the dynamics of water sorption/desorption

under real operating conditions of adsorption heat pumps: Modelling of coupled heat and mass transfer in a single adsorbent grain," vol. 51, no. 1-2, pp. 246-252, 2008.

[27] Y. I. J. J. o. E. T. Aristov, "New family of solid sorbents for adsorptive cooling: material scientist approach," vol. 16, no. 2, pp. 63-72, 2007.

[28] W. Wongsuwan, S. Kumar, P. Neveu, and F. J. A. t. e. Meunier, "A review of chemical heat pump technology and applications," vol. 21, no. 15, pp. 1489-1519, 2001.

[29] H. Liu, K. Nagano, D. Sugiyama, J. Togawa, and M. Nakamura, "Honeycomb filters made from mesoporous composite material for an open sorption thermal energy storage system to store low-temperature industrial waste heat," *International Journal of Heat and Mass Transfer,* vol. 65, pp. 471-480, 2013/10/01/ 2013.

[30] M. Gaeini, A. L. Rouws, J. W. O. Salari, H. A. Zondag, and C. C. M. Rindt, "Characterization of microencapsulated and impregnated porous host materials based on calcium chloride for thermochemical energy storage," *Applied Energy,* vol. 212, pp. 1165-1177, 2018/02/15/ 2018.

[31] D. Aydin, S. P. Casey, X. Chen, and S. Riffat, "Novel “open-sorption pipe” reactor for solar thermal energy storage," *Energy Conversion and Management,* vol. 121, pp. 321-334, 2016/08/01/ 2016.

[32] B. Michel, N. Mazet, and P. Neveu, "Experimental investigation of an open thermochemical process operating with a hydrate salt for thermal storage of solar energy: Local reactive bed evolution," *Applied Energy*, vol. 180, pp. 234-244, 2016/10/15/ 2016.

[33] Y. N. Zhang, R. Z. Wang, and T. X. Li, "Experimental investigation on an open sorption thermal storage system for space heating," *Energy*, vol. 141, pp. 2421-2433, 2017/12/15/ 2017.

[34] P. D'Ans *et al.*, "Humidity dependence of transport properties of composite materials used for thermochemical heat storage and thermal transformer appliances," *Journal of Energy Storage*, vol. 18, pp. 160-170, 2018/08/01/ 2018.

[35] P. Tatsidjodoung, N. Le Pierrès, J. Heintz, D. Lagre, L. Luo, and F. Durier, "Experimental and numerical investigations of a zeolite 13X/water reactor for solar heat storage in buildings," *Energy Conversion and Management*, vol. 108, pp. 488-500, 2016/01/15/ 2016.

[36] J. Jänchen *et al.*, "Performance of an open thermal adsorption storage system with Linde type A zeolites: Beads versus honeycombs," vol. 207, pp. 179-184, 2015.

[37] L. Shere, S. Trivedi, S. Roberts, A. Sciacovelli, and Y. J. H. T. E. Ding, "Synthesis and Characterization of Thermochemical Storage Material Combining Porous Zeolite and Inorganic Salts," pp. 1-6, 2018.

[38] R. van Alebeek, L. Scapino, M. Beving, M. Gaeini, C. Rindt, and H. J. A. T. E. Zondag, "Investigation of a household-scale open sorption energy storage system based on the Zeolite 13X/water reacting pair," vol. 139, pp. 325-333, 2018.

[39] C. Xu, Z. Yu, Y. Xie, Y. Ren, F. Ye, and X. J. A. T. E. Ju, "Study of the hydration behavior of zeolite-MgSO4 composites for long-term heat storage," vol. 129, pp. 250-259, 2018.

[40] A. Mehrabadi and M. Farid, "New salt hydrate composite for low-grade thermal energy storage," *Energy,* vol. 164, pp. 194-203, 2018/12/01/ 2018.

[41] F. Kuznik, D. Gondre, K. Johannes, C. Obrecht, and D. J. R. E. David, "Numerical modelling and investigations on a full-scale zeolite 13X open heat storage for buildings," vol. 132, pp. 761-772, 2019.

[42] C. Bales *et al.*, "Laboratory tests of chemical reactions and prototype sorption storage units," vol. 32, 2008.

[43] A. Hauer, "Open absorption systems for air conditioning and thermal energy storage," in *Thermal energy storage for sustainable energy consumption*: Springer, 2007, pp. 429-444.

[44] G. Krese, V. Butala, U. J. E. Stritih, and Buildings, "Thermochemical seasonal solar energy storage for heating and cooling of buildings," 2018.

[45] B. Mette, H. Kerskes, and H. Drück, "Process and reactor design for thermo-chemical energy stores," in *ISES Solar World Congress*, 2011, vol. 28.

[46] D. Aydin, S. P. Casey, X. Chen, and S. J. A. E. Riffat, "Numerical and experimental analysis of a novel heat pump driven sorption storage heater," vol. 211, pp. 954-974, 2018.

[47] S. Xu, R. Wang, L. Wang, J. J. E. C. Zhu, and Management, "A zeolite 13X/magnesium sulfate–water sorption thermal energy storage device for domestic heating," vol. 171, pp. 98-109, 2018.

[48] M. Al-Zareer, I. Dincer, and M. A. J. J. o. H. T. Rosen, "Heat Transfer and Thermodynamic Analyses of a Novel Solid–Gas Thermochemical Strontium Chloride–Ammonia Thermal Energy Storage System," vol. 140, no. 2, p. 022802, 2018.

[49] H. Zondag, B. Kikkert, S. Smeding, R. de Boer, and M. J. A. e. Bakker, "Prototype thermochemical heat storage with open reactor system," vol. 109, pp. 360-365, 2013.

[50] B. Zettl, G. Englmair, and G. J. A. T. E. Steinmaurer, "Development of a revolving drum reactor for open-sorption heat storage processes," vol. 70, no. 1, pp. 42-49, 2014.

[51] K. Johannes, F. Kuznik, J.-L. Hubert, F. Durier, and C. J. A. e. Obrecht, "Design and characterisation of a high powered energy dense zeolite thermal energy storage system for buildings," vol. 159, pp. 80-86, 2015.

[52] A. Krönauer, E. Lävemann, S. Brückner, and A. J. E. P. Hauer, "Mobile sorption heat storage in industrial waste heat recovery," vol. 73, pp. 272-280, 2015.

[53] J. Wyttenbach *et al.*, "Performances and modelling of a circular moving bed thermochemical reactor for seasonal storage," vol. 230, pp. 803-815, 2018.

[54] Y. A. Cengel and M. A. J. S. Boles, "Thermodynamics: an engineering approach," vol. 1000, p. 8862, 2002.

[55] t. s. c. Sensirion, *fileadmin/user_upload/customers/ sensirion/ Dokumente/ Humidity_Sensors/Sensirion_Humidity_Sensors_Introduction_to_Relative_Humidity_V2.pdf* >.

[56] M. S. Buker, B. Mempouo, and S. B. Riffat, "Performance evaluation and techno-economic analysis of a novel building integrated PV/T roof collector: An experimental validation," *Energy and Buildings*, vol. 76, pp. 164-175, 2014/06/01/ 2014.

[57] F. Ozgen, M. Esen, and H. Esen, "Experimental investigation of thermal performance of a double-flow solar air heater having aluminium cans," *Renewable Energy*, vol. 34, no. 11, pp. 2391-2398, 2009/11/01/ 2009.

[58] S. P. Casey, J. Elvins, S. Riffat, and A. Robinson, "Salt impregnated desiccant matrices for ‘open’ thermochemical energy storage—Selection, synthesis and characterisation of candidate materials," *Energy and Buildings*, vol. 84, pp. 412-425, 2014/12/01/ 2014.

[59] E. Courbon *et al.*, "Further improvement of the synthesis of silica gel and CaCl2 composites: Enhancement of energy storage density and stability over cycles for solar heat storage coupled with space heating applications," vol. 157, pp. 532-541, 2017.

[60] A. Mehrabadi and M. J. E. Farid, "New salt hydrate composite for low-grade thermal energy storage," vol. 164, pp. 194-203, 2018.